Scuola Universitaria Superiore IUSS Pavia

SEISMIC BEHAVIOUR AND RETROFITTING OF MASONRY VAULTS IN HISTORICAL CHURCHES: AN APPLIED ELEMENT MESO-MODELLING STUDY

A Thesis Submitted in Partial Fulfilment of the Requirements
for the Degree of Doctor of Philosophy in

EARTHQUAKE ENGINEERING AND ENGINEERING SEISMOLOGY

Obtained in the framework of the Doctoral Programme in
Understanding and Managing Extremes

by

Martina Cogliano

30 November, 2025

Scuola Universitaria Superiore IUSS Pavia

SEISMIC BEHAVIOUR AND RETROFITTING OF MASONRY VAULTS IN HISTORICAL CHURCHES: AN APPLIED ELEMENT MESO-MODELLING STUDY

A Thesis Submitted in Partial Fulfilment of the Requirements
for the Degree of Doctor of Philosophy in

EARTHQUAKE ENGINEERING AND ENGINEERING SEISMOLOGY

Obtained in the framework of the Doctoral Programme in
Understanding and Managing Extremes

by

Martina Cogliano

Supervisor: Gian Michele Calvi

30 November, 2025

ABSTRACT

Unreinforced masonry buildings are widely recognized as structures characterized by high seismic vulnerability, even when referring to historical constructions located in seismic-prone areas. While the seismic behaviour of bending and shear walls has been extensively investigated by past studies, the knowledge about the response of vaulted systems, which are the most common horizontal element in historic buildings, remains largely limited. As a result, assessing their seismic behaviour becomes a key research topic.

In this study, as a novelty in literature, the application of the Applied Element Method (AEM) in simulating the response of masonry vaults when subjected to ground shaking is explored. Due to its discrete nature, AEM is fully capable of reproducing the response of a structure starting from the elastic range, through the crack initiation and propagation, up to failure and debris detachment.

A meso-modelling approach is proposed and developed within the AEM framework, originating from the need to assess historic churches in the area of Groningen, where seismicity is induced by gas extraction. This methodology is chosen to expedite the numerical modelling and limit the computational demand without losing accuracy.

In this context, the progress in the study of efficient strengthening measures with limited architectural impact allows the retrofitting of masonry vaults without offending their original beauty. Consequently, the numerical modelling of reinforcement is also investigated.

After an introduction on the historical developments of masonry vaulted constructions and the AEM formulation, this work presents the meso-modelling approach, its validation against experimental tests, and finally, its application on real historic churches. The obtained results demonstrate its capability in reproducing crack patterns, damage evolution, and failure mechanisms, thereby establishing it as a reliable and efficient tool for evaluating the seismic response of masonry vaults.

SOMMARIO

Gli edifici in muratura non armata sono caratterizzati da un'elevata vulnerabilità sismica, anche se costruite in zone riconosciute come soggette ad azione sismica. Mentre il comportamento sismico di elementi murari (maschi e fasce) è ancora oggi oggetto di uno studio intensivo, la conoscenza della risposta sismica delle volte murarie, che rappresentano uno dei più comuni sistemi di orizzontamento specialmente negli edifici storici, risulta piuttosto limitata. Di conseguenza, la valutazione del loro comportamento sismica è diventato un argomento di estrema rilevanza nella ricerca.

In questo studio, come novità in letteratura, è analizzata l'applicazione dell'AEM per simulare la risposta sismica di volte murarie. L'AEM deriva dai metodi di modellazione discreta ed è in grado di riprodurre l'evoluzione della risposta di una struttura partendo dal campo elastico, formazione e propagazione delle fessure, fino al collasso con conseguente distacco di macerie.

La proposta di una meso-modellazione sviluppata tramite AEM nasce dal bisogno di valutare un piccolo gruppo di chiese storiche della regione di Groningen, dove la sismicità è indotta dalle estrazioni di gas. Tale metodologia permette una elevata velocità di modellazione numerica con un ridotto onere computazionale senza perdere accuratezza.

Inoltre, i progressi nello sviluppo di misure di rinforzo efficaci e caratterizzate da un limitato impatto architettonico permettono di rinforzare le volte murarie preservandone il valore artistico. Di conseguenza, in questa tesi viene trattata anche la modellazione numerica del rinforzo.

Dopo aver richiamato gli sviluppi storici delle costruzioni con orizzontamenti voltati e illustrato la formulazione dell'AEM, viene presentata la metodologia della meso-modellazione, la sua validazione confermata da test sperimentali, e infine la sua applicazione a casi studio reali. I risultati ottenuti mostrano che questo approccio è in grado di riprodurre la formazione delle fessure, la propagazione del danno e i meccanismi di collasso, dimostrando di essere uno strumento efficace e robusto per la valutazione della risposta sismica delle volte.

ACKNOWLEDGEMENTS

TABLE OF CONTENTS

LIST OF FIGURES

CHAPTER 1

INTRODUCTION

CHAPTER 2

MASONRY VAULTS: HISTORY, STRUCTURAL DESIGN AND NUMERICAL MODELLING

CHAPTER 3

APPLIED ELEMENT METHOD AND ITS APPLICATION

Chapter 4

AEM meso-modelling approach and its validation on vaults

CHAPTER 5

SENSITIVITY ANALYSES

CHAPTER 6

VAULTS SEISMIC VULNERABILITY

CHAPTER 7

MASONRY VAULTS: RETROFITTING SOLUTIONS

Chapter 8

Case studies

LIST OF TABLES

CHAPTER 4

AEM MESO-MODELLING APPROACH AND ITS VALIDATION

CHAPTER 5

SENSITIVITY ANALYSES

CHAPTER 7

MASONRY VAULTS: RETROFITTING SOLUTIONS

1 INTRODUCTION

1.1 MOTIVATION

Masonry vaults have been frequently used as the main ceiling type among historic buildings. Disregarding their architectural importance, their role in favouring a global sound response connecting walls and columns and their high sensitivity to imposed displacements and deformations made them crucial components to assess the global response and safety. While the response of masonry structural elements generally inclined to adsorb horizontal actions (such as bending and shear walls connected by lintels) have been the object of extended past studies, it became soon clear that the effects and potential collapse modes of vaulted ceilings was a field in which knowledge was generally lacking.

Furthermore, unreinforced masonry buildings are known as characterized by high seismic vulnerability. This applies, in particular, to the architectural heritage in the Groningen area, where seismicity induced by gas extraction led to a series of ground shakings, Figure 1.1. The large number of historic churches present in the area was not designed considering seismic actions, which even for low magnitude induced event caused several damages.

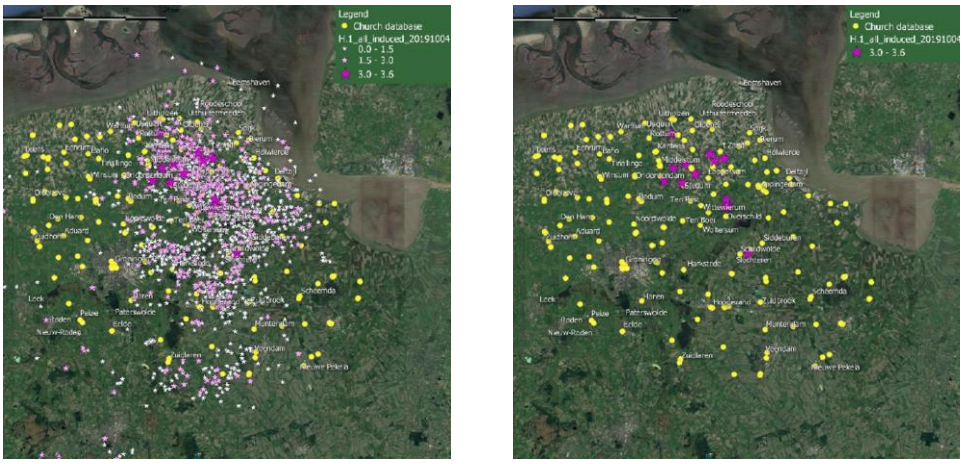

(a) (b)

Figure 1.1 Occurred induced earthquakes in the Groningen area: all magnitudes (a), magnitude M_w>3 (b)

For the purpose of rapidly assessing the seismic performance of a large portfolio of churches, the project, also known as Seismic Multilevel Assessment of Churches (SMAC), was developed by (Moratti et al., 2019). The main goal was to handle a large number of churches, on the order of hundreds, understanding which buildings may need retrofitting, which certainly will need retrofitting, and which can be considered as safe according to as-built configuration. In other words, the aim of the SMAC procedure is the definition of a prioritisation, because carrying out a full fledge of analysis on each church is time demanding, excessively expensive and incompatible with the need of where resources should be allocated to further investigate the situation prior to intervention.

The process involves both data collection and vulnerability assessment, with progressive refinements, and has been applied to a portfolio of 52 churches in the Groningen area, (Moratti et al., 2019). SMAC procedure consists of three levels of analysis each of increasing details, Figure 1.2:

- O.0 – Level 0 procedure results.
- O.1 – Level 1 assessment procedure results.
- O.2 – Level 2 assessment procedure results.

In order to perform these assessments, three data collection levels are required: geographic data, geotechnical data, and seismic hazard data; together with two levels of inspection of the buildings, V.1 and V.2.

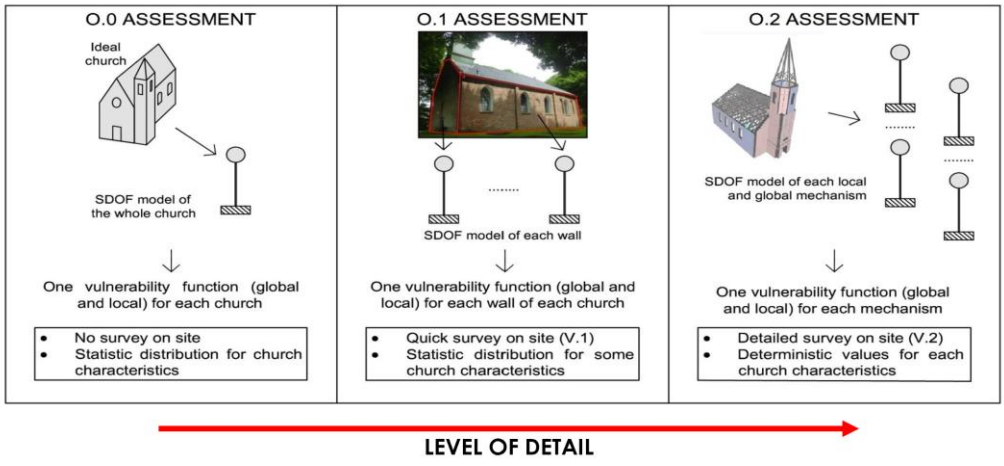

Figure 1.2 SMAC procedure

The Level O.0 foresees the representation of the whole church using a simple model, single pier, without any inspection needed because statistical assumptions are made on

main geometric and structural characteristics with self-improving system. This level makes use of Nonlinear Pushover Analyses (NLPO) for the in-plane behaviour, Nonlinear Kinematic Analyses (NLKA) for the out-of-plane response, and Monte Carlo simulation is performed for each church. It does not give information about safety condition of each specific church, but an estimate of the general behaviour of the whole portfolio of churches. Level O.0 is valuable to define the average cost and strategy of intervention with reference to the complete database.

Level O.1 needs short inspection to retrieve the main characteristics of the churches, because each wall is represented by an equivalent pier, still using a simple model. Some characteristics still come from statistical assumptions (e.g. material) and NLPO, NLKA and Monte Carlo simulations are performed for each wall of the church. Level O.1 is capable to give which parts are the most vulnerable and returns evidence whether the inadequacy is limited to some elements in the church or it is widespread. Despite it is not NPR compliant because based on statistical assumption, it is currently beneficial to the prioritisation of further activities on each church.

Level O.2 builds refined models and analyses to define the capacity of churches according to guided semiautomatic steps. For this reasons it requires detailed inspections of the structures, during which pre-existing state of deformations or deficiencies should be reported in order to consider them in the numerical model. A global assessment through NLPO and a local verification with NLKA are performed. The main advantage is that this level is fully NPR compliant.

The consistency of results at different levels confirms the effectiveness of the multilevel procedure in assessing the prioritisation of interventions on churches and warnings associated to each church are given to address topics which might be critical and need further investigations at the following phases (e.g. vaults, gable, ties, steeple). Consequently, the results of Level O.2 have been the starting point for the following phases:

- Inspections of churches based on the warnings.
- Level 3, which consists of refined analyses on the churches which are uncompliant at level O.2, most of them characterized by vaulted ceilings.
- Level 4, in which strengthening measures are designed on the analysed churches.

1.2 OBJECTIVE AND SCOPE

Within the context described above, the Applied Element Method (AEM) is proposed to address both Level 3 and Level 4 as a natural continuity of the SMAC procedure. Several recent studies have demonstrated the capabilities of AEM in reproducing in-plane, out-of-plane and global responses of masonry walls and buildings when subjected to seismic loading., also highlighting its computational efficiency.

The objective of this thesis is to develop and validate a reliable and computationally efficient meso-modelling approach based on the Applied Element Method for the seismic assessment of historic masonry churches characterized by vaulted systems. with the aim of create a standardised framework which can be applied to churches of any dimension and any typology.

The research was developed by the author in an academic context, while benefiting from the interaction with professional practice and selected case-study experience at Studio Calvi Beam, which provided a valuable practical background without influencing the scientific autonomy of the study.

The challenge of this study is mainly the lack of deep knowledge on the numerical modelling of masonry historic vaults using AEM formulation, together with the presence of very few shaking table tests on full scale vaulted specimens. This has led to a series of sensitivity analyses simulating LNEC shaking table tests, (Bianchini et al., 2023), in order to find a procedure to assess the churches of Level 3 balancing accuracy of results and speed of analysis.

1.3 OUTLINE OF THE THESIS

Chapter 2 presents through a deep literature review the historical evolution of masonry vaults from empirical construction practices, which led to long-lasting buildings, up to theoretical formulations explaining their mechanical behaviour. An overview of the numerical modelling approaches for masonry structures and masonry vaults for their structural assessment is given. This chapter provides the cultural and technical foundations necessary to interpret both vulnerability and strengthening strategies.

Chapter 3 is dedicated to the introduction of the theoretical formulation of the Applied Element Method (AEM). The first part traces its development starting from earlier discrete modelling techniques, highlighting how its characteristics make it a powerful innovation in numerical modelling. The second part illustrates how the methodology is applied in the assessment of the masonry structures, and it recalls validations against

experimental results, which demonstrate the ability of AEM to reproduce their structural responses. A brief introduction to the Extreme Loading for Structures (ELS) software, which has been employed in this thesis is give. This chapter lays the foundation to present the proposed meso-modelling approach presented in this study.

Chapter 4 presents the meso-modelling approach developed in this study to numerically simulate masonry structures and vaults. According to this method, masonry is treated as a homogenized material, made of rigid blocks and nonlinear interfaces springs. An overview of the AEM meso-modelling is given, together with constitutive laws employed for tension, compression and shear. After discussing the modelling assumptions, the chapter is strongly dedicated to the validations both on walls and vaults behaviour. A particular attention is given to the numerical simulations of the LNEC shaking table tests campaign, already presented in (Cogliano et al., 2025a). The validation is also performed considering different modelling strategies from different authors.

Chapter 5 investigates the influence of key numerical and mechanical parameters through a series of sensitivity analyses. Particular attention is devoted to the separation strain, already treated in the Chapter 4, but here deeply assessed through Local Sensitivity Analysis (LSA). Other parameters are discussed, such as mesh size, and interface properties, assessing the robustness and stability of the numerical model.

Chapter 6 examines the seismic vulnerability of masonry vaults in historical churches. The discussion integrates theoretical considerations, an evaluation on emblematic case studies (Pavia Cathedral, Basilica of St. Francis of Assisi), and the effects of induced seismicity in Groningen, highlighting recurrent weaknesses and collapse mechanisms.

Chapter 7 presents an extensive review of retrofitting solutions for masonry vaults, from traditional measures to modern composite systems, defining advantages and disadvantages for each strengthening solution. The two case studies presented in Chapter 6, Pavia Cathedral and Basilica of St. Francis of Assisi, are recalled and the consolidation of their vaulted systems are illustrated and discussed. Subsequently, the chapter shows the validations of FRCM/TRM strengthening modelling within the AEM framework, starting from scaled model (wallets and arches), to the numerical simulation of the strengthened with Textile Reinforced Mortar LNEC vault.

Chapter 8 applies the modelling framework developed in the previous chapters to three Dutch churches selected within the SMAC framework. For each case study, the chapter describes the as-built and retrofitted configurations and their seismic assessment following (NEN, 2020) regulation.

Chapter 9 summarises the main findings of the research, highlighting both virtues and limitations of the proposed AEM meso-modelling approach applied to masonry vaults. Potential future developments in numerical modelling which could improve the accuracy and reliability are also discussed.

2 MASONRY VAULTS: HISTORY, STRUCTURAL DESIGN AND NUMERICAL MODELLING

2.1 INTRODUCTION

Masonry vaults represent one of the most emblematic components in architectural and structural history, combining construction creativity, geometric instinct, and mechanical behaviour. Their study requires a multidisciplinary perspective, starting from historical analysis to modern structural mechanics and advanced computational modelling. This chapter provides an overview of the evolution and scientific understanding of masonry vaults.

Section 2.2 shows the historical development of vaulted ceilings, from prehistoric corbelled constructions to Roman concrete domes, Gothic rib vaults, and Renaissance and Baroque masterpieces. Particular attention is placed on how different cultural and technological contexts affected construction techniques and architectural forms.

Section 2.3 illustrates the structural behaviour of vaults, starting from empirical construction practices, the rules of thumb, up to theoretical formulations, with the first contributions of Hooke, Gregory, and Heyman. The section explores how geometric reasoning and limit analysis theories laid the foundation for modern structural assessment, also highlighting the issue of vault vulnerability, their sensitivity to degradation and seismic actions, and reviews experimental investigations that have been developed until now.

Finally, Section 2.4 discusses numerical modelling strategies for masonry and masonry vaults. It introduces the two main approaches, micro- and macro-modelling, and analyses their application to vaulted systems. The review includes continuum-based finite element methods, limit state analysis, and discrete element modelling, as well as recent developments in homogenisation and reinforcement modelling. Pros and cons of each method are evaluated in order to provide a critical framework for selecting the most appropriate strategy depending on the objective of the analysis.

2.2 HISTORY OF VAULTED CEILING

Masonry vaults have a long history, dating back to the earliest civilizations, where they represented both functional and symbolic achievements in architecture. The oldest known example is most likely the corbelled vault, used in megalithic structures of the Neolithic and Early Bronze Age. The funerary chamber of the Newgrange mound in Ireland, Figure 2.1, dated to around 3200 BCE, is generally considered the earliest surviving vault (Eogan, 1991). This passage tomb, with its corbelled roof, predates Stonehenge and the Pyramid of Cheops by several centuries and is also earlier than the Mycenaean culture of Ancient Greece. The mound covers an area of approximately 4,500 m^2, with a diameter of 80 m and a height of 12 m. Its tunnel extends 20 m and leads to a vaulted chamber about 6 m high, Figure 2.2.

Figure 2.1 Newgrange: UNESCO World Heritage Site

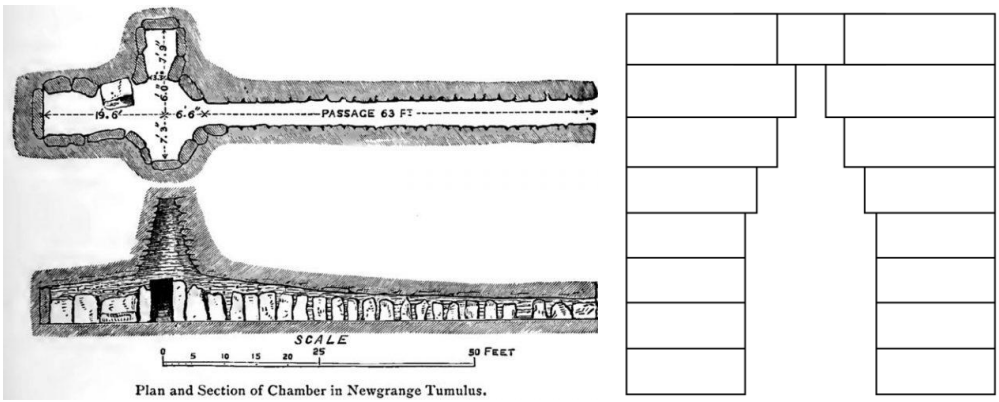

(a) (b)

Figure 2.2 Plan and section of chamber in Newgrange tumulus** (Eogan, 1991) **(a) and a typical scheme of a corbelled arch

During 19th century, different scientists, such as (Cooke, 1903), saw the Newgrange chamber as a dome constructed by corbelling: successive layers of stones were projected inward until they met at the vertex Figure 2.2 (b). However, later studies challenged this view. (Nelms, 1981), for instance, argued that the structure employed a different system that he called "beam-wall construction," where massive stones were arranged in a polygonal base, acting simultaneously as wall and roof. Unlike true corbelling, which is short in span and vulnerable to settlement or seismic events, this method was more robust and durable, comparable to pyramid construction. Despite these debates, Newgrange remains the elderly example of a masonry vault.

During the Late Bronze Age, civilizations such as the Mycenaeans built tholos tombs, including the Tomb of Atreus (c. 1300 BCE), shown in Figure 2.3. These subterranean chambers employed corbelled vaulted system by placing rings of stone progressively inward to form conical domes (G De Matteis et al., 2019). While visually similar to later domes, these structures lacked true compressive arch action and remained tension-free systems. As noted by (G De Matteis et al., 2019) and (Kurrer, 2008), corbelled systems were inherently limited: the greater the diameter, the higher the risk of collapse, so that the vertical expansion was more feasible than horizontal span.

(a) (b)

Figure 2.3 Tomb of Atreus, Mycenae (Greece) external view (a), inner view of the vault (b)

The Romans marked a decisive turning point in vault construction, mastering the use of arches to create large-scale masonry vaults. Two main typologies were employed: the barrel vault, obtained by extending a semicircular or segmental arch longitudinally, and the groin vault, formed by the perpendicular intersection of two barrel vaults. The latter employed diagonal internal ribs to strengthen critical zones (Como, 2015). Roman innovation lay in the extensive use of *opus caementicium* (Roman concrete), which enabled continuous compressive force distribution along curved surfaces. This material

allowed for the construction of unprecedented architectural spaces, as seen in the Pantheon Figure 2.4, and the Baths of Caracalla, Figure 2.5, (Gaetani et al., 2016).

The Pantheon is the largest unreinforced concrete dome in the world with a span equal to 43.3 m, built around 126 CE under Emperor Hadrian. Its structural efficiency derives from an accurate use of materials: heavy aggregates at the base and lighter ones, such as pumice, toward the crown. Its thickness decreases with the height: from 6.4 m at the base up to 1.2 m at the oculus. The oculus, with a diameter of 8.3 m, works both as a light source and as a stress-relieving opening. Resting on a massive drum, the dome forms a perfect hemisphere, symbolizing cosmic harmony and imperial grandeur.

(a) (b)

Figure 2.4 Pantheon, Rome (Italy) external view (a), internal view of the dome (b)

The Baths of Caracalla (212–216 CE) represents an additional Roman understanding of vaulted system, putting together technical and monumental designs. Their monumental entrances were roofed with massive barrel, groin, and cloister vaults, where *opus caementicium* was employed with brick and stone. The frigidarium spanned over 30 m, while the caldarium was enclosed by soaring domes and half-domes.

(a) (b)

Figure 2.5 Bath of Caracalla, Rome (Italy) external view (a), internal view of the vaults (b)

Between the 10th and 13th centuries, with the development of Gothic architecture ribbed vaults and pointed arches were born, enabling taller and lighter structures with more flexible configurations. Structural loads were transferred directly to ribs and external flying buttresses; in this way, it was possible to have thinner walls and large stained-glass windows. Rib vaults evolved from intersecting barrel vaults, with additional diagonal and transverse ribs starting to work as structural elements. Depending on rib configuration, several forms can be built: sexpartite vaults (six bays), quadripartite vaults (four bays), stellar vaults (with tertiary ribs), and fan vaults (radiating ribs). One of the most iconic examples is the interior of Notre-Dame Cathedral in Paris, begun in 1163, whose sexpartite vaults exemplify the Gothic synthesis of structural efficiency and aesthetic verticality (Bony, 2023).

(a) (b)

Figure 2.6 Notre-Dame Cathedral, Paris (France) external view (a), internal view of the six-part ribbed vaults (b)

The Renaissance returns back to classical ideals, combining structural rigor with architectural harmony, as exemplified by the dome of Santa Maria del Fiore in Florence, Figure 2.7, designed by Filippo Brunelleschi in 1420. With a span of 45.5 m and a rise of 103.4 m, it is the largest brick masonry dome ever built. From the structural point of view, it consists of two shells connected by ribs: an inner dome, 2.2 m thick, and an outer protective shell, whose thickness varies from 0.8 m to 0.4 m. Brunelleschi constructed it without centering, relying on successive horizontal courses to ensure stability (Bartoli et al., 2015).

(a) (b)

Figure 2.7 Cathedral of Santa Maria del Fiore, Florence (Italy) external view (a), internal view of the frescoed dome(b)

Vaults were used to create spatial illusion in the Baroque era. A distinctive example is the Church of Sant'Ignazio di Loyola in Rome, which was designed by Orazio Grassi and decorated by Andrea Pozzo. Pozzo transformed the simplicity of a barrel vault into an illusionistic masterpiece, *The Glory of Saint Ignatius*, which depicts the saint ascending into heaven among allegories and figures representing the continents. He created the illusion of an open sky, extending the architecture beyond its physical boundaries (Fasolo & Mancini, 2019).

(a) (b)

Figure 2.8 Church of Sant'Ignazio di Loyola, Rome (Italy) external view (a), internal view of the frescoed barrel vault(b)

A representative example of this long historical trajectory is the Cathedral of Pavia. Initiated in 1488 following the ideals of Romanesque cathedrals, its design was linked to Renaissance figures such as Donato Bramante and Amadeo, and accompanied by the

construction of a large wooden model that guided the building process for centuries, (Calvi & Palenzona, 2013). The construction was discontinuous, lasting more than five hundred years, and it highlights the influence of economic, political, and cultural changes on the realization of vaulted structures. The central dome, completed only in the late nineteenth century, represents the persistence of Renaissance ideals across time. It was raised on an eighteenth-century octagonal drum between 1885 and 1889, following Carlo Amati's design, and crowned by a lantern and a gilded copper statue of the Redeemer in1890. It consists of a double shell, with an inner hemispherical calotte and a slender external one, separated by a walkable cavity. Reinforced with iron chains and rings, it demonstrates the integration of traditional masonry vaulting, based on Reanaissance, with modern structural devices. It exemplifies how cultural ambition and technological innovations shaped the evolution of vaulted ceilings well beyond their original historical context.

(a) (b)

Figure 2.9 Cathedral of Pavia (Italy) external view (a), internal view of the dome (b) (Calvi & Palenzona, 2013)

In summary, the history of masonry vaults is characterized by a progressive refinement from experience-driven construction methods to more advanced theoretical frameworks. From the corbelled chambers to the structural understanding of Roman concrete, from the ribbed vaults of Gothic cathedrals to the geometric harmonies of the Renaissance and the visual effects of the Baroque, each period introduced solutions that reflected its culture and technical expertise.

With the advent of modern structural mechanics in the eighteenth century, analytical tools were introduced transforming vaults from objects of empirical tradition into subjects of scientific investigation. Nevertheless, as (Benvenuto, 1991) observes, the discrete and frictional nature of masonry has often been misunderstood, because its

behaviour was often considered elastic. This difference between theoretical abstraction and material reality highlights how vaults have always considered as architectural components, while their true structural behaviour requires a careful balance between geometry, material properties and boundary conditions.

In order to assess vaults vulnerability and to develop appropriate conservation and intervention strategies, it is essential to understand how there were conceived, built and interpreted over the centuries. The next step, therefore, is to examine the fragility of these structures in relation to modern needs and explore the knowledge gained from experimental tests that integrate theoretical and numerical approaches.

2.3 VAULTS STRUCTURAL DESIGN: FROM ANCIENTS TO MODERN ANALYSTS AND EXPERIMENTAL TESTS

The structural analysis of masonry arches and vaults represents one of the most fascinating intersections of empirical knowledge, geometric reasoning, and theoretical mechanics in architectural history. From ancient Rome to the scientific advancements of the 20th century, the design of vaults evolved from rule-of-thumb practices to rigorous formulations based on equilibrium and limit state theories. Until the 18th century, genuine structural science did not exist; nevertheless, master builders succeeded in creating durable structures of remarkable stability. As (Huerta, 2008) notes, ancient builders relied primarily on geometry and construction experience rather than analytical calculations. Roman engineers, for example, mastered the use of barrel vaults, groin vaults, and domes, as seen in structures like the Pantheon, by applying empirical knowledge. They understood that the geometry governed the stability: a well-shaped arch stood because its thrust was absorbed by the surrounding walls. This practical wisdom was codified in treatises such as Vitruvius' *De Architectura*, though without a rigorous mathematical framework.

When analysing vaults, reference to the arch is essential, since even complex forms, such as Gothic vaults, can be interpreted as a composition of arches. (Huerta, 2001), who refers to the work of Joseph Durm (1885), illustrates the fundamental behaviour of the arch, Figure 2.10: wedge-shaped stones are placed on wooden centring, closed by the keystone, and thereafter self-supporting. At each joint, a compressive force, called the thrust, develops, which must remain within the contact surface to ensure stability. The locus of these thrust points defines the line of thrust. This equilibrium persists along the arch until it reaches the supports, where abutments must resist the outward forces. Masonry design, therefore, involves two principal challenges: guaranteeing the internal

stability of the arch and providing adequate buttressing against lateral thrust. The line of thrust must lie within the masonry thickness, in accordance with the material's properties: heterogeneity, high compressive capacity, negligible tensile strength, and high friction coefficient (Huerta, 2001).

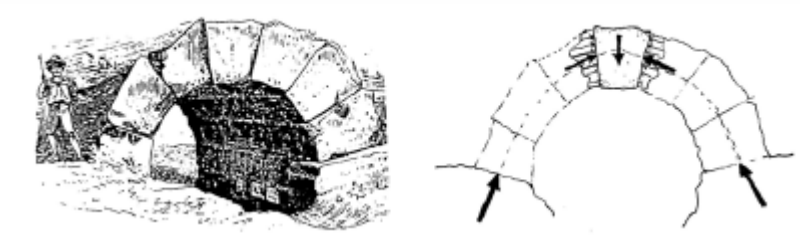

Figure 2.10 Etruscan voussoir arch (Drum, 1885) figure reported in *(Huerta, 2001)*

The first conceptual breakthrough occurred in 1675, when Robert Hooke famously stated: "*As hangs the flexible line, so but inverted will stand the rigid arch*". This insight, later clarified by (Gregory, 1697) established the basis of funicular theory: the stable form of an arch corresponds to the inverted shape of a hanging chain, or catenary. An arch is stable if a catenary curve can be inscribed within its thickness. Since multiple equilibrium lines may exist within the masonry, the arch is statically indeterminate.

During the 18th and 19th centuries, significant advances were achieved with graphical statics and elasticity theory, developed by figures such as Coulomb, Navier, and Rankine. Winkler (1879) was the first to apply elasticity theory to masonry arches, but, as (Huerta, 2001) notes, perturbations such as centring deformation, buttress yielding, and thermal effects could not be neglected. These produced cracking, which elastic analysis could not adequately explain. As (Heyman, 1995) demonstrated, it is only possible to evaluate the extreme positions of the line of thrust, corresponding to minimum and maximum thrusts. Cracks, acting as hinges, allow for structural adjustment. Both (Huerta & Lopez, 1997) and (Benvenuto, 1991) criticized purely elastic approaches, emphasizing instead the discrete and frictional nature of masonry.

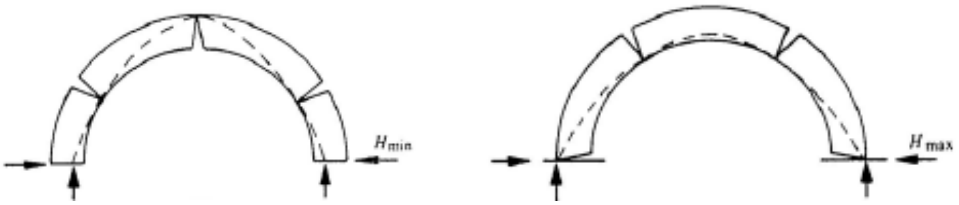

(a) (b)

Figure 2.11 Semicircular arch under its own weight. (a) Minimum thrust; (b) maximum thrust *(Heyman, 1995)*

A decisive shift came with (Heyman, 1966, 1982), who formalized the structural behaviour of masonry within the framework of limit state and plastic theory. He established three key assumptions: masonry has infinite compressive strength, zero tensile strength, and no sliding between blocks. Under these hypotheses, stability is guaranteed if a statically admissible line of thrust lies within the structure's geometry. (Heyman, 2008) also noted the indeterminacy of boundary conditions, which may evolve over time, but emphasized that the collapse load depends only on geometry. Within this framework, a structure is safe if at least one set of internal forces satisfies both equilibrium and yield conditions. This approach, rooted in limit analysis, translated the intuitive practices of historic builders into a consistent mathematical theory.

Modern developments in the analysis of domes and vaults, among the first is the work done by (Oppenheim et al., 1989), extend Heyman's framework to three-dimensional shells, exploring the conditions under which a dome may form a kinematic collapse mechanism. They demonstrate how to calculate the minimum thickness of a dome under self-weight and show that compressive hoop stress is necessary in the upper cap of a dome for stability, a conclusion that aligns with historical construction patterns like the use of rings in St. Peter's dome in Rome. Their work demonstrates that the principles of limit analysis, first applied to two-dimensional arches, are equally effective in analysing complex three-dimensional forms. In practice, limit analysis has become a cornerstone of modern conservation engineering, offering a rigorous yet historically faithful toolset for assessing ancient structures. It validates much of the historical construction practice while enabling contemporary engineers to intervene wisely and respectfully. (D'Ayala & Casapulla, 2001) introduces a finite friction coefficient into the limit analysis of masonry vaults, enhancing the accuracy and realism of the structural prediction with respect to classical Heyman-based approaches, which assume infinite friction and no tension. This study demonstrates that the value of friction strongly influences the location of failure mechanism, the distribution of internal forces and the load-bearing capacity of the vaults; the method is especially relevant for the structural assessment of historic vaults, where interventions must be minimal and reversible. By accurately estimating the collapse load and identifying critical regions, the model aids in targeted reinforcement design and prioritisation of structural interventions. (Block & Ochsendorf, 2008) applies Heyman's lower-bound theorem, i.e. if a compression-only equilibrium can be found within the geometry of the vault, the structure is safe. The authors develop a three-dimensional thrust-network analysis for masonry vaults,

offering a powerful extension of traditional thrust-line methods (graphics statics) to complex 3D vaulted forms. Their method provides rigorous lower-bound solutions based on masonry's compression-only behaviour.

The evolution of vault analysis, from empirical rules to limit state mechanics, demonstrates both the ingenuity of historic builders and the explanatory power of modern structural theory. While theoretical models have greatly advanced the understanding of masonry vaults, their actual behaviour is inevitably affected by material irregularities, construction and retrofitting defects, and external actions such as earthquakes (Theodossopoulos & Sinha, 2008). For this reason, the concept of vulnerability has become central in modern studies, particularly in the context of cultural heritage preservation. To complement analytical and numerical approaches, a wide range of experimental tests has been conducted, offering valuable insights into the load-bearing capacity, collapse mechanisms, and seismic response of masonry vaults. The scientific community has been putting a lot of effort in studying how masonry vaults behave when horizontal actions are considered, but still, this represents an open challenge which requires historical investigation, literature review, inspections, structural modelling and numerical analyses (ICOMOS-ISCS, 2023). As a matter of fact, (Bertolesi et al., 2019) highlighted, through a bibliometric analysis of publications, that within the broader literature on masonry structures, studies specifically focused on arches and vaults remain limited, representing approximately 10% of the analysed portfolio, as shown in Figure 2.12.

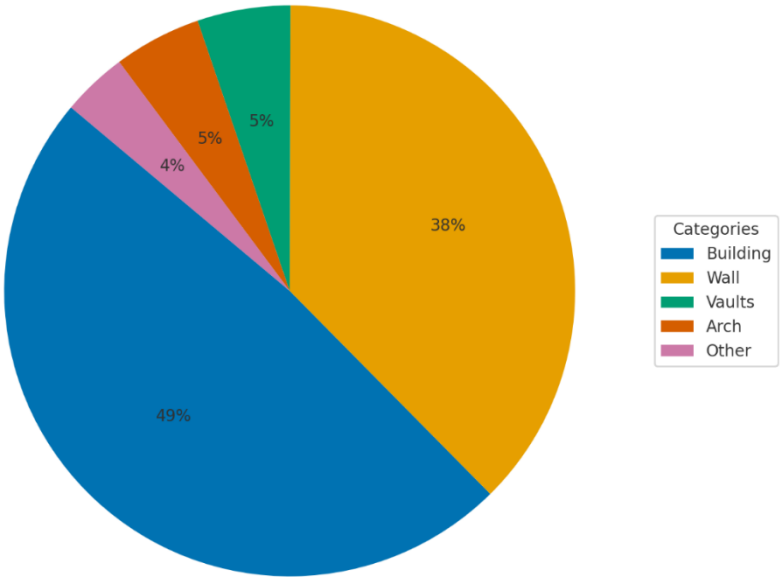

Figure 2.12 Documents published on "masonry" from 1960 to 2018

The very first shaking table test on a scaled model was performed in 2012 (Williams et al., 2012) on Roman-style scaled barrel vaults. The main goal was to evaluate the dynamic response of masonry vaults, how existing cracks due to gravity loads affect their seismic performance, and validate numerical modelling of historic vaults. The study found that the mechanism that occurs due to seismic load is characterized by four hinges, whose location depends on material's tensile strength; a damaged vault (i.e., with existing open cracks) is more fragile, because cracks work as weak planes.

The first 1:1 scaled vaults was tested on a shake-table in 2020 (Rossi et al., 2020). This work investigates the seismic response of a full-scale unreinforced masonry cross vault inspired by one of the vaults in the Dey Mosque in Algeris, Algeria, trying to assess the collapse mechanisms and how steel tie bars and wooden inserts affect the global behaviour of the vault. They conclude that the presence of steel ties improves the seismic performance by reducing in-plane deformations and preventing early collapse, which was instead achieved by the specimen without any tie; furthermore, the study highlights the importance of both geometric configuration and structural details in seismic performance of historical masonry vaults.

An additional shaking table test on a full-scale masonry cross-vault took place at *Laboratorio Naciónal de Engenharia Civil* (LNEC), Portugal, in 2021 aiming to understand

the seismic behaviour of masonry cross-vault and assess the capability in simulating its seismic response of different modelling strategies. The experimental campaign is deeply described in (Bianchini et al., 2024) and it has been used to validate the proposed numerical modelling subject of this thesis.

2.4 NUMERICAL MODELLING OF MASONRY AND MASONRY VAULTS

Masonry has been used for centuries in construction, yet it still lacks design tools as comprehensive as those available for concrete or steel. The difficulty lies in the material's nature: it is a composite made of units (bricks, stones, or blocks) and mortar joints, and is characterized by anisotropy, heterogeneity, and a quasi-brittle behaviour. Accurate numerical modelling is therefore crucial, particularly for the assessment of heritage structures. With the increase in computational power and the development of advanced structural analysis software, it has become possible to model complex historic architecture with greater accuracy. This is typically achieved through contact-element formulations and nonlinear brittle material models, which allow both static and seismic vulnerability assessments.

In the scientific literature, two main modelling strategies are recognised: micro-modelling and macro-modelling. Micro-modelling explicitly represents the individual components of masonry, while macro-modelling treats masonry as a homogeneous continuum governed by phenomenological constitutive laws. Each approach offers different advantages in terms of accuracy, computational cost, and suitability for specific applications.

2.4.1 Micro-modelling approach

According to (Lourenco, 1996), two levels of micro-modelling can be distinguished: detailed and simplified. In the detailed approach, bricks and mortar are represented as separate continuum elements, while their interfaces are described with discrete interface elements governed by nonlinear constitutive laws. This enables the simulation of tensile cracking, shear slip, and compressive crushing. In the simplified approach, mortar thickness is absorbed into the geometry of the masonry units, while joints are represented by zero-thickness interface elements. These are the only elements assigned nonlinear behaviour, reducing the number of degrees of freedom without losing the capacity to reproduce the main failure mechanisms.

An early and influential micro-modelling strategy was presented by (Lourenço et al., 1995), who developed a composite interface model combining a tension cut-off

criterion, Coulomb friction law, and an elliptical cap for compressive failure. This formulation enabled the simulation of cracking, sliding, and crushing, and incorporated inelastic behaviour through softening and hardening laws. Micro-modelling is particularly suited to small-scale structures or localised analyses of critical zones such as piers and connections, although its computational cost remains high.

2.4.2 Macro–modelling approach

Macro-modelling treats masonry as a homogeneous orthotropic continuum, typically assigning different tensile and compressive behaviour along the bed and head joint directions. (Lourenço et al., 1995) proposed a constitutive model based on a Rankine-type yield surface for tension, a Hill-type yield surface for compression, and different strengths and fracture energies in the material directions.

This approach is computationally efficient and well suited to large-scale structures, particularly when the global response is of primary interest. One of its most practical applications is the Equivalent Frame Model (EFM), in which walls are idealised as an assembly of vertical piers and horizontal spandrels connected by rigid nodes (Lagomarsino et al., 2013). Based on post-earthquake observations, this method recognises that damage tends to concentrate in piers and spandrels. While EFM focuses on in-plane behaviour and assumes sufficient connections to prevent out-of-plane failure, it provides an efficient tool for seismic assessment at the building scale.

In summary, macro-modelling achieves a balance between accuracy and efficiency, making it the preferred approach for global structural analyses and seismic vulnerability assessment of entire buildings.

2.4.3 Numerical modelling for masonry vaults

When moving from walls and piers to vaulted systems, additional challenges arise. While the same numerical techniques employed for walls, piers and other structural components can be extended to vaulted systems, their application requires additional considerations. Cross vaults are characterised by a double curvature geometry, the presence of groins or ribs, and a complex interaction between arches and supporting walls, all of which significantly influence their mechanical behaviour. Moreover, the collapse mechanisms of vaulted structures are often governed not only by the local behaviour of the masonry material, but also by global geometric instabilities and support conditions. For these reasons, the transition from the general modelling of masonry to the numerical simulation of masonry vaults involves adapting constitutive assumptions,

computational strategies and boundary conditions in order to capture the specific response of such systems under static and seismic loading. In the following, the main modelling approaches that have been applied to masonry vaults are critically reviewed, highlighting their underlying assumptions, constitutive models, and the strengths and limitations of each method with reference to the most relevant literature. These approaches can be classified into three families: continuum-based approaches (FEM), limit state analysis (LSA), and discrete element modelling (DEM).

Within continuum-based approaches, the Finite Element Method (FEM) has been the most widely adopted to study masonry cross vaults. Two different levels of refinement can be distinguished. In macro-modelling, masonry is considered as a homogeneous anisotropic or isotropic continuum, often represented by nonlinear constitutive laws such as no-tension materials or damage–plasticity models (Creazza et al., 2002; Milani & Tralli, 2012; Pelà et al., 2016; Pellegrini, 2023). This approach allows for the analysis of large-scale and geometrically complex structures, such as ribbed or irregular cross vaults, without explicitly reproducing the texture of masonry. However, some intrinsic features, such as orthotropy induced by the bond pattern or localised cracking, tend to be smeared within the continuum. To overcome this drawback, orthotropic elastic–plastic models with softening have been proposed and calibrated against experimental results (Berto et al., 2002; Lourenço et al., 1997). On the other hand, micro-modelling strategies reproduce explicitly the units and the joints. In their complete form, masonry blocks are modelled as deformable elements and mortar joints as continuum layers with their own constitutive behaviour, usually defined in terms of tensile strength, cohesion, friction angle and compressive capacity (Lourenço & Rots, 1997). In the so-called simplified micro-modelling, mortar thickness is incorporated into the geometry of the blocks, and the nonlinear behaviour is concentrated in zero-thickness interfaces, governed by constitutive models such as Mohr–Coulomb or fracture-energy based softening (Formica et al., 2002; Lotfi & Shing, 1994) This approach allows for the reproduction of orthotropy and sliding mechanisms, but remains computationally expensive when applied to large-scale vaults. Relevant examples include the pioneering work on the Holyrood Abbey cross vault (Theodossopoulos et al., 2003) and the more recent heterogeneous modelling of small-scale prototypes tested under tilting conditions (Milani et al., 2016).

A further refinement is represented by homogenisation techniques, which attempt to bridge the gap between micro- and macro-modelling. These methods exploit the periodicity of the masonry texture to derive equivalent continuum properties at the structural scale (Cecchi & Sab, 2002; Milani et al., 2006b). Rigorous mathematical

formulations, finite element multi-scale frameworks, or simplified two-step homogenisation procedures have been proposed (Luciano & Sacco, 1997; Pegon & Anthoine, 1997). Despite their effectiveness in capturing some intrinsic features of masonry, these methods require strong assumptions such as material periodicity and often involve double discretisation, which limits their application to large and irregular cross vaults.

Limit State Analyses (LSA), either kinematic (upper-bound) or static (lower-bound), represent a complementary family of methods (Heyman, 1966; O'Dwyer, 1999). They are based on the limit theorems of plasticity and allow for a rapid evaluation of collapse loads, thrust lines and active mechanisms. Advanced formulations, such as Thrust Network Analysis (TNA), have been applied to ribbed cross vaults, predicting the formation of typical hinge lines such as the crown hinge and the Sabouret's crack (Block & Ochsendorf, 2007; Fraternali, 2010). More recent contributions coupled limit analysis with FEM, adopting mesh adaptation strategies to reduce mesh-dependence and improve accuracy (Chiozzi et al., 2017; Milani & Lourenço, 2009).

Finally, Discrete Element Modelling (DEM) has gained increasing popularity due to its ability to capture the discontinuous nature of masonry. In DEM, blocks are represented as rigid or deformable elements, while mortar joints are described as contact interfaces where nonlinearities such as sliding, separation, and friction are concentrated (Lengyel, 2017; Lengyel & Bagi, 2015) This approach is particularly suitable for unreinforced masonry, where the mechanical response is governed by the joints. DEM has been applied to investigate the role of ribs in groin vaults (Lengyel & Bagi, 2015) the influence of geometry (Lengyel, 2017), and the three-dimensional effects of support displacements (Foti et al., 2018; Van Mele et al., 2012). More recent contributions have further enriched this method: (Pulatsu et al., 2019) introduced DEM formulations enhanced with fracture-energy-based constitutive models, enabling the simulation of both cracking and crushing phenomena; (Oktiovan et al., 2023) applied a simplified micro-modelling DEM approach for the seismic assessment of vaults, effectively reproducing the complex interactions between blocks and mortar interfaces; (Bianchini et al., 2022) conducted experimental and numerical investigations on the collapse of masonry vaults subjected to seismic displacements, highlighting the predictive capability of DEM in capturing three-dimensional failure patterns.

The modelling of strengthened vaults has also been addressed. FEM and DEM approaches have been used to investigate the effectiveness of reinforcement materials such as FRP, CFRP, GFRP, TRM and FRCM, showing significant increases in collapse

loads and modifications of crack patterns (De Lorenzis et al., 2007; Foraboschi, 2004; Szołomicki et al., 2015) Numerical simulations confirmed that reinforcement can prevent the formation of crown hinges, meridian cracks and Sabouret's cracks under both vertical and seismic loads (Fraternali et al., 2015; Milani et al., 2009).

In summary, macro-FEM approaches are the most efficient for large-scale analyses, although they neglect some aspect, such as local failures; micro-FEM and DEM allow the reproduction of discontinuous behaviour and local failure mechanisms, but with higher computational costs; homogenisation offers an intermediate solution but relies on restrictive assumptions; and limit analysis provides a rapid tool for collapse safety evaluation. The choice of modelling strategy thus depends on the specific objective of the analysis, whether estimating global capacity, identifying local mechanisms, or assessing strengthening interventions.

2.5 Historical Dutch churches: architectural and structural features

The architectural heritage of Dutch churches reflects a complex historical development shaped by regional materials, cultural influences, and evolving construction techniques. Early Romanesque churches, built from the 11th century onwards, were characterized by massive masonry walls, squat towers, and the extensive use of tuff stone in the earliest phases. With the advent of Gothic architecture between the 13th and 15th centuries, more elaborate spatial configurations emerged, including ribbed, cross, and net vaults, often combined with tall nave structures and slender buttresses. In the northern provinces, particularly in Groningen and Friesland, the scarcity of natural stone encouraged the widespread adoption of fired clay brick, resulting in distinctive large-scale brick churches whose aesthetic and structural expression differs markedly from the stone-built Gothic of Brabant in the south (Abrahamse et al., 2009; Brown, 2013). Many of these churches underwent multiple construction and modification phases over several centuries, leading to heterogeneous structural configurations where Romanesque elements coexist with later Gothic or post-medieval additions.

Beyond their architectural evolution, these churches also embodied a strong cultural and symbolic dimension. As highlighted by (Kroesen, 2021), medieval churches in the Northern Netherlands functioned as "storytelling spaces," where biblical narratives and theological concepts were materially inscribed into the architecture, decoration, and liturgical furnishings. This cultural role reinforces the dual significance of these

monuments: they are not only engineering artefacts but also vehicles of collective memory and identity that demand preservation.

From the late medieval to the early modern period, Dutch ecclesiastical architecture incorporated Renaissance and later Neoclassical elements, yet the defining structural typologies of the northern provinces remained strongly tied to multi-leaf brick masonry walls and, in later centuries, cavity-wall systems. Vaulting systems also displayed considerable variety: while cross vaults were common in main naves and chancels, many Groningen churches feature starred or net vaults with complex bond patterns, whose rib systems in stone or brick had a genuine loadbearing function (Bacigalupo et al., 2012; Wendland, 2005). Foundations were typically shallow, often consisting of brick or tuff courses on sand or gravel layers, an expedient solution in soft clay soils that, however, contributes to long-term settlement issues (Barends, 2002). These construction choices, while effective under gravity loading, resulted in limited robustness against differential settlements and imposed horizontal actions.

Structurally, these churches present vulnerabilities intrinsic to their material and construction techniques. The relatively weak lime mortars and the presence of multi-leaf or cavity-wall assemblages result in poor interleaf connectivity and susceptibility to moisture-induced damage (Van Der Pluijm, 1997). Vaults, while historically celebrated for their aesthetic and liturgical symbolism, often act as non-structural components with limited lateral resistance, making them highly vulnerable under seismic excitation. Furthermore, buttresses and towers were frequently not adequately bonded to adjacent walls, creating discontinuities that exacerbate seismic fragility (Lourenço & Silva, 2020). These characteristics, combined with centuries of environmental exposure, explain the progressive cracking and deformation observed in many of these structures.

More recently, the changing role of rural sacral buildings in Groningen has added an additional dimension to their preservation. As noted by (Arno, 2021), many of these churches, particularly in depopulating rural areas, have been repurposed for cultural or social functions, raising new challenges for their adaptive reuse while maintaining their historical and symbolic integrity. This trend further emphasizes the importance of safeguarding their structural stability, as their continued use in modern society depends on ensuring both safety and heritage value.

The recent challenge of induced seismicity in Groningen, caused by decades of natural gas extraction, has brought renewed urgency to the assessment of such monuments (Bommer & van Elk, 2017; Moratti et al., 2019). Although designed in regions with no

tradition of seismic design, these churches now face recurrent low-magnitude earthquakes, which amplify pre-existing vulnerabilities and threaten the preservation of an irreplaceable cultural heritage. Their conservation requires not only advanced numerical modelling and structural assessment, but also a careful balance between safety, authenticity, and cultural value.

3 APPLIED ELEMENT METHOD AND ITS APPLICATION

The Applied Element Method (AEM) has emerged over the past decades as one of the most versatile numerical tools for the simulation of structural behaviour up to collapse. Unlike conventional continuum-based approaches, AEM enables the explicit representation of cracking, separation, contact, and debris interaction, thereby bridging the gap between finite element formulations and discrete element methods. Its progressive development stems from earlier discrete modelling techniques, such as the Rigid Body Spring Model (RBSM) and the Modified Distinct Element Method (MDEM), which introduced fundamental concepts later refined into the full AEM framework.

Section 3.1, a literature review traces the evolution of discrete modelling approaches, outlining how the limitations of RBSM and MDEM motivated the formulation of AEM and highlighting the key innovations that distinguish it from other numerical strategies.

Section 3.2 discusses how the method has been employed to investigate the behaviour of masonry structures under various loading conditions. Particular attention is given to its validation against experimental data, ranging from small-scale wallet tests to full-scale shake-table experiments, and to its application in the seismic assessment of historical buildings. The review also emphasizes AEM's ability to capture both in-plane and out-of-plane mechanisms, as well as its extension to non-seismic scenarios such as blast loading.

By providing both the theoretical background and a synthesis of practical applications, this chapter aims to demonstrate the methodological foundations and the proven effectiveness of AEM, thereby setting the stage for its use in the present research on the seismic assessment and strengthening of masonry vaults.

3.1 LITERATURE REVIEW ON THE ORIGINS OF THE APPLIED ELEMENT METHOD

3.1.1 Rigid Body Spring Method

The origins of the Applied Element Method (AEM) can be traced back to the pioneering work of Tadahiko Kawai in the late 1970s. In particular, (Kawai, 1977) introduced a novel discrete element formulation in which the solid body was idealized as a rigid system (3D), and the interaction between rigid bodies was represented by springs. This concept constitutes the fundamental basis of AEM. The method was developed in parallel with

the Distinct Element Method (DEM), introduced in the early 1970s by (Cundall & Strack, 1979). The essential difference lies in the way interactions are treated: in DEM, elements are not connected by springs, but rather interact through repulsive forces generated upon contact, whereas in Kawai's approach, continuity is immediately introduced through predefined springs. While DEM proved highly effective in geotechnical applications, its computational demand for structural and civil engineering problems was excessive. For this reason, Kawai proposed the new formulation, which became known as the Rigid Body Spring Method (RBSM).

The similarity with DEM lies in the fact that discrete rigid bodies interact through springs at their contact points. The displacement field of each rigid body is defined with respect to its centroid, while the displacements of points on the body's surface are calculated as functions of the centroidal displacement. A distinctive feature of this method is that the initial contact spring includes two components, normal and tangential, defined with respect to the local contact plane. When two bodies come into contact, the contact surface must be defined; however, in AEM, this limitation is removed. From the displacement field, the strain energy of the springs can be expressed as a function of the relative displacements at the contact points and the corresponding normal and tangential stiffness. Applying Castigliano's theorem, a symmetric 12×12 stiffness matrix can then be derived.

The early RBSM formulation did not explicitly address material or geometric nonlinearities, and the normal and tangential stiffnesses were introduced as scalar values. Nonetheless, this was a significant step forward, as it provided a physically transparent model in contrast to the highly complex mathematical formulations of that period. Importantly, it offered the ability to represent fracture and separation phenomena, features not easily achievable in the Finite Element Method (FEM) without prohibitive computational costs. To this end, rotational stiffness was also introduced at the contact points, so that the overall stiffness was concentrated in a single contact location defined by three springs: axial, shear, and rotational.

In (Kawai, 1978), the method was further developed for seismic response analysis. Furthermore, Kawai proposed the development of different elements; a beam-column element, similar to a modern rigid link, was introduced by concentrating the member's behaviour into a rotational spring, significantly reducing computational effort through stiffness condensation, which was of great importance in the 1970s due to limited computing power. Similarly, plate elements were modelled using triangular elements connected by distributed rotational springs. In all cases, the degrees of freedom were

assigned to the rigid body centroids, independent of the number of springs introduced, ensuring that increasing the number of springs refined the stiffness distribution without enlarging the global system size. This property laid the foundation for the computational efficiency of AEM.

Another contribution, (Kawai, 1980), provided a critical assessment of FEM in specific contexts, such as geotechnical problems. It was highlighted that FEM, being grounded in continuum mechanics, was not well suited for problems involving fracture initiation and propagation, where discrete approaches were more effective. Although the comparison should have been made primarily with DEM, these critiques were justified. RBSM positioned itself as an intermediate approach between FEM and DEM, enabling the solution of both structural and geotechnical problems within a unified framework.

During the early 1980s, further developments were introduced in (Kawai & Toi, 1983), where nonlinear springs were incorporated for contact problems: axial springs worked only in compression, while shear springs were governed by purely frictional resistance. Nonlinear displacement fields were also introduced, analogously to FEM, together with a geometric stiffness matrix to account for geometric nonlinearities and to allow eigenvalue analysis for critical load multipliers in buckling problems.

One of the final developments of this method appeared in (Kikuchi et al., 1992), focusing on fracture mechanics. The innovative aspect was the management of springs during failure: when the deformation of a spring exceeded its ultimate strain, its stiffness was reduced to zero in all components, effectively modelling crack propagation. Incremental load-control analyses using the Newton-Raphson method were performed, alongside explicit dynamic simulations inspired by DEM formulations. Damping matrices were defined proportionally to stiffness. Distinctive modelling choices, such as very small time steps in explicit analyses, were required. Comparisons were also made between different failure criteria, such as Mohr-Coulomb and von Mises.

Finally, later studies further refined the method (Bolander et al., 1999). Building on RBSM concepts, these works introduced the use of Voronoi diagrams for mesh generation, enabling automatic and optimised (though random) partitioning of the model into irregular blocks. Each block, regardless of its shape or size, was connected by a triplet of springs (axial, tangential, rotational) defined from material elasticity, thickness, contact surface length, and centroid-to-centroid distances. The challenge remained in evaluating internal forces for irregularly shaped blocks, which was addressed by computing resultant forces at each centroid as the summation of edge contributions.

3.1.2 Modified Distinct Element Method

A further advancement in discrete approaches was introduced by (Meguro & Hakuno, 1989). This work represented a turning point, linking earlier formulations with what would later become the Applied Element Method (AEM). Meguro, together with Tagel-Din, is considered one of the founders of AEM, and the influence of RBSM on their work is evident.

The Modified Distinct Element Method (MDEM) was conceived by adapting DEM, which had originally been developed for geotechnical applications, in order to extend its applicability to reinforced concrete and masonry structures. In this formulation, the body was discretized into inert particles to which mortar was added, thus making it possible to model cementitious and masonry materials. The resulting system incorporated two sets of springs, two normal and two tangential, to simulate the mechanical behaviour of the two constituent materials (blocks and mortar). Unlike RBSM, where springs were introduced at contact points with explicit rotational components, in MDEM the springs worked in tension, compression, and shear, but the rotational spring was eliminated as superfluous.

Conceptually, the method positioned itself between FEM and DEM, Figure 3.1. In FEM, the continuum is represented as a fully connected and homogeneous system, where all particles are continuously linked. In DEM, by contrast, particles are modelled as fully detached and independent, interacting only when they come into contact. MDEM offered an intermediate formulation: particles were initially connected to one another (though not necessarily homogeneously), while still allowing for contact interactions. Importantly, fracture mechanisms could be directly represented: when a tensile or shear limit was reached, the springs lost their tensile resistance, allowing relative displacements and collisions among discrete bodies. This capability represented a significant step towards modelling fracture propagation in quasi-brittle materials such as concrete and masonry.

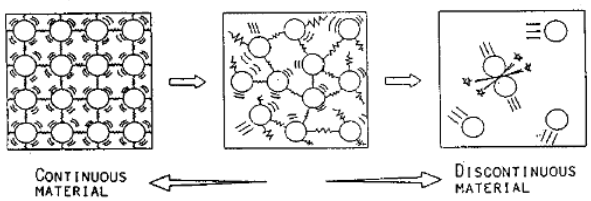

Figure 3.1 Behaviour of MDEM or EDEM, Extended Distinct Element Method, *(MEGURO et al., 1991)*

As in DEM, explicit dynamic integration was employed. The forces acting on each element were computed by accounting for all contact interactions, but accurate calculation of reaction forces required that the stress wave within each element remained sufficiently small relative to the selected time step. To ensure stability, a simplified estimate of the critical time step Δt was proposed (1):

$$\Delta t < \frac{D_{min}}{V} \quad \textbf{(1)}$$

where V is the stress wave propagation velocity and D_{min} is the minimum distance between the centroids of two elements.

The final significant contribution was (Meguro & Hakuno, 1994), in which MDEM was applied to structural collapse analyses. The method was first validated on simple problems, such as beams under concentrated loads, and subsequently extended to real-scale structural cases, including bridge collapse simulations.

3.1.3 FEM, DEM, and AEM brief comparison

Before addressing the specific developments of the Applied Element Method, it is useful to briefly contrast its formulation with the two dominant numerical strategies in structural analysis, namely the Finite Element Method (FEM) and the Discrete Element Method (DEM). Such a comparison highlights the respective advantages and limitations of each approach, clarifying the context in which AEM was conceived and the reasons for its increasing adoption in the analysis of masonry structures.

The Finite Element Method (FEM) represents the most established and widely adopted numerical tool in structural engineering, rigorously derived from continuum mechanics. It is particularly effective in describing deformable continua, where stresses and strains must be resolved with high precision, and has proven reliability for both linear and nonlinear analyses in elastic and plastic regimes. FEM's major strengths lie in its versatility for complex geometries and multi-physics coupling. However, when applied to brittle materials such as masonry, FEM faces intrinsic challenges: cracks must often be introduced via special interface elements or cohesive laws, and element separation requires user-defined fracture paths. This makes it difficult to capture the spontaneous initiation and evolution of fractures, as well as progressive collapse, without introducing significant complexity and computational cost.

The Discrete Element Method (DEM), initially developed by (Cundall & Strack, 1979), takes the opposite standpoint: it represents materials as an assembly of rigid particles

that can move independently, with interactions governed by contact laws, friction, and restitution. This allows DEM to naturally model discontinuities, fragmentation, and large displacements, making it extremely powerful for particulate systems such as soils, rocks, powders, and rubble. DEM has been successfully applied to simulate phenomena such as flow, compaction, crushing, and segregation. Its limitations, however, become evident when applied to structural continua: because every unit must be represented as a discrete particle, the number of elements required to model a realistic structure becomes prohibitively high, and calibration of contact parameters is not straightforward. Moreover, DEM does not explicitly provide a global stiffness matrix, which can complicate static or quasi-static analyses.

Situated between these two paradigms, the Applied Element Method (AEM) combines the strengths of FEM and DEM in a unified framework. In AEM, structures are divided into small elements connected by normal and shear springs distributed along their interfaces. These springs transfer stresses and strains, and are progressively removed when separation strains are reached, allowing cracks to initiate, propagate, and coalesce automatically. When detached elements collide, new contact springs are generated without requiring predefined crack paths or user intervention. This formulation enables AEM to follow the entire collapse sequence of a structure: from elastic behaviour, through cracking and reinforcement yielding, to large displacements, collisions, and debris interaction. Compared to FEM, AEM provides a more natural representation of discontinuities and progressive collapse; compared to DEM, it is computationally more efficient for large structures because it preserves a global stiffness matrix while still allowing discrete interactions. These characteristics have led to its growing use in the analysis of unreinforced masonry (URM), where both continuum behaviour (e.g., elastic stiffness, in-plane shear cracking) and discrete phenomena (e.g., out-of-plane rocking, wall detachment, debris generation) must be considered simultaneously (Matuttis & Chen, 2014; Meguro & Tagel-Din, 2000)

The contrasting strengths and weaknesses of FEM and DEM thus revealed the need for a more versatile methodology. The Applied Element Method emerged precisely in this context, conceived as a hybrid approach able to combine continuum accuracy with discrete interaction modelling, and thereby enabling the realistic simulation of structural collapse. The following section reviews in detail the formulation and subsequent developments of AEM, emphasizing its theoretical foundations and its progressive validation in the context of masonry structures.

3.1.4 Applied Element Method

The first work laying the foundations of the Applied Element Method (AEM), although the name was not yet used, was (Kimiro Meguro & Tagel-Din, 1997), the method's actual founders. This study introduced all the key theoretical aspects that later defined AEM.

The central innovation was the discretisation of the structure into rigid blocks, with degrees of freedom concentrated at their centroids rather than at individual particles. The deformability of the system was not assigned to the rigid blocks themselves, but to a set of springs distributed over the contact surfaces between adjacent blocks. Unlike RBSM, which employed a single spring at the centroid of the contact, AEM introduced a bed of springs along the entire interface, each spring associated with an influence area extending from centroid to centroid. These springs acted axially and in shear, capturing both deformation and damage.

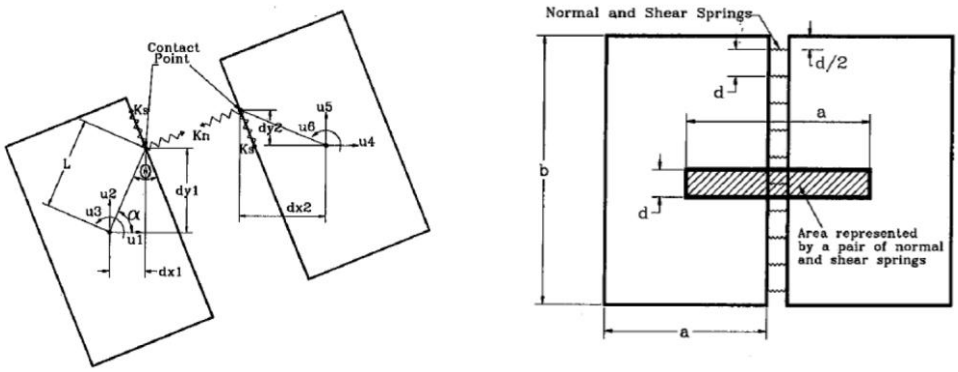

(a) (b)

Figure 3.2 (a) Element shape, contact point and degrees of freedom for two elements. (b) Spring distribution and area of influence of each spring, (K Meguro & Tagel-Din, 1997)

In two-dimensional systems, each element is characterized by three degrees of freedom, which results in a 6×6 stiffness matrix for each spring. A crucial innovation lies in the fact that the number of springs on the contact surface does not affect the size of the global stiffness matrix, since the degrees of freedom are assigned exclusively to the rigid bodies. From a computational perspective, this is of paramount importance: increasing the number of springs improves the accuracy of the solution without significantly increasing computational demand. Indeed, one of the most expensive operations in structural analysis is the inversion of the global stiffness matrix, an operation that is not easily parallelized. By contrast, calculations at the spring level

(deformations, stresses, etc.) are easily parallelized, so increasing their number does not cause prohibitive computational costs.

The stiffness matrix is constructed from two stiffness values (normal and tangential), together with the distance between the centroid of each element and the spring's contact point. In the initial algorithm proposed by Meguro and Tagel-Din, geometric nonlinearity was not explicitly considered, no Newton–Raphson iterations were performed, and singularity of the stiffness matrix was admitted, leading to a form of "numerical collapse."

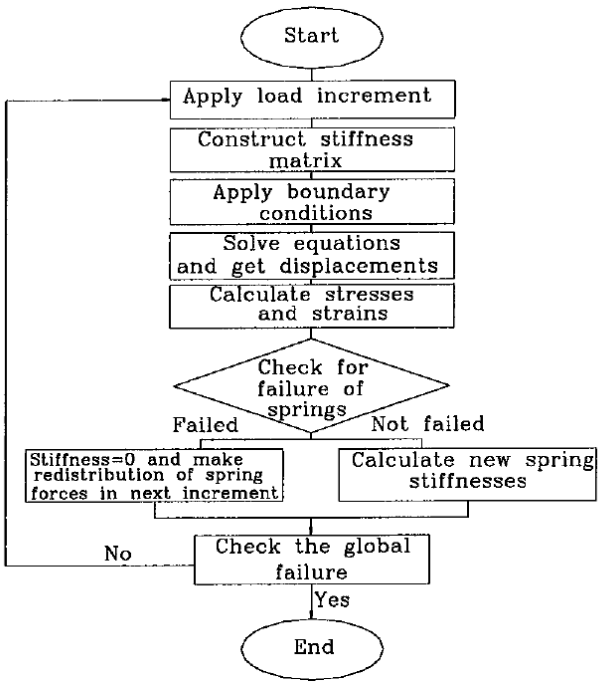

Figure 3.3 Flow of analysis (Kimiro Meguro & Tagel-Din, 1997)

The constitutive laws implemented were linear elastic up to rupture for tension; plastic behaviour up to a maximum stress, beyond which failure occurs, in compression; and, for shear linear behaviour up to a limiting value, followed by residual shear strength, Figure 3.4.

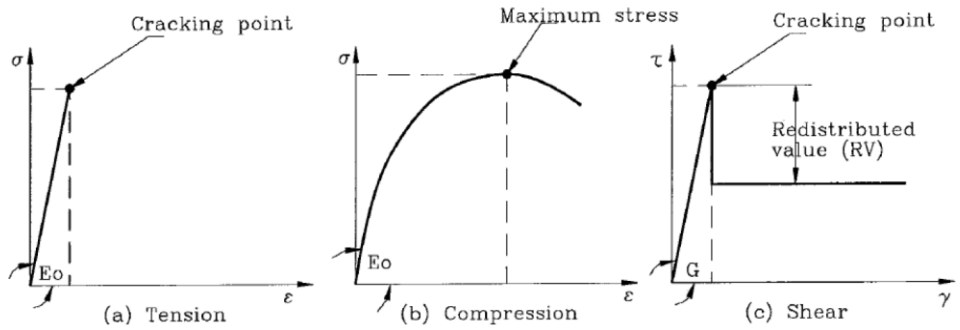

Figure 3.4 (a) Tension, (b) compression and (c) shear models for concrete (Kimiro Meguro & Tagel-Din, 1997)

(Meguro & Tagel-Din, 1999) marked the first use of the term AEM. While the underlying approach remained unchanged, the authors extended the formulation to address geometric nonlinearity. Unlike RBSM, where geometric stiffness was introduced, AEM accounted for nonlinear geometry through residual force vectors (2):

$$[K][\Delta U] = \Delta f + R_m + R_G \quad \textbf{(2)}$$

- R_m: residual forces arising from material failure (spring rupture),
- R_G: residual forces arising from geometric deformation (change of spring orientation during the analysis).

The procedure for computing these vectors was described in detail, with particular emphasis on updating R_G to capture the reorientation of springs as the structure deforms.

Several methodological observations were highlighted:

1. To trigger structural instability, model symmetry must be artificially broken, either by introducing small load perturbations or by varying material properties in selected zones, an approach analogous to FEM, where small imperfections are required to capture buckling;
2. At each incremental step, the small deformation theory was applied; therefore, load increments had to remain sufficiently small. This condition was valid for both static and dynamic analyses.

In (Tagel-Din & Meguro, 1999), the authors refined the treatment of contact mechanics. Borrowing from DEM, they introduced collision springs: when the centroids of two previously unconnected particles moved closer than a threshold distance, additional

normal and shear collision springs were created to generate contact forces. These collision springs differed fundamentally from the pre-existing interface springs: interface springs were oriented perpendicular to the element face; collision springs directly connected the centroids of approaching blocks, independently of their geometry (geometry being relevant only for centroidal distance).

The authors also introduced an energy dissipation mechanism through a restitution coefficient, which defined the loss of energy upon impact. Unlike interface springs, collision springs could not "break" but disappeared once separation occurred. Importantly, AEM analyses could employ implicit dynamic integration, which was less computationally demanding than DEM's fully explicit schemes.

In the subsequent contribution (Tagel-Din & Meguro, 2000a), the framework was consolidated by defining the mass matrix, adopting a damping matrix proportional to mass (in contrast with RBSM, where damping was proportional to stiffness), and combining both static and dynamic formulations under the same methodology.

Overall, AEM introduced a paradigm shift: it allowed large displacement and collapse simulations, with explicit representation of crack patterns, failure mechanisms, and debris fields. This capability was particularly revolutionary for masonry structures, where both in-plane and out-of-plane responses could be modelled until complete collapse.

An essential aspect of the dynamic formulation concerns the representation of energy dissipation, which in AEM is treated differently from conventional numerical approaches. The following subsection describes how damping and energy loss are inherently reproduced within the AEM framework.

3.1.4.1 Energy dissipation and damping in AEM

In the original formulation of the Applied Element Method (AEM), no explicit viscous or Rayleigh damping term is introduced in the governing equations of motion. Energy dissipation naturally arises from the intrinsic mechanisms of the method itself: the progressive cracking and separation of normal and shear springs, the inelastic impact between adjacent elements, and the frictional interaction along contact surfaces. As these nonlinear processes develop, part of the system's strain and kinetic energy is irreversibly lost, reproducing the damping effect observed experimentally in real structures (K Meguro & Tagel-Din, 1997; Tagel-Din & Meguro, 2000b).

The absence of artificial damping makes AEM fundamentally different from traditional finite-element approaches, where Rayleigh damping is often required to approximate unmodelled hysteretic or frictional losses. In AEM, such mechanisms are explicitly captured by the cracking and contact formulations, providing a physically consistent description of energy degradation during dynamic loading and collapse. For purely numerical stability purposes, a small mass-proportional term or a restitution coefficient may occasionally be introduced, but these parameters serve only to suppress high-frequency oscillations and do not represent real material dissipation (Applied Science International, 2024a).

3.1.4.2 Extreme Loading for Structures

The Extreme Loading® for Structures (ELS) software, developed by Applied Science International (ASI), is the main commercial implementation of the Applied Element Method (AEM). The following overview is primarily based on the (Applied Science International, 2024b)

ELS allows users to model structures as an assembly of rigid elements connected by normal and shear springs distributed along their interfaces, automatically capturing crack initiation, propagation, separation, and collision phenomena without requiring predefined failure surfaces or special interface elements. A key strength of the software lies in its ability to simulate the entire sequence of structural behaviour under extreme events, from the elastic stage, through cracking and yielding, up to large deformations, collapse, and debris interaction. This makes it particularly suitable for the analysis of progressive collapse, seismic performance, blast effects, and impact loading, where both continuum and discrete behaviours must be reproduced within the same computational framework.

The rationale for the development of ELS stems from the need to address these dual behavioural stages. Structures subjected to extreme loading conditions inevitably transition from a continuum phase, characterized by elastic response, cracking, and yielding, to a discrete phase, involving element separation, debris motion, and collisions. Conventional FEM cannot accurately capture this transition, while DEM lacks the ability to reproduce the continuum stage. By contrast, AEM as implemented in ELS was specifically conceived to overcome these limitations, enabling analysts to address critical questions such as whether collapse will occur, whether it will be partial or total, how long the process will last, what debris patterns will form, and how adjacent structures will be affected.

In addition, ELS incorporates a wide range of material constitutive laws, including reinforced concrete, masonry, steel, and composites, together with nonlinear static and dynamic solvers, enabling collapse simulations that extend beyond the capacity of conventional FEM tools.

3.1.4.3 Material modelling

Extreme Loading for Structures allows the employment of both standard and user-defined constitutive models. The response of concrete under uniaxial cyclic tension–compression loading can be simulated by (Okamura & Maekawa, 1983) model, Figure 3.5a. This constitutive law is limited to one-dimensional stress states and does not take into account for confinement effects due to the reinforcement layout. To overcome this issue, a user-defined material can be calibrated. A simplified Mohr–Coulomb constitutive model is typically adopted for shear-compression stress states, Figure 3.5b. This formulation captures the initial shear resistance, expressed through cohesive and frictional components, and reproduces a brittle degradation of strength. However, a progressive softening law based on a linear degradation of cohesion, including the contribution of shear fracture energy, is not implemented. Instead, interface springs are completely separated once a user-defined threshold strain, referred to as separation strain, is reached. Axially loaded reinforcement springs can be assigned the hysteretic model proposed by (Menegotto & Pinto, 1973), shown in Figure 3.5c. Failure of the reinforcement occurs either when a target strain (separation strain) is exceeded or when the Euclidean norm of the surface traction vector reaches the ultimate strength f_u. The tangent stiffness of the reinforcement is evaluated as a function of the spring strain, loading or unloading state, and loading history, thereby allowing the Bauschinger effect to be captured.

Under the above assumptions, failure mechanisms such as reinforcement buckling and concrete spalling are neglected. Nevertheless, shear transfer between reinforced concrete components and shear softening behaviour can be adequately represented within the adopted modelling framework.

In the post-cracking stage, elastic parameters are progressively modified according to the implemented constitutive laws by updating the stiffness and strength of the interface springs at each load increment, thus accounting for damage evolution.

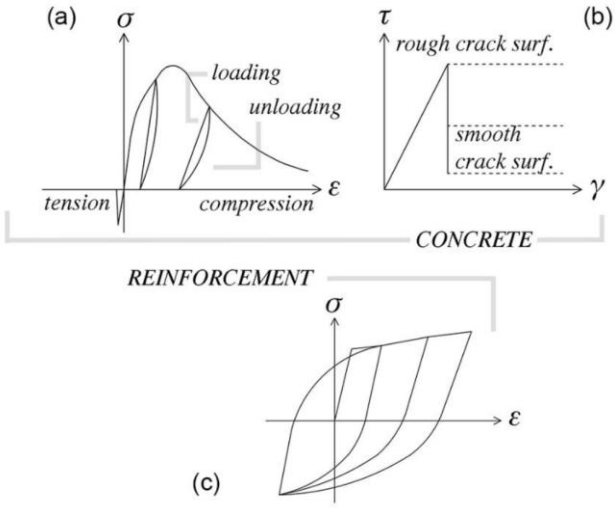

Figure 3.5 AEM constitutive laws for concrete (Malomo et al., 2020a)

3.2 AEM APPLICATION TO MASONRY STRUCTURES

One of the earliest systematic applications of the Applied Element Method (AEM) to masonry structures was presented by (Pandey & Meguro, 2004), who investigated the in-plane lateral response of clay brick walls. Their formulation, which discretized masonry into rigid blocks connected by springs along mortar interfaces, was able to reproduce experimentally observed mechanisms such as diagonal cracking, stepped failure, and joint sliding. This pioneering work highlighted AEM's potential to capture both local and global shear–sliding responses. Further developments were provided by (Guragain et al., 2007), who simulated the cyclic response of brick masonry walls. Despite employing simplified joint assumptions, the numerical models reproduced the progressive stiffness degradation and crack propagation observed in laboratory tests, confirming the suitability of AEM for assessing the seismic vulnerability of masonry components under repeated in-plane loading. More recently, (Malomo et al., 2020c) extended the method to the shake-table simulation of full-scale unreinforced masonry cavity-wall buildings. Using a simplified micro-modelling strategy, they showed that AEM could reproduce the global seismic response of complete systems up to near-collapse, with satisfactory accuracy in terms of hysteretic behaviour and crack patterns.

The capability of AEM to address out-of-plane response has also been demonstrated. (Sathiparan et al., 2005) showed through combined in-plane and out-of-plane tests that

while unreinforced masonry panels failed abruptly after first cracking, retrofitted specimens retained residual strength and ductility, behaviours that AEM is able to capture through progressive element separation. At the building scale, (Karbassi & Nollet, 2013) applied AEM to a six-storey URM structure, showing that both in-plane degradation and out-of-plane mechanisms such as rocking and wall detachment could be simulated within a performance-based seismic evaluation framework. Likewise, (Malomo et al., 2020b) validated AEM against shake-table tests on full-scale single-leaf and cavity walls, confirming its ability to reproduce crack initiation, bending mechanisms, and collapse patterns under different boundary conditions. Beyond the seismic field, (Keys & Clubley, 2017) demonstrated the versatility of AEM in simulating fragmentation, panel separation, and debris ejection of masonry subjected to blast loading, reinforcing its general applicability to extreme out-of-plane actions.

A further notable large-scale application of AEM is the forensic investigation of the collapse of the Morandi Bridge in Genoa (2018). In this study, (Calvi et al., 2019) employed the commercial implementation of AEM, Extreme Loading for Structures (ELS), to explore possible collapse mechanisms of the viaduct. The simulations reproduced different scenarios of progressive failure, including deterioration of stays, local deck failures, and the sudden loss of stay–deck or stay–antenna connections. Among the tested hypotheses, the latter produced collapse sequences and debris distributions that closely matched post-event evidence. This work showcased the ability of AEM/ELS not only to capture complex dynamic interactions and debris generation, but also to provide valuable insights for forensic engineering investigations of large infrastructure failures, extending the method's scope beyond conventional seismic or blast scenarios.

In parallel, several studies have employed AEM for the seismic assessment of large-scale historical buildings. (Garofano & Lestuzzi, 2016) employed a detailed three-dimensional AEM model to assess the seismic safety of the Ancien Hôpital de Sion in Switzerland, highlighting the method's ability to reproduce complex behaviours and potential collapse mechanisms of heritage masonry. Similarly, (Karbassi & Lestuzzi, 2012) developed a numerical-based methodology for the fragility analysis of existing unreinforced masonry (URM) buildings, where AEM proved particularly effective in capturing both in-plane and out-of-plane damage modes within nonlinear dynamic simulations. These building-scale applications are reinforced by complementary studies focusing on debris assessment and experimental validation. (Domaneschi et al., 2019) introduced a simplified approach to quantify seismic debris generated by masonry collapses, supported by AEM-based parametric simulations calibrated against

shaking table experiments. At a smaller scale, (Sathiparan et al., 2012) performed one-quarter scale shake-table tests on URM houses retrofitted with polypropylene band meshes, demonstrating an agreement between experimental observations and AEM predictions of damage patterns and collapse sequences. At the full-scale level, (Malomo et al., 2020a) applied AEM to the dynamic response of a clay brick masonry building with flexible diaphragms, confirming the method's capability to reproduce crack initiation, hysteretic response, and collapse modes under seismic excitation.

Taken together, these contributions demonstrate that AEM is a robust and versatile framework for the seismic analysis of unreinforced masonry, capable of simulating progressive collapse, debris generation, and both in-plane and out-of-plane mechanisms across multiple scales, from small wallets to full-scale historical buildings, and under diverse loading conditions, including seismic and blast actions.

A recent critical appraisal by (Malomo & Pulatsu, 2024) further consolidates the role of AEM within the broader family of discontinuum approaches for masonry analysis. In their comprehensive review, the method is identified as one of the most mature and widely adopted discontinuum-based strategies for the structural and seismic assessment of unreinforced masonry. The authors emphasize AEM's capability to explicitly simulate progressive damage, contact loss, large displacements, and complete separation between structural components, features that are particularly suited to the inherently discontinuous nature of masonry assemblies. The effectiveness of the methodology is confirmed at different scales, from the detailed micro-modelling of walls to full three-dimensional buildings, demonstrating its capability to reproduce in-plane cycling degradation and out-of-plane collapse mechanisms. In addition to the main advantages of the AEM, the authors also highlight the issues that are still unsolved, such as the definition of appropriate damping schemes, sensitivity to discretisation strategies, and the calibration of the equivalent mechanical input parameters.

4 AEM MESO-MODELLING APPROACH AND ITS VALIDATION ON VAULTS

This chapter presents a pragmatic meso-modelling framework for unreinforced masonry (URM) within the Applied Element Method (AEM), together with its validation against established numerical strategies and experimental evidence.

Section 4.1 introduces the meso-scale approach: masonry is homogenized into larger rigid blocks connected by interface springs whose elastic and inelastic properties are obtained through upscaling relations. The section summarizes the constitutive ingredients (tension, compression and shear under cyclic loading) and highlights how the scheme preserves key deformation and failure mechanisms while remaining computationally tractable for large historic systems.

Section 4.2 validates the proposed approach by comparing AEM predictions with those from an Equivalent Frame Method (EFM, macro-FEM) and a Discrete Element Method (DEM, micro-model) on two representative church façades from the Phase-3 portfolio. The comparison focuses on initial stiffness, peak strength, post-peak response, and failure modes, and includes a mesh-sensitivity study (0.4 m vs 0.3 m block sizes). The results motivate AEM as an effective compromise between DEM's kinematic fidelity and EFM's efficiency, suitable for near-collapse and collapse simulations at realistic computational cost.

Section 4.3 provides an experimental validation based on the LNEC shaking-table campaign on cross-vaults, extensively building on the article (Cogliano et al., 2025a). The section outlines specimen geometry, identification tests, model calibration (including the role of separation strain), and nonlinear time-history analyses, and discusses agreement between simulated and observed damage patterns, modal properties, and response histories.

4.1 MESO-MODELLING APPROACH

To address the prohibitive computational demand of detailed micro-modelling in large unreinforced masonry (URM) structures, a meso-scale modelling scheme has been developed within the Applied Element Method (AEM) framework.

In classical micro-modelling, each brick is represented as a rigid unit connected by zero-thickness interface springs, which reproduce the deformability and nonlinear behaviour of mortar joints. This strategy provides high fidelity in simulating tensile, compressive, and shear failures, enabling accurate reproduction of crack patterns and progressive disintegration. However, its applicability to full-scale structures, such as historical churches, is severely limited by the enormous number of degrees of freedom required.

The meso-scale strategy mitigates this limitation by homogenizing masonry into larger square rigid blocks, each representing an equivalent assemblage of several bricks and mortar joints. Equivalent stiffness and strength properties are then assigned to the interface springs through homogenization and scaling procedures, consistent with masonry parameters defined in (NEN, 2020).

For a masonry texture characterized by brick height h_b, elastic modulus E_m, and shear modulus G_m, the equivalent elastic properties are expressed as:

$$E_{eq} = E_m \frac{h_b}{H_b}, G_{eq} = G_m \frac{h_b}{H_b} \quad (3)$$

Where H_b is the side length of the meso-block. The corresponding stiffnesses of the interface springs are obtained as

$$k_n = \frac{E_{eq} A}{H_b}, k_s = \frac{G_{eq} A}{H_b} \quad (4)$$

With A denoting the contact area between adjacent blocks. This upscaling technique, presented in (Davis et al., 2024), preserves the deformability of the original material while drastically reducing the computational effort, thus enabling the simulation of separation, impact, and re-contact phenomena intrinsic to AEM.

The cyclic behaviour of masonry is reproduced by assigning inelastic constitutive laws to the interface springs, Figure 4.1. In compression, degradation under cyclic uniaxial loading is described by a simplified elasto-plastic fracture formulation (El-Kashif & Maekawa, 2004), whereas tensile behaviour follows a bilinear law with linear softening up to the ultimate strain capacity. In shear, a hysteretic Mohr–Coulomb model is

adopted, where cohesion drops to zero immediately after the peak shear resistance is attained. Local failures of individual springs progressively reduce the stiffness and strength at the element scale, leading to crack initiation and propagation. Ultimately, when all springs between two blocks have fully degraded (i.e., stiffness reduces to zero), complete loss of connection occurs.

This constitutive framework allows AEM at the meso-scale to reproduce progressive cracking, separation, and collapse mechanisms of masonry structures with significantly reduced computational cost, ensuring applicability to large-scale systems such as historical vaulted churches.

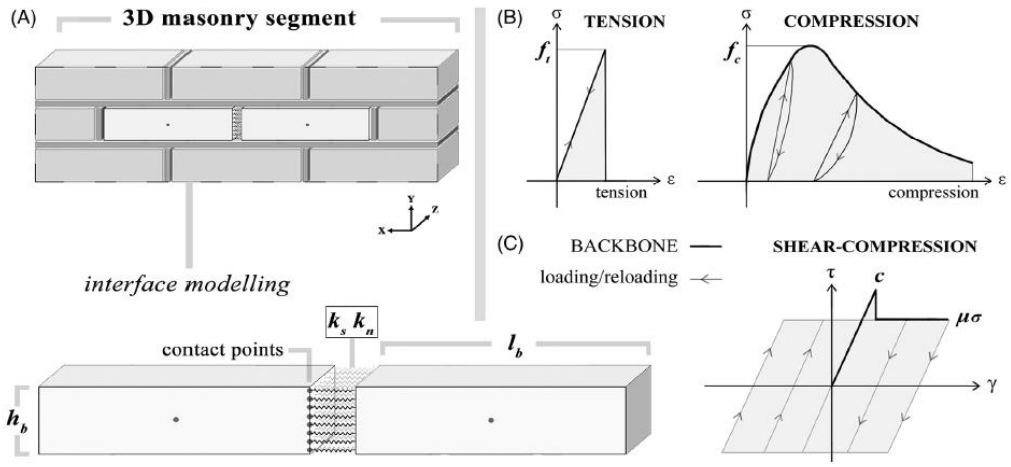

Figure 4.1 Discretisation of a masonry segment according to AEM (a), interface springs constitutive laws under normal (b) and shear (c) cyclic loading *(Davis et al., 2024)*.

An essential aspect of the dynamic formulation concerns the treatment of energy dissipation. In the present AEM-based meso-model, damping is not introduced explicitly but arises from the intrinsic nonlinear interactions among elements, as discussed in the following subsection.

4.1.1 Treatment of energy dissipation and damping in the proposed AEM-based meso-model

In the proposed meso-scale modelling strategy, no Rayleigh or viscous damping has been applied. The exclusion of any artificial damping ensures that the simulated dynamic response arises solely from the physical mechanisms explicitly represented within the AEM framework, rather than from numerically imposed attenuation. Energy

dissipation is instead governed by the intrinsic processes of the method, namely, cracking and separation of normal and shear springs, re-contact between detached elements, and frictional interactions along interfaces (K Meguro & Tagel-Din, 1997). These local nonlinearities inherently reproduce the hysteretic energy losses typically observed in experimental tests on masonry structures, providing a physically consistent representation of damping.

Nevertheless, during repeated contact interactions, perfectly elastic impacts between adjacent elements can induce spurious high-frequency oscillations that affect numerical stability. To mitigate this issue, the contact formulation includes a restitution coefficient slightly lower than unity (typically 0.9–0.95), as recommended in the Extreme Loading for Structures Theory Manual (Applied Science International, 2024a). This parameter reduces the post-impact velocity by a small fraction, emulating the natural inelasticity of real impacts. It is therefore introduced purely as a numerical stabilization tool within the explicit integration scheme, without influencing the overall energy balance or representing any form of material or structural damping.

4.2 Comparison of FEM, DEM and AEM

To validate the proposed meso-scale AEM approach, comparative analyses were carried out against Equivalent Frame Method (EFM, a macro-FEM strategy) and Discrete Element Method (DEM, micro-modelling) simulations on isolated URM wall sub-structures subjected to lateral pushover loading. two representative façades of churches investigated within the Phase 3 of the project discussed in Chapter 1.

As shown in Figure 4.2, the three modelling strategies produced comparable initial stiffnesses and peak base shear capacities. All predicted similar failure mechanisms, characterized by diagonal shear/flexure cracking in spandrels followed by flexural failure of slender piers. However, post-peak responses diverged:

- EFM exhibited a more abrupt strength degradation (−35% drop) and underestimated ultimate displacement capacity, confirming its limited applicability for collapse analysis.
- DEM and AEM showed consistent post-peak behaviour, providing reliable predictions of displacement capacity and collapse progression.

Computational efficiency was a decisive factor: the EFM simulation required ~4 minutes, AEM ~30 minutes, while DEM demanded ~6 hours, underscoring the advantage of the proposed meso-scale AEM in balancing accuracy and efficiency.

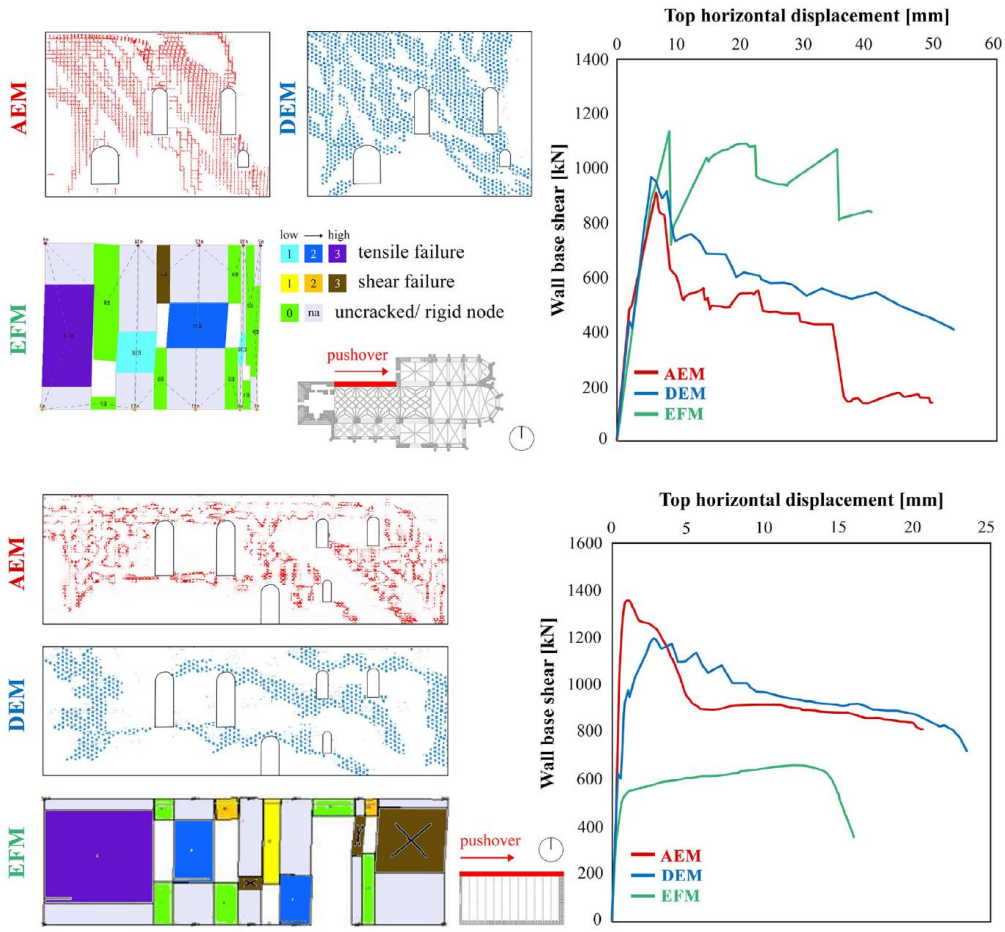

Figure 4.2 Damage and pushover curve comparisons between AEM, EFM, and DEM for two different walls *(Davis et al., 2024)*.

A further validation test compared AEM discretisation of 0.4 m × 0.4 m and 0.3 m × 0.3 m rigid blocks for another wall, Figure 4.3. Both discretisation reproduced similar crack patterns and base shear histories. The finer mesh (0.3 m) resulted in only slightly higher residual displacements (+15%), a variation deemed acceptable. This confirmed that the coarser 0.4 m discretisation can be employed without significant loss of accuracy, ensuring computational feasibility for large-scale church models.

In summary, while FEM is efficient but unsuitable for collapse analysis, and DEM is accurate but computationally prohibitive, the meso-scale AEM provides a pragmatic

compromise, capturing progressive cracking and collapse mechanisms at manageable computational cost.

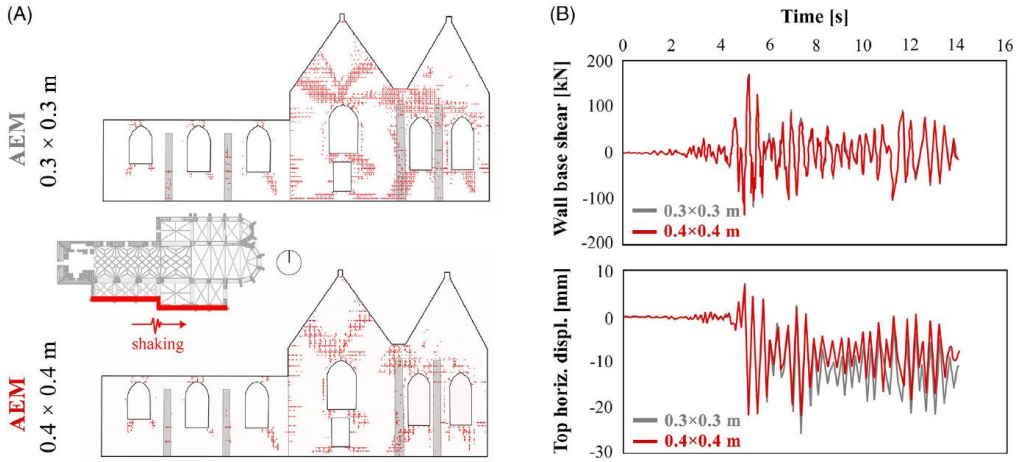

Figure 4.3 Comparison between (A) damage, (B) base-shear and displacement time histories predicted by AEM models with different block sizes *(Davis et al., 2024)*.

4.3 SIMULATION ON FULL-SCALED CROSS VAULTS AT LNEC SHAKING TABLE TEST

The experimental benchmark adopted in this study derives from the large-scale campaign carried out at the *Laboratório Nacional de Engenharia Civil* (LNEC) in Lisbon, 2021, deeply described in (Bianchini et al., 2024), within the framework of the SERA Project Blind Prediction (Bianchini et al., 2023). The main goal of the programme was to gain further insight into the seismic behaviour of masonry cross-vaults and to evaluate the predictive capacity of different numerical modelling strategies. Three specimens were tested: (i) a 1:5 scale vault assembled from 3D-printed blocks with dry joints, (ii) a full-scale unreinforced masonry cross-vault, and (iii) a full-scale vault retrofitted with textile reinforced mortar (TRM). The reduced-scale (1:5) experimental campaign, performed through both quasi-static and shake table tests (Bianchini et al., 2022), was conceived as a preparatory step for the subsequent full-scale testing at LNEC, providing essential insights into boundary conditions, failure mechanisms, and calibration data for numerical modelling. In this study, attention is restricted to the full-scale specimens; specifically, this chapter addresses the unstrengthened configuration, while the retrofitted case is discussed in Chapter 7.

4.3.1 Brief description of the experimental campaign

The vaulted specimen has a square plan dimension of approximately 3.5 m x 3.5 m, with a net span of 2.9 m and a rise of 0.8 m. The vault thickness is constant at 0.12 m. Structural supports include two masonry piers fully fixed at the base and two steel block of 0.84 x 0.84 m serving as additional masses, standing on movable supports. Three pairs of steel tie-rods link the four abutments in order to confine the whole specimen, Figure 4.4. The material properties are derived from tests on masonry wallets and reported in Table 4.1.

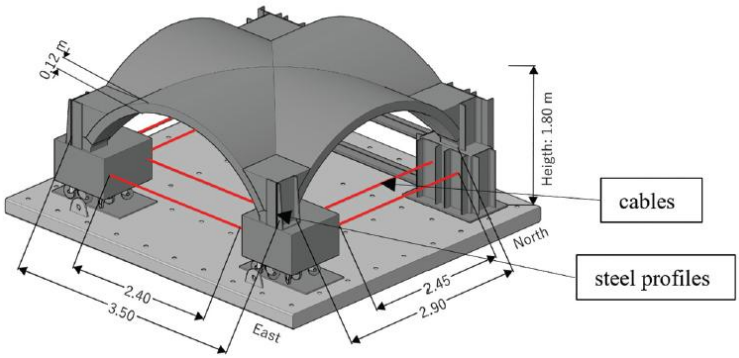

Figure 4.4 Geometrical model of the full-scale specimen *(Bianchini et al., 2023)*

Table 4.1. Summary of masonry and retrofitting mortar (TRM) mechanical properties.

Material	ρ [kg/m^3]	E [MPa]	G [MPa]	f_c [MPa]	f_t [MPa]	*cohesion* [MPa]	Φ [-]
Masonry	2255.2	2223.0	762.0	9.1	0.31	0.031	0.785
TRM	1870.0	16620.0	-	22.7	5.82	-	-

The monitoring system was equipped with displacement transducers, load cells, and piezoelectric accelerometers, which enabled the recording of structural response during both seismic simulations and dynamic identification tests. The overall layout of the instrumentation is illustrated in Figure 4.5.

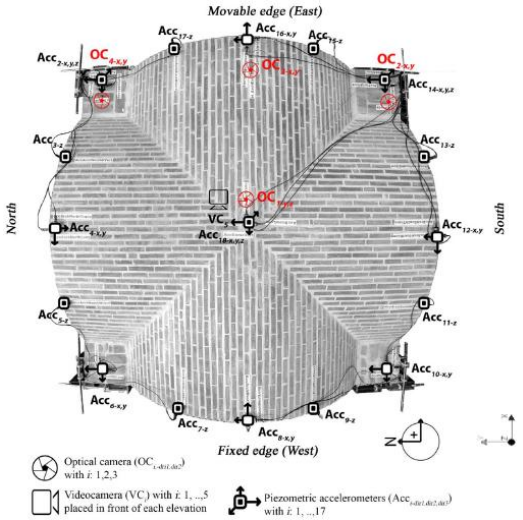

Figure 4.5 Instrumental setup of the unstrengthened specimen *(Bianchini et al., 2023)*

The record of L'Aquila earthquake, occurred on the 6th of April 2009 (also known as AQA signal), was adopted as seismic input for both the unreinforced and reinforced specimens. Only the North-South component of the acceleration time series was applied to the longitudinal direction of the specimen, which corresponds to the Y axis, North-South direction. The sequence consisted of a series of shaking table simulations with progressively increasing input amplitudes, Table 4.2, designed to account for damage accumulation under cyclic seismic demand.

Table 4.2. Summary of the sequential seismic test

Specimen	***% AQA Earthquake***						
Unstrengthened	10%	25%	50%	75%	Repairing and Strengthening		
Strengthened	-	25%	50%	75%	100%	125%	150%

Between consecutive shaking events, dynamic identification tests were performed to capture the evolution of the modal properties as degradation progressed. The initial identification test provided the undamaged reference condition, while subsequent measurements allowed for the tracking of frequency shifts associated with the propagation of cracks and stiffness loss.

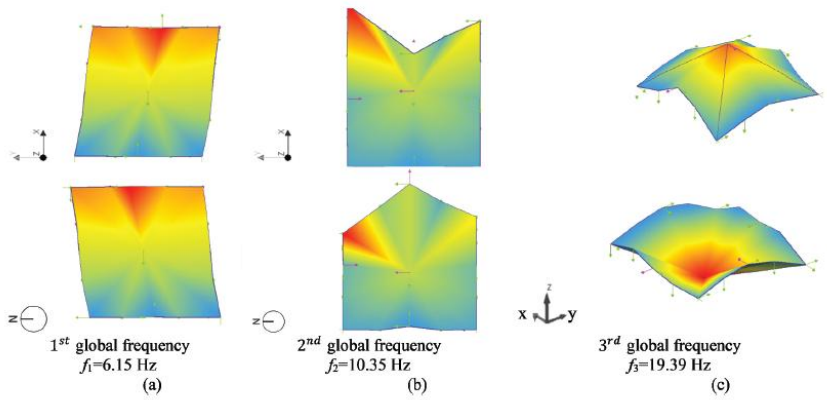

Figure 4.6 Natural frequencies and mode shapes of the unstrengthened specimen: (a) first global longitudinal mode; (b) second global transverse mode; (c) third global vertical mode *(Bianchini et al., 2023)*

4.3.2 Numerical modelling and preliminary validations

The meso-modelling approach is used to simulate the seismic response of the tested masonry cross-vault. Since this represents the first application of meso-modelling to a masonry vault, and given that the influence of mesh size relative to the vault dimensions is not yet established, the meso-modelling strategy is herein applied exclusively at the material level. In this framework, masonry is treated as a homogenized material, while still accounting for the actual size of the brick units. The numerical geometry is generated from AutoCAD drawings provided within the blind prediction, aiming to replicate the actual brick arrangement of the cross-vault, Figure 4.7, through the use of 8-node hexahedral elements, within ELS software. Each brick unit was represented with dimensions equal to the real brick size plus a 10 mm mortar thickness, the latter idealized as a zero-length joint. Masonry was thus modelled as an equivalent homogeneous material, with mechanical properties summarized in Table 4.1. For the retrofitted configuration, a textile reinforced mortar layer is incorporated into the model in the form of a reinforcement grid, whose material properties were provided by Kerakoll, plus a mortar layer at the vault's extrados. The adopted element type (RFT element) corresponds to that employed in ELS to represent reinforcement bars in reinforced concrete beams. The TRM layer was thus idealized as a mesh of rebars arranged with a spacing of 20 × 20 mm.

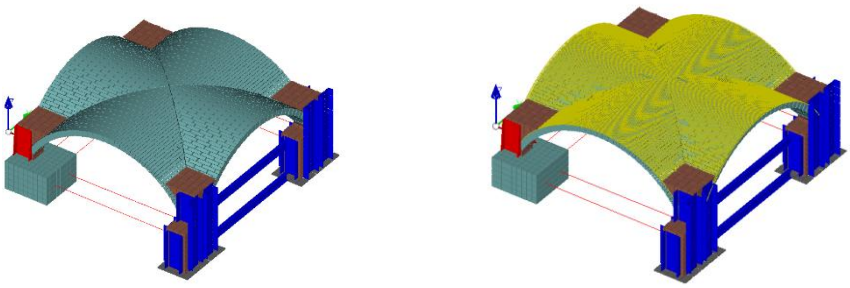

(a) (b)

Figure 4.7 Numerical model developed within ELS software: (a) unstrengthened and (b) strengthened specimens

The numerical modelling strategy is first informed by material characterisation tests and subsequently refined through dynamic identification analyses, ensuring proper calibration of mechanical parameters and modal properties prior to seismic simulation.

4.3.2.1 Simulation of axial-compression (AC) tests

Axial compression tests on masonry wallets were carried out to derive the constitutive parameters of the material, providing the fundamental input for numerical modelling. These tests were reproduced within the adopted modelling framework in order to calibrate stiffness, peak compressive strength, and post-peak degradation behaviour. The simulations were performed by imposing a constant vertical loading rate of 0.003 mm/s, consistent with the experimental campaign setup.

(a) (b)

Figure 4.8 Simulation of AC tests: (a) one of the four tested wallet, and (b) numerical model of the wallet in ELS

Sensitivity analyses were then conducted to refine the calibration of the material parameters, with particular attention to the separation strain, a key variable governing the onset of fracture. This parameter defines the strain level at which the springs connecting adjacent faces are removed, and, as noted in (Applied Science International, 2024a), it represents the resultant strain of matrix springs.

The influence of this parameter is shown in Figure 4.9. When adopting the default value of 0.1, the post-peak behaviour deviates significantly from the experimental results (red curve). Conversely, reducing the parameter to 0.01 yields a much closer correspondence to the observed response (blue curve), although this agreement is limited to pure compression scenarios. In fact, under combined loading conditions (axial plus shear), the lower value of 0.01 leads to an overly restrictive material response, no longer representative of the actual vault behaviour. Unfortunately, results of shear tests on triplets were not available for directly calibrating this parameter.

Despite these limitations, the comparison between experimental and numerical stress–strain curves confirmed that the calibrated stiffness and compressive strength values were consistent, while also emphasising the importance of properly accounting for nonlinear strength degradation in the model.

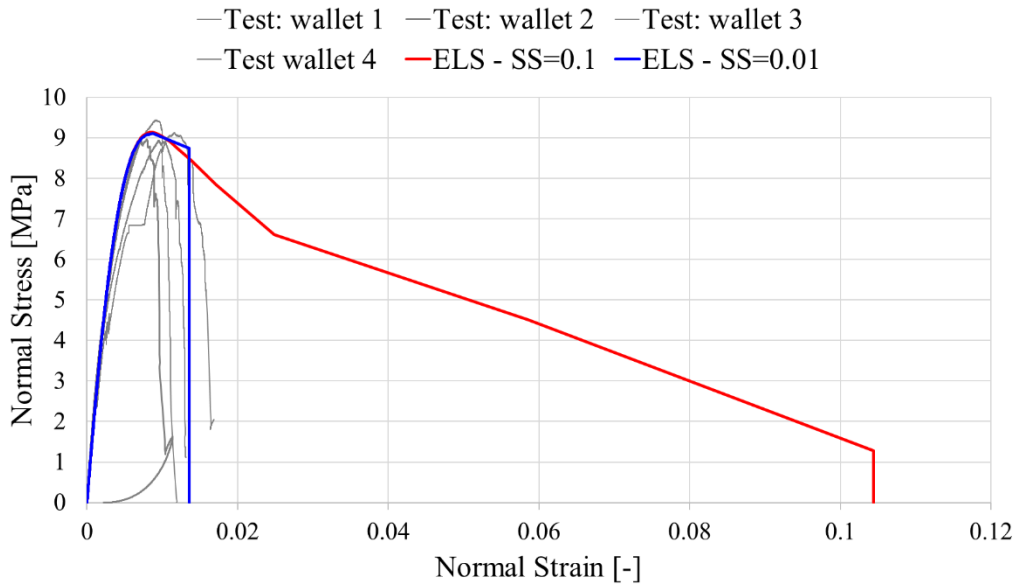

Figure 4.9 Simulation of AC tests: stress-strain curves for two different values of separation strain

4.3.2.2 Comparison between dynamic identification and eigenvalue analysis

The dynamic identification phase provided a fundamental basis for the calibration of the numerical models. An eigenvalue analysis was carried out to investigate the global dynamic behaviour of the numerical model. The computed modal properties, reported in Figure 4.10, were compared against those obtained from the initial dynamic identification test on the undamaged unstrengthened specimen Figure 4.6. The comparison, summarised in, indicates a discrepancy of only 3% for the first global mode, corresponding to the longitudinal direction of excitation.

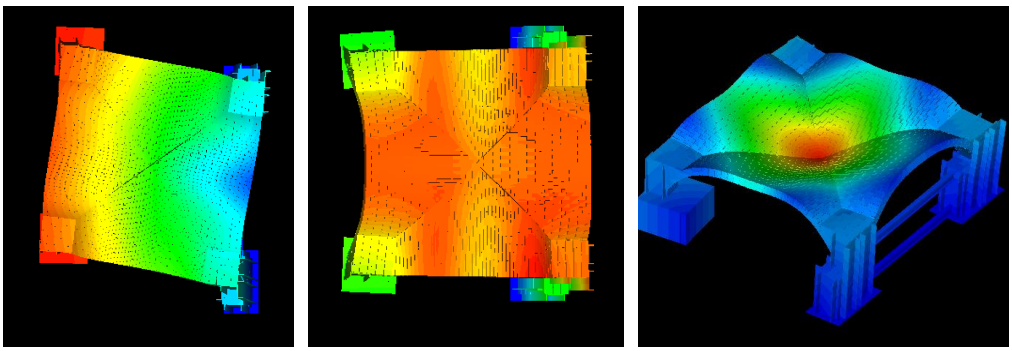

f_1 = 5.98 Hz (a) | f_2 = 14.83 Hz (b) | f_3 = 24.67 Hz (c)

Figure 4.10 Natural frequencies and mode shapes of the unstrengthened specimen obtained within ELS: (a) first global longitudinal mode; (b) second global transverse mode; (c) third global vertical mode *(Bianchini et al., 2023)*

Table 4.3. Comparison of natural frequencies obtained from the first dynamic identification test and eigenvalue analysis of the numerical model within ELS

	Natural frequencies [Hz]		
	f_1	***f_2***	***f_3***
Dynamic identification test	6.15	11.62	19.39
Numerical model ELS	5.98	14.83	24.97
Difference	3%	28%	27%

The effective global longitudinal stiffness was influenced by the Young's and shear moduli of the mortar at the steel–masonry interface, which were calibrated to achieve consistency between the numerical model and the experimental results.

4.3.3 Discussion on the calibration and uncertainty of the Separation Strain parameter

The separation strain (SS) in the Applied Element Method (AEM) represents the deformation threshold beyond which the connection between adjacent elements is released. While this parameter has a clear mechanical meaning in tension, corresponding to the crack opening strain at complete decohesion. it may lose physical significance under compression or shear, where failure is instead governed by crushing or sliding criteria. For this reason, most authors recommend assigning high SS values in compression and shear, and focusing calibration efforts on the tensile response only.

No universal procedure exists for calibrating SS. Its influence depends not only on the adopted constitutive model but also on the element size, the accumulation of damage, and the loading history. As a result, SS cannot be considered a true material property; rather, it behaves as a global numerical parameter, whose effect manifests at the scale of the entire component rather than at the micro-structural level of bricks or mortar joints.

Consequently, the calibration of SS should be carried out by matching the global response of structural components (e.g., masonry walls or panels) rather than small-scale tests. Ideally, this calibration should rely on quasi-static monotonic and cyclic experiments, where the SS value is tuned to reproduce the ultimate displacement observed experimentally or predicted by analytical references such as (DD:ENV:1996-2:2001, 2001) or (Beyer & Mangalathu, 2014). Empirically, values around 0.01 (1% strain) often provide reasonable agreement for in-plane (IP) behaviour, whereas smaller values are typically required for out-of-plane (OOP) analyses to avoid excessive ductility.

Despite its empirical nature, the SS parameter has a clear mechanical role: once a pre-defined strain limit is reached, the contact fails, allowing the structure to exhibit realistic cracking and collapse mechanisms. In fact, the absence of such a strain-based limit, as in some discrete element formulations, can lead to overly stable quasi-static in-plane responses, preventing a correct simulation of progressive cracking and local failure.

There is therefore no general or transferable value for the separation strain; its determination must rely on targeted calibration against component-scale experiments, performed case by case. Unfortunately, such data are scarce for masonry vaults, and the few available tests generally concern small specimens under quasi-static loading conditions. Similarly, the literature still contains only a limited number of dynamic simulations of vaulted systems employing discrete or applied element formulations. As

highlighted by (Lourenço, 1996), the advancement of reliable numerical models for masonry cannot rely solely on theoretical or computational formulations. It must be grounded in a combined experimental and numerical framework, where simulations are systematically validated and refined through comparison with experimental evidence. Only through this integrated approach can move numerical analyses beyond qualitative interpretation and evolve into predictive tools capable of capturing the actual structural behaviour and supporting the definition of rational design principles.

4.3.4 Scale dependence and calibration of softening parameters in AEM

Although the separation strain is a parameter specific to the Applied Element Method, its conceptual foundation aligns with principles already established in fracture-based modelling of masonry. (Lourenço, 1996) demonstrated that softening parameters such as tensile and shear fracture energies cannot be regarded as intrinsic material constants, since their value depends on both the finite-element size and the adopted constitutive law.

From a mechanical standpoint, the separation strain can be defined as the ratio between the ultimate crack opening and the characteristic element length l_{char},

$$SS = \frac{w_f}{l_{char}} \quad \textbf{(5)}$$

This formulation establishes a direct link between the strain-based limit used in AEM and the fracture energy of the material, since the ultimate crack width w_f is proportional to the energy dissipated during fracture. For a linear softening law in tension (Mode I), the fracture energy is defined as:

$$G_{f,I} = \frac{1}{2} f_t w_f \;\Rightarrow\; w_f = \frac{2G_{f,I}}{f_t} \quad \textbf{(6)}$$

Substituting this expression into the previous relation leads to the formulation of the separation strain in tension:

$$SS_n = \epsilon_{n,f} = \frac{w_f}{l_{char}} = \frac{2G_{f,I}}{f_t l_{char}} \quad \textbf{(7)}$$

For shear (Mode II), assuming a linear softening behaviour governed by the shear fracture energy $G_{f,II}$, and the peak shear strength τ_p, an analogous relationship can be expressed as:

$$SS_s = \gamma_f = \frac{2G_{f,II}}{\tau_p l_{char}} \quad \textbf{(8)}$$

These formulations show that the separation strain can be interpreted as a compact, energy-equivalent parameter that encapsulates the effects of the fracture energy, tensile or shear strength, and the characteristic element length of the model. Because the fracture energy itself depends on multiple factors, such as material composition, mortar–brick interface behaviour, loading rate, and the adopted crack-band width, the corresponding values of SS_n and SS_s are inevitably sensitive to these same variables as well as to the chosen discretisation.

(van Zijl, 2004) further reinforced this idea by highlighting that fracture energy and post-peak response are mesh-dependent quantities; to overcome this limitation, he proposed a normalization through the crack-band approach and argued that fracture energy should be treated as a global parameter calibrated at the structural-component level rather than at the material level. This interpretation directly parallels the behaviour of the separation strain in AEM, which is inherently influenced by the characteristic element length and therefore by the discretisation scale. More recently, (D'Altri et al., 2020) stated that constitutive parameters must be calibrated at the same scale as the intended structural application, since values derived from small-scale material tests often fail to reproduce the overall behaviour of masonry components. They also recognized that discrete and applied element models require case-specific calibration and that experimental data on vaulted structures remain limited. Similarly, (Milani et al., 2006b, 2006a) observed that the mechanical parameters used in homogenized analyses cannot be considered true material constants, as they reflect the collective response of the entire element rather than the intrinsic behaviour of its constituents.

Taken together, these studies converge on a consistent conclusion: fracture-related and softening parameters are inherently scale-dependent and must be calibrated against the global behaviour of real structural components. Within the AEM framework, this implies that the separation strain, which encapsulates the entire softening process in a single strain-limit parameter, should not be derived from laboratory properties of bricks or mortar joints. Instead, it must be tuned to reproduce experimentally observed component-scale responses, such as load-displacement or drift capacities, ensuring

that the numerical model accurately captures both the onset and the progression of damage.

4.3.5 Sensitivity analyses on mechanical parameters

Building upon these considerations, the calibration of the separation strain was performed through a set of sensitivity analyses aimed at reproducing the experimental behaviour of the tested vault. As discussed in the previous sections, the SS parameter is not a measurable material property but a numerical quantity that must be tuned according to the global response of the component. Following the recommendations from the literature (Applied Science International, 2024a) and the outcomes of the compression tests, additional values were explored to assess their influence on the global stability and cracking pattern of the vault. Figure 4.11 summarises the results of the nonlinear time-history analyses (NLTHAs) at 75% of the Accelerogram Qualifying Amplitude (AQA) for three different SS values.

- SS = 0.01: the model collapses prematurely, exhibiting an unrealistically brittle response that is not supported by the test evidence (the experimental vault did not fail);
- SS = 0.05: widespread cracking and localized damage develop, and global stability is retained. While this setting improves over SS = 0.01, the predicted damage extent remains larger than observed;
- SS = 0.1: the model reproduces a damaged-but-stable configuration, consistent with the experiment in which the vault suffered visible cracking without collapse. Both the extent and distribution of cracking are more representative when compared qualitatively with the test outcome.

Among the values explored, SS = 0.1 provides the most representative match to the experimental behaviour at 75% AQA: the vault sustains damage yet preserves global integrity, in agreement with the shaking-table observations, as described in next section.

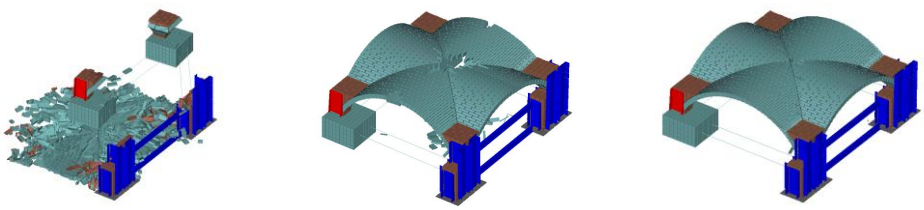

SS = 0.01 SS = 0.05 SS = 0.1

Figure 4.11 Results of the NLTHAs at the end of the 75% of AQA for different SS values

Additional analyses were also performed for higher values of the parameter (SS = 0.2 and 0.3), Figure 4.12, to investigate the upper sensitivity of this parameter. As expected, increasing SS delays the onset of detachment between adjacent elements, resulting in a more contained crack pattern and lower deformation demand. While these models exhibit an overall stable behaviour, the extent of cracking becomes slightly underestimated when compared to the experimental observations, Figure 4.13. Therefore, the adopted value SS = 0.1 can be regarded as a lower bound of the realistic separation capacity for the masonry interfaces, since higher values tend to over-stiffen the model and reduce the amount of dissipated energy. As a matter of fact, from a quantitative perspective, the maximum peaks of displacement and acceleration tend to decrease and increase, respectively, increasing SS, as reported in Table 4.4.

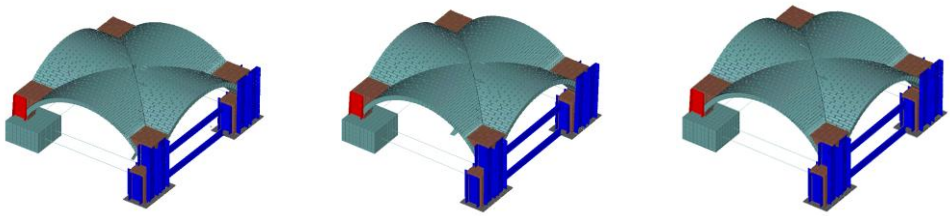

SS = 0.1 SS = 0.2 SS = 0.3

Figure 4.12 Results of the NLTHAs at the end of the 75% of AQA for higher SS values

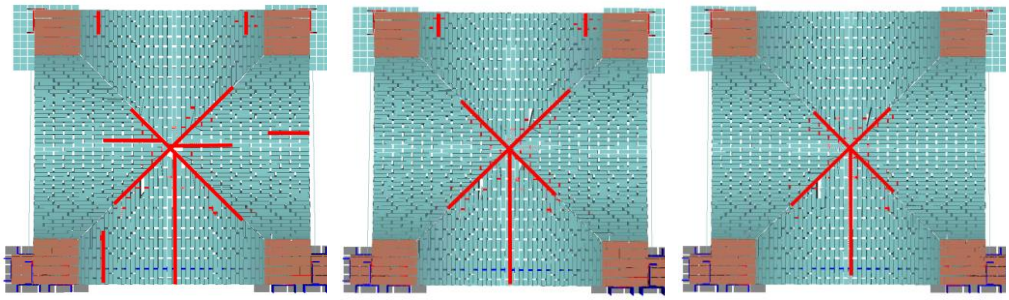

SS = 0.1 SS = 0.2 SS = 0.3

Figure 4.13 Comparison of crack pattern at the end of the 75% of AQA for higher SS values

Table 4.4. Comparison of experimental and numerical absolute maximum total displacements and accelerations for the unstrengthened specimen for higher values of separation strain

			SS		
		Exp.	*0.1*	*0.2*	*0.3*
Displacement [mm]	OC1-y	30.7	25.9	24.62	22.22
	OC2-y	52.5	32.3	30.50	27.87
	OC4-y	32.1	24.9	29.84	28.74
Acceleration [m/s^2]	Acc18-y	3.5	4.9	4.73	5.27
	Acc14-y	4.5	4.4	4.74	4.31
	Acc2-y	4.5	3.9	4.29	4.57

The reliability of the adopted material parameters and the stability of the numerical results were further investigated through dedicated sensitivity analyses, as presented in Chapter 5.

4.3.6 Nonlinear time history analyses results

According to shaking sequence, a series of nonlinear time history analyses (NLTHA) were performed to replicate the experimental shaking table tests. The simulations successfully reproduced the mechanical response of the cross-vault, from the elastic phase through to severe damage states. The numerical crack patterns showed strong consistency with the experimental observations, particularly in relation to diagonal cracking along the vault webs and the formation of hinges at the haunches, Figure 4.14.

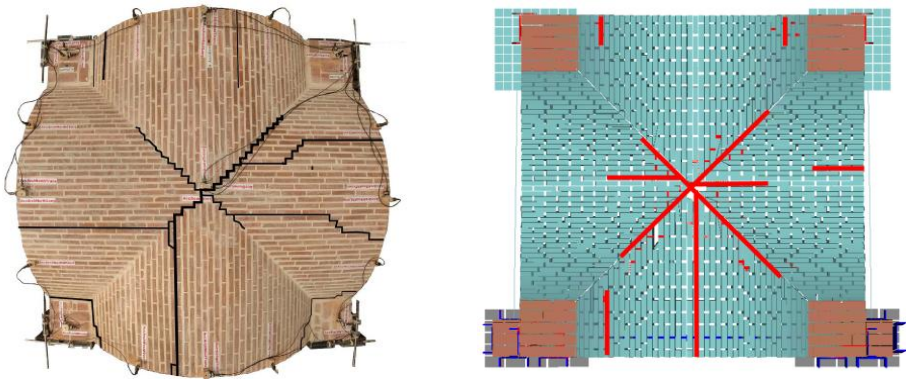

(a) (b)

Figure 4.14 Comparison of experimental** (Bianchini et al., 2023) **(a) and numerical (b) crack patterns at the end of 75% of AQA signal

The analyses confirmed that the dominant failure mechanism was governed by in-plane shear; indeed, Figure 4.15 highlights the progressive damage of the vault, with the subsequent formation of a plastic hinge at the restrained pitch, occurring when the input motion reaches 75% of the AQA signal intensity.

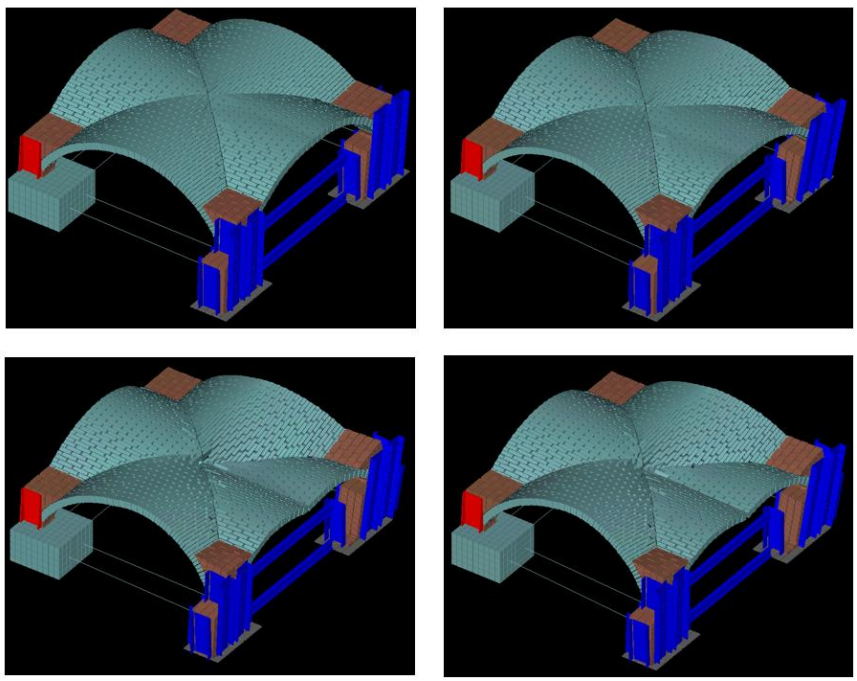

Figure 4.15 Progressive vault damage and plastic hinge formation during 75% of the AQA

The comparison between experimental and numerical results highlights a generally consistent trend, although with varying levels of accuracy depending on the monitored location and response type, Table 4.5. For the displacement response the numerical model tends to underestimate the experimental displacements, with errors ranging between –8.8% and –38.6%. A notable exception is observed at OC2–x, where the numerical prediction significantly overestimates the experimental value (+152.3%). This discrepancy suggests a localized sensitivity of the model in reproducing lateral displacements at that specific point. The correlation of the acceleration response is overall satisfactory, with relative errors mostly within ±15%. However, larger deviations appear at Acc18–x (+60%) and Acc14–x (–57%), indicating that the model may have difficulties in accurately capturing acceleration demand at certain positions, possibly due to local dynamic effects. In summary, the model reproduces the global seismic behaviour of the vault with reasonable accuracy, particularly in terms of acceleration trends, while larger discrepancies in displacement response highlight the need for further refinement in the representation of local deformation mechanisms.

Table 4.5. Comparison of experimental and numerical absolute maximum total displacements and accelerations for the unstrengthened specimen

		Experimental	*Numerical*	*Relative Error [%]*
Displacement [mm]	OC1-y	30.7	25.9	-15.6
	OC2-y	52.5	32.3	-38.6
	OC2-x	4.4	11.1	152.3
	OC4-y	32.1	24.9	-22.3
	OC4-x	7.7	8.4	-8.8
Acceleration [m/s²]	Acc18-y	3.5	4.9	44
	Acc18-x	3.8	6	60
	Acc14-y	4.5	4.4	-1
	Acc14-x	5.2	2.2	-57
	Acc2-y	4.5	3.9	-13
	Acc2-x	4.4	3.9	-10

The displacement time histories at nodes OC1, OC2, and OC4, Figure 4.16, show that the numerical simulations reproduce the overall dynamic response observed during the shaking table test. Both experimental and numerical signals capture the same dominant frequency content and general decay trend. Nevertheless, some discrepancies are evident in terms of amplitude: while the model tends to underestimate the displacement demand at OC1 and OC4, it clearly overestimates the peak value at OC2. Despite these local differences, the global correspondence between the two datasets confirms that the modelling strategy is able to reproduce the primary deformation mechanisms governing the vault's seismic behaviour.

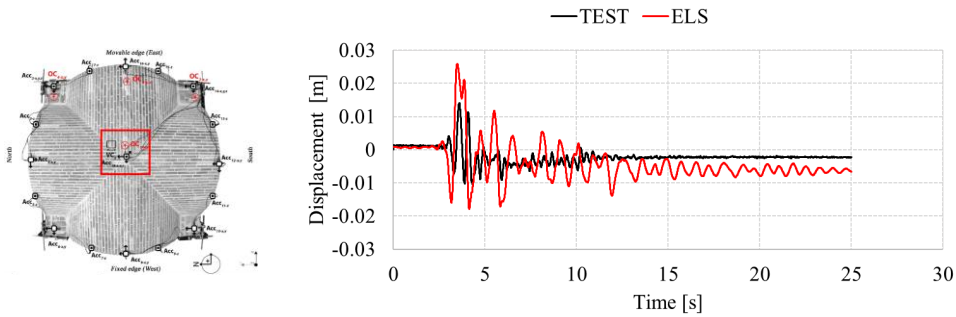

(a)

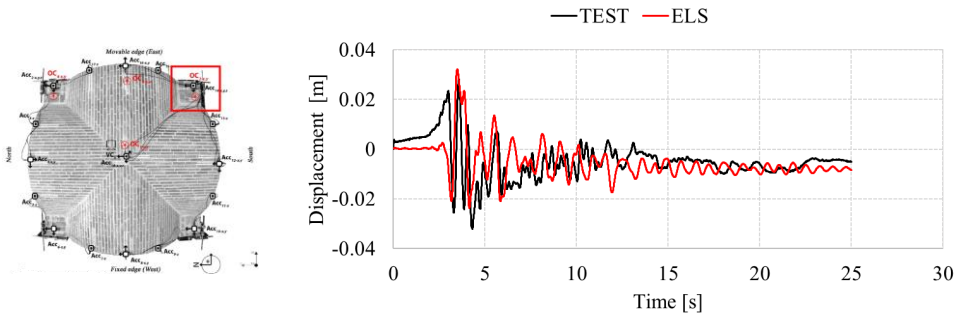

(b)

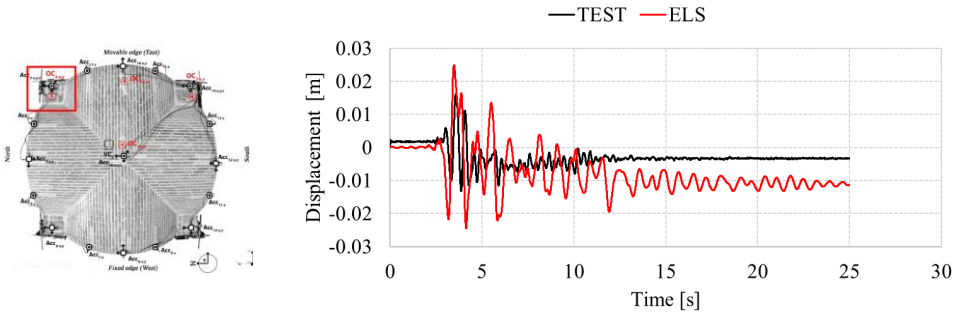

(c)

Figure 4.16 Displacement time histories along N-S direction for OC1 (a), OC2 (b), and OC4 (c) node during 75% of the AQA

The acceleration records at sensors Acc18, Acc14, and Acc2, Figure 4.17, indicate an even closer match between experimental and numerical results compared to the displacement case. The two sets of curves exhibit almost identical frequency content and phase alignment, with discrepancies mainly limited to peak amplitudes. At Acc18 and Acc2, the model slightly overestimates the experimental values, whereas at Acc14 the numerical response underestimates the recorded acceleration. Overall, the comparison demonstrates that the model provides a reliable representation of the global dynamic behaviour, even though local effects may still lead to variations in amplitude.

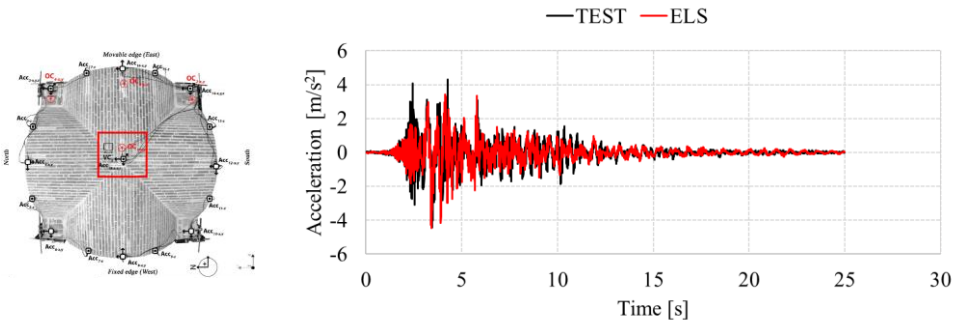

(a)

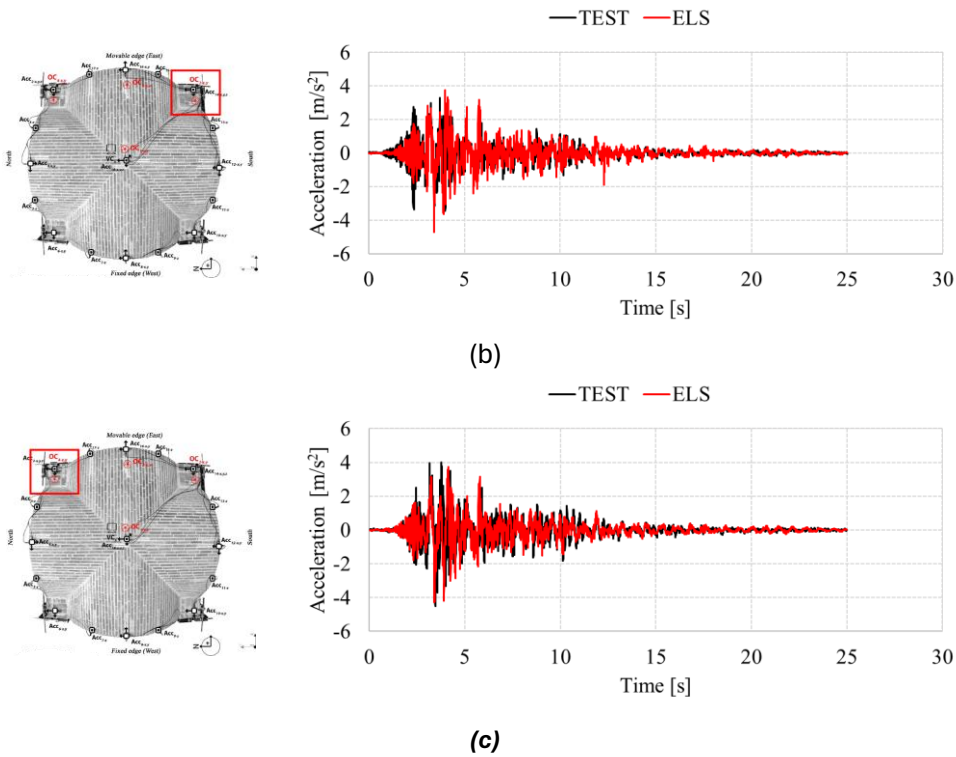

Figure 4.17 Acceleration time histories along N-S direction for Acc18 (a), Acc14 (b), and Acc2 (c) node during 75% of the AQA

4.3.7 Conclusions on LNEC test simulation using AEM

A series of nonlinear time history analyses (NLTHA) was performed to reproduce the shaking table tests conducted on a brick masonry cross-vault. Preliminary static and dynamic assessments confirmed that the Applied Element Method (AEM) is capable of reproducing both the mechanical and dynamic properties of the vault, in agreement with the experimental observations. The adopted modelling strategy enables the investigation of the vault behaviour from the initial elastic range to severe damage states, while also providing insight into the progressive evolution of cracking. The present chapter focuses exclusively on the unstrengthened specimen, whereas the retrofitted configuration is discussed in Chapter 7.

4.3.8 Numerical modelling of the LNEC vault: comparative approaches

Several authors have numerically reproduced the LNEC full-scale shaking-table tests on masonry cross vaults using different modelling strategies, ranging from continuum finite elements to discrete block-based approaches. These studies provide valuable insights into the predictive capacity of diverse methods, their advantages, and their limitations.

(Kesavan et al., 2024) developed a discontinuum finite element model in STKO+OpenSees, where units and mortar joints were represented explicitly with thick-shell Reissner–Mindlin elements and a damage–plasticity law (DamageTC3D). The implicit–explicit integration scheme (IMPL-EX) ensured stable convergence in the post-peak range. Simulations were carried out for both unstrengthened and TRM-strengthened vaults and validated against the LNEC campaign. The results demonstrated the ability of the model to reproduce the dominant in-plane shear mechanism along the groins, as well as the beneficial effect of strengthening, which nearly doubled the seismic capacity of the vault. Limitations included the computational cost and the need for extensive calibration of material softening and low-cycle fatigue effects.

A systematic comparison of continuous homogeneous modelling (CHM) and discrete block-based approaches was presented by (Ferrante et al., 2024) In the CHM framework, masonry is treated as a homogenised anisotropic continuum with a damage-plasticity constitutive law (Endo3D in LMGC90). In the discrete strategy, the vault is discretised into rigid or deformable blocks with cohesive–frictional contact interfaces. The study highlighted that CHM efficiently captures global dynamic behaviour but tends to underestimate discontinuities and block detachment, whereas discrete approaches reproduce cracking and collapse mechanisms more realistically at higher computational cost.

(Oktiovan et al., 2023) applied a simplified micro-modelling strategy in 3DEC, where the vault geometry was generated parametrically and represented as deformable blocks interacting through zero-thickness interface springs. The contact laws incorporated elasto-softening behaviour in tension, shear, and compression, calibrated against fracture energy. The DEM simulations reproduced both qualitative crack patterns and quantitative response parameters observed in the LNEC blind and post-diction phases. Strengths of the DEM include its native ability to capture joint opening, closure, and large block displacements; however, the approach requires careful parameter identification (e.g., damping, interface properties) and remains computationally demanding.

Despite methodological differences, all the referenced studies consistently identified the same governing failure mechanism in the unstrengthened vault: in-plane shear cracking concentrated along the groins, starting from the crown. FEM-based models proved effective in reproducing the global dynamic behaviour, modal properties, and overall deformation patterns, and were particularly useful in assessing the beneficial role of TRM strengthening, which significantly enhanced both strength and energy dissipation capacity. Conversely, DEM approaches excelled in capturing localized damage phenomena, such as crack initiation, block detachment, and collapse kinematics, thanks to their intrinsic ability to simulate contact, separation, and re-contact among discrete units.

However, these higher-fidelity DEM formulations demand extensive calibration of interface parameters, e.g., cohesion, friction, damping. Regarding damping parameter, (Oktiovan et al., 2023) calibrated the model in different seps since it seemed to affect too much the displacement responses. Furthermore, these approaches entail substantially higher computational costs. As reported by (Ferrante et al., 2024), the average runtime for DEM simulations (≈ 29 days) was more than twice that of comparable FEM analyses (≈ 14 days), highlighting the trade-off between accuracy and efficiency typical of discontinuum approaches. In contrast, the AEM meso-scale model developed in this work completed the same class of nonlinear dynamic simulations in approximately 5 hours, achieving a similar level of accuracy while drastically reducing the computational demand. Moreover, unlike several previous numerical studies where only the strongest portion of the seismic record was applied, by truncating the accelerogram to reduce analysis time, the AEM simulations presented here employed the entire duration of the ground motion for each amplitude increment. This ensured a more realistic representation of the cumulative damage process and allowed for the evaluation of stiffness degradation and crack propagation under full cyclic loading histories, closely replicating the experimental testing protocol.

The results of the modal analyses are aligned with the experimental data. The mean frequency obtained from the four numerical models (6.22 Hz) differs from the experimental value of 6.15 Hz by approximately +1.14%, indicating a slight tendency toward overestimation in the simulations. The dispersion among the models, quantified through the coefficient of variation (CV ≈ 4.9%), remains relatively low, reflecting a satisfactory numerical consistency despite the methodological differences between the approaches adopted. Among the considered models, the Discontinuum FEM shows the closest agreement with the experimental frequency, with a deviation lower than 0.2%. Furthermore, considering the 95% confidence interval of the mean frequency, ranging

from 5.74 Hz to 6.70 Hz, it can be stated that the overall estimate is consistent with the experimental observation within the bounds of numerical uncertainty, confirming the general reliability of the set of models employed. A detailed comparison is provided in Table 4.6.

Table 4.6. Comparison of experimental and numerical first mode frequencies

Model	***f [Hz]***	***Absolute Error [Hz]***	***Relative Error [%]***
(Kesavan et al., 2024) - FEM	6.16	0.01	0.16
(Ferrante et al., 2024) - FEM	6.08	0.07	1.14
(Cogliano et al., 2025) – AEM (present work)	5.98	0.17	2.76
(Oktiovan et al., 2023) - DEM	6.66	0.51	8.29
Experimental test frequency [Hz]	6.15		
Numerical mean frequency [Hz]	6.22		
Standard Deviation σ [Hz]	0.3		
Coefficient of Variation CV [%]	4.86		

Across all simulations, displacement amplitudes along the direction of excitation were systematically underestimated compared to experimental measurements. This difference is probably due to the absence of initial geometric imperfections in the numerical models, which represent “perfect” configurations, unlike the real specimen that inevitably is characterized by small irregularities and residual deformations. Additionally, none of the models successfully reproduced the acceleration peaks observed between 2 s and 3 s, a discrepancy likely associated with localized dynamic effects and transient stiffness variations in the physical test that are not fully captured by the simplified numerical representations.

In this context, the Applied Element Method (AEM) stands as a hybrid and pragmatic alternative, bridging the gap between FEM and DEM. Its formulation retains the computational efficiency of continuum models while naturally incorporating the

discontinuous mechanics of discrete approaches. As demonstrated in this study, the meso-modelling strategy developed within AEM allows for a reliable representation of the nonlinear dynamic response and progressive failure evolution of masonry vaults, offering a robust framework for collapse assessment and comparative validation against experimental data.

5 SENSITIVITY ANALYSES

Numerical models of masonry structures involve several parameters that are derived through empirical relationships, calibration, or simplifying assumptions. Consequently, the predictive reliability of such models depends critically on the choice and calibration of these parameters. Sensitivity analyses constitute a fundamental step in the verification and validation process, as they allow for the quantitative evaluation of how variations in the input parameters influence the numerical predictions.

The present chapter focuses on the evaluation of the model's robustness through local sensitivity analyses, aimed at assessing the influence of individual mechanical and numerical parameters on the predicted structural response. The analyses provide insight into both the stability of the numerical solution and the physical consistency of the adopted parameters within reasonable uncertainty ranges.

Section 5.1 introduces the theoretical background and motivation for performing sensitivity analyses, summarising key contributions from the literature.

Section 5.2 outlines the adopted methodological framework, describing the procedure implemented for the local sensitivity and stability assessment of selected mechanical parameters.

Section 5.3 resents and discusses the results of the parametric study on the separation strain, a key AEM parameter controlling the onset of element detachment and the propagation of cracks. Both qualitative and quantitative assessments are provided to evaluate its influence on the global seismic response of the vault.

Section 5.4 extends the discussion to additional parameters, such as mesh discretisation, contact stiffness, and interface materials, highlighting their interactions and combined effects on the overall model robustness.

5.1 THEORETICAL BACKGROUND AND MOTIVATION

According to (Helton & Davis, 2003; Saltelli et al., 2004), sensitivity analysis is an essential component of any scientific modelling process, as it provides a quantitative framework to identify which parameters most affect the model output and to assess the robustness of the predictions. In structural engineering, local sensitivity analyses are commonly employed as a first-order approximation of parameter influence: each

parameter is independently varied within a small range (typically ±10–20%) around its calibrated value, and the corresponding change in the model response is evaluated.

Formally, the local sensitivity index S can be expressed as:

$$S = \frac{\Delta R/R}{\Delta p/p} \quad (9)$$

where p is the parameter being varied and R is the corresponding structural response quantity. Large values of S indicate a strong dependence of the results on the parameter, while small values imply a robust and stable numerical behaviour.

The adopted formulation corresponds to the local sensitivity index defined by (Saltelli et al., 2004), which expresses the logarithmic derivative of the model output with respect to the input variable, $S_l = \partial \ln Y / \partial \ln P$. This local measure quantifies the proportional change in the model response resulting from a proportional perturbation of a single input parameter, thereby allowing a straightforward evaluation of parameter influence around a given reference configuration. According to their study, local sensitivity indices S_l can be interpreted as follows: values below 0.1 indicate a negligible or weak influence of the parameter, values between 0.1 and 0.5 correspond to a moderate sensitivity, and values close to or above 1.0 denote a strong or dominant influence of the parameter on the model response. These thresholds provide a useful benchmark for classifying parameters in terms of their impact on model behaviour and for distinguishing between stable and highly sensitive configurations.

Several studies have emphasized the importance of performing such local parametric analyses to assess model reliability and to identify critical parameters. (Lourenço & Rots, 1997), for instance, investigated the sensitivity of interface parameters in masonry models to evaluate their impact on shear and tensile behaviour. Within this framework, the separation strain used in AEM formulations represents a particularly critical parameter, as it controls the strain threshold for element detachment and strongly influences the progression of cracking and collapse mechanisms. The evaluation of its sensitivity is therefore necessary to ensure that the chosen value leads to a physically meaningful and numerically stable response.

5.2 METHODOLOGICAL FRAMEWORK

The analyses presented in this chapter are classified as local sensitivity and stability analyses, focusing on the effect of small perturbations of selected parameters around their calibrated reference values. For each parameter, a reference value was first

determined through calibration against experimental results. Variations of ±10% and ±20% was then considered, and their influence on the global structural response, such as displacements, accelerations, and crack evolution, was evaluated.

This approach, also referred to as a parametric stability study or robustness assessment, aims to determine whether the numerical response remains qualitatively and quantitatively consistent under small variations of key input parameters. In particular, it provides insight into whether the model exhibits stable mechanical behaviour or if it is highly sensitive to the assumed values, thus identifying the parameters that govern the nonlinear response of the system.

Such an approach is especially relevant in discrete and applied element formulations, where many parameters (e.g., separation strain, fracture energies, interface stiffnesses) are not fixed material constants but depend on the mesh discretisation and contact definitions. For this reason, the first part of this chapter focuses on the separation strain.

5.3 LOCAL SENSITIVITY AND STABILITY ANALYSIS OF THE SEPARATION STRAIN

To evaluate the stability and robustness of the numerical model with respect to the separation strain parameter, a series of Local Sensitivity Analyses (LSA) were carried out. The reference value adopted for the calibration of the vault model was SS_{ref} = 0.1, which provided the best agreement with the experimental results in terms of global deformation and cracking pattern. Starting from this value, additional simulations were performed by varying the parameter over a wider range, namely

Table 5.1. Values and variations of separation strain explored for LSA

SS	*0.05*	*0.08*	*0.09*	0.11	0.12	*0.15*
Variation	*-50%*	*-20%*	*-10%*	*+10%*	*+20%*	*+50%*

Although these variations extend beyond the ±20 % range typically considered in local sensitivity studies, they were introduced to better illustrate the stabilising effect of the parameter: very low SS values induce premature separation between adjacent elements and lead to unrealistic brittle collapse, whereas higher SS values delay the detachment process and produce a stiffer but globally stable behaviour.

5.3.1 Qualitative assessment of model responses varying separation strain values

To qualitatively assess the influence of the separation strain on the overall behaviour of the vault, the final damage patterns obtained from all simulations were compared. The comparison aims to identify possible changes in the cracking mechanism, failure mode, or global stability of the structure as the SS parameter varies within the considered range (0.05–0.15). The resulting configurations are shown in Figure 4.11, where the damage distributions corresponding to each SS value are reported.

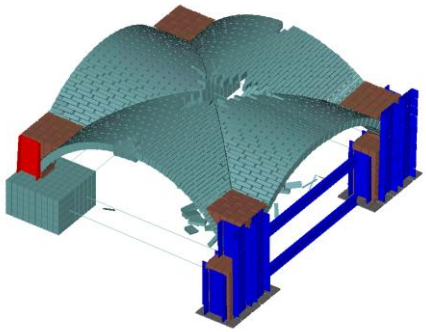

SS = 0.05

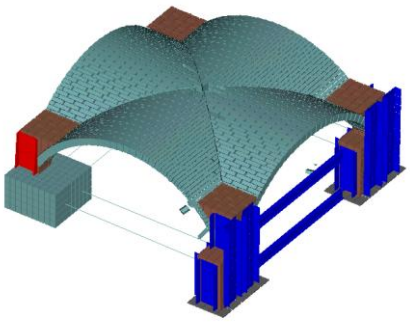

SS = 0.08

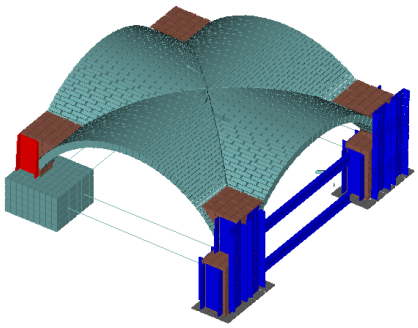

SS = 0.09

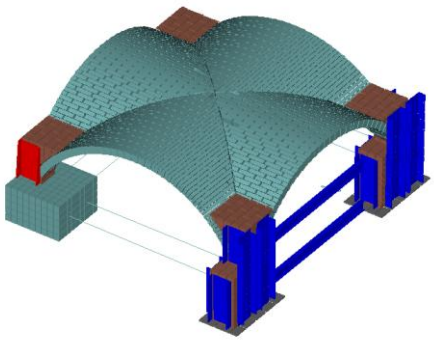

SS = 0.11

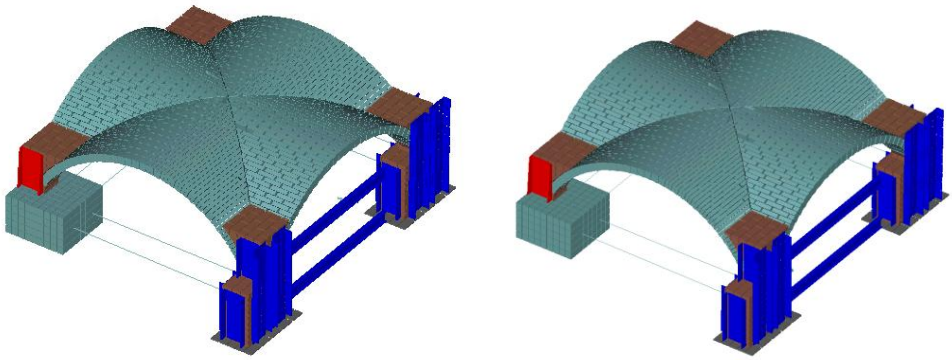

SS = 0.12 SS = 0.15

Figure 5.1 Results of the NLTHAs at the end of the 75% of AQA for different SS values for LSA

A clear distinction emerges between the lowest value (SS = 0.05) and the remaining configurations.

- SS = 0.05: the vault experiences a severe and premature degradation of its structural integrity; a pronounced crack initiates at the crown, leading to a partial collapse of the central portion of the vault. This configuration displays extensive fragmentation and loss of continuity, with localised detachment of elements near the key. Such behaviour was not observed experimentally and reflects an unrealistically low separation capacity, marking the lower bound beyond which the model becomes numerically unstable and physically inconsistent.
- SS = 0.08: the vault recovers a stable and coherent structural behaviour. Cracking develops along the haunches and near the supports, with moderate openings at the crown but without any element detachment. The crack pattern remains continuous and compatible with the in-plane shear mechanism observed experimentally.
- SS = 0.09: The configuration exhibits a very similar mechanism but with slightly reduced damage extension. The cracks at the crown are less pronounced, and the overall pattern appears more cohesive, suggesting a marginally stiffer and less dissipative response as the separation strain increases.
- SS = 0.11: more contained damage distribution. Cracking remains localised near the vault intersections and along the lower portions of the shells, whereas the central region remains largely intact. The global mechanism is unchanged, but the vault behaves more rigidly and exhibits limited tensile opening.

- SS = 0.12: the damage becomes even more restricted. Only minor separations appear near the supports and along the haunches, with negligible cracking in the upper regions. The response is predominantly elastic, and the detachment initiation is significantly delayed compared with smaller SS values.
- SS = 0.15: this value yields the stiffest configuration among the analysed cases. The vault shows an almost undamaged pattern, with minimal or no cracking and no indication of instability. The behaviour becomes overly rigid compared with the experimental observations.

Overall, the analyses show that the damage pattern remains substantially unchanged across most configurations, confirming that variations in SS within moderate limits do not significantly alter the global failure mechanism. Cracking is concentrated along the vault's haunches and near the supports, with minor tensile openings along the crown, consistent with the experimental observations, highlighting the in-plane shear mechanism. This qualitative stability of the response supports the interpretation that the SS mainly governs the timing of cracking initiation rather than the global failure mode. For SS values between 0.08 and 0.15, the evolution of damage progressively decreases, reflecting an increasingly stiff response but without modifying the underlying collapse mechanism.

The only configuration that deviates from this trend is the case with SS = 0.05, where the vault experiences partial collapse initiated at the key. This behaviour results in a more damaged configuration, with the central portion of the vault detaching and falling in the numerical model. However, such a failure was not observed in the experimental test, indicating that the reduced SS value is unrealistically low and does not represent the actual separation capacity of the masonry.

The outcome therefore highlights the lower bound of physically meaningful SS values, beyond which the numerical response becomes unstable and no longer consistent with the experimental evidence. The qualitative analysis thus confirms the stabilizing effect of the parameter: once SS exceeds approximately 0.08, the predicted damage pattern and failure mechanism remain consistent, demonstrating the robustness of the model with respect to this parameter.

5.3.2 Quantitative assessment of model responses varying separation strain values

Building on the qualitative observations presented in the previous section, a quantitative analysis was carried out to evaluate how the variation of SS affects the numerical response of the vault. The assessment focuses on the evolution of maximum displacements and accelerations recorded at selected monitoring points, as well as on the corresponding sensitivity indices derived for each configuration. These quantities provide an objective measure of the model's stability and allow for a more rigorous interpretation of the influence of SS on the simulated seismic behaviour.

For each simulation, the responses in terms of displacement and acceleration were monitored at three representative monitoring points (OC1_y, OC2_y, OC4_y and Acc18_y, Acc14_y, Acc2_y) on the vault along the seismic direction and evaluated at 75% of AQA signal.

Table 5.2. Summary of experimental and numerical absolute maximum total displacements and accelerations for the unstrengthened specimen for different values of separation strain

			Numerical for different values of SS						
		Exp.	***0.1***	***0.05***	***0.08***	***0.09***	***0.11***	***0.12***	***0.15***
Displacement [mm]	OC1-y	30.7	25.9	46.96	19.8	19.4	21.3	20.15	22.22
	OC2-y	52.5	32.3	30.73	25.2	24.1	27.4	25.20	27.98
	OC4-y	32.1	24.9	30.18	26.0	23.4	27.43	24.53	28.90
Acceleration [m/s^2]	Acc18-y	3.5	4.9	70.1	6.0	4.64	4.42	4.91	5.31
	Acc14-y	4.5	4.4	4.12	4.5	4.56	4.46	4.60	4.68
	Acc2-y	4.5	3.9	4.08	4.4	5.19	4.27	4.82	4.23

Table 4.5 summarises the main results, confirming the stabilising influence of the separation strain parameter, which prevents premature detachment between elements and promotes a more realistic and stable global response. As expected, the largest displacement and acceleration peaks correspond to the configuration with SS = 0.05, for which the vault undergoes an early local failure at the crown. In this case, the

monitoring point located near the key records an abrupt increase in displacement followed by extremely large acceleration values[1].

It is essential to stress that these peaks do not reflect the dynamic response of the vault, but rather the free-fall motion of detached elements after the onset of collapse. Once detachment occurs, the recorded time histories capture the kinematics of the falling block rather than the structural response. Consequently, the numerical values associated with SS = 0.05, although mathematically produced by the solver, are not physically meaningful, and cannot be used for comparison with either the experimental reference or the other numerical configurations. The premature collapse is therefore a modelling artefact caused by an unrealistically low separation strain, which does not represent the actual tensile capacity of the masonry interfaces.

The sensitivity index S was then computed according to Equation (9) as the ratio between the relative variation of the response and the relative variation of the parameter. The obtained values are summarized in Table 5.3.

Table 5.3. Values of the sensitivity index S

SS/SS_{ref}	*-0.5*	*+0.1*	*-0.1*	+0.2	-0.2	*+0.5*
S_{mean}	*0.41*	*1.48*	*1.64*	*0.53*	*0.62*	*0.22*

It should be noted that the extremely large response associated with SS = 0.05 artificially inflates the sensitivity index for the −50% perturbation. In this case, the high value of S does not indicate a genuine physical sensitivity, but simply reflects the non-physical collapse mechanism triggered by the unrealistically low parameter. For this reason, the −50% configuration must be interpreted as outside the physically meaningful range, and its numerical outputs should not contribute to the evaluation of parameter sensitivity.

The sensitivity indices range between 0.22 and 1.64, indicating that the model response exhibits a moderate-to-high sensitivity to variations in the parameter. The largest sensitivity values correspond to the ±10% perturbations of the reference value, revealing

[1] Once the vault initiates collapse, the monitoring points located on the detached elements no longer record the structural response but the free-fall motion of individual fragments. As a result, the displacement and acceleration peaks obtained for SS = 0.05 do not reflect the seismic behaviour of the vault and should not be included in the quantitative comparison with the experimental reference or with the other numerical simulations. The configuration must therefore be regarded as outside the physically meaningful parameter range.

that the model seems to be slightly more sensitive to small variations of SS around its calibrated value. This behaviour is consistent with the physical interpretation of SS as the strain threshold controlling the detachment between elements: near this limit, even a small modification in the parameter shifts the onset of contact opening, significantly altering stiffness, energy dissipation, and local deformation mechanisms. When the parameter is further reduced (−50%) or increased (+20 % to +50 %), the sensitivity index decreases, suggesting two cases: in the first one, the detachment due to in-plane shear failure occurred and the response is not affected anymore by SS; in the second case, the model enters a numerically stable regime in which additional variations of SS produce only minor effects on the global response.

This trend highlights the nonlinear influence of the SS parameter: its effect is most pronounced near the transition between bonded and detached states, whereas outside this range the model behaviour becomes less sensitive. The mean sensitivity index ($S \approx 0.8$) therefore indicates a moderate average sensitivity, confirming that the parameter meaningfully influences the model response but does not cause instability within the physically realistic range ($0.08 \leq SS \leq 0.12$).

The ratio between the numerical and experimental responses (R_{num}/R_{exp}) is plotted in Figure 5.2 as a function of the normalised separation strain (SS/SS_{ref}). The grey lines represent the individual responses recorded at each monitoring point, OC labels refer to displacements, while Acc labels refer to accelerations, whereas the red line corresponds to their mean value. The black horizontal line represents the experimental reference ($R_{num}/R_{exp}=1$), providing a direct measure of the model accuracy. Overall, the results show that the mean numerical response remains consistently close to the experimental one, with deviations below ±10 % for most configurations.

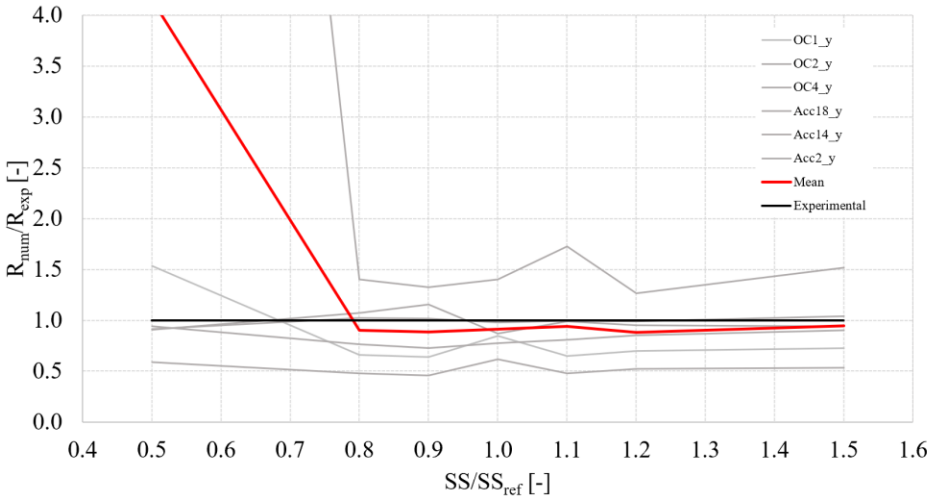

Figure 5.2 Global sensitivity of the numerical response to the separation strain (SS)

The only configuration that diverges significantly from the experimental behaviour is the case with SS/ SS_{ref}=0.5 (SS = 0.05), for which the vault experiences partial collapse initiated at the crown. In this case, the mean ratio R_{num}/R_{exp} reaches ≈ 4.15, indicating an unrealistic amplification of both displacements and accelerations. This divergence is attributed again to the excessively low SS value, which causes premature detachment between elements and loss of stiffness, leading to a numerically unstable configuration that does not reflect the experimental behaviour. When this non-physical configuration is excluded, the mean ratios for all other cases range between 0.88 and 0.94, confirming an excellent agreement between the numerical and experimental responses.

To better visualise the response stability within the physically meaningful range of parameter variation, Figure 5.3 provides a zoomed-in view of the local sensitivity (±10–20 %) around the calibrated value. Within this interval, the red mean curve remains nearly coincident with the experimental reference line (R_{num}/R_{exp}≈1.0), and the individual monitoring points exhibit small and well-distributed fluctuations.

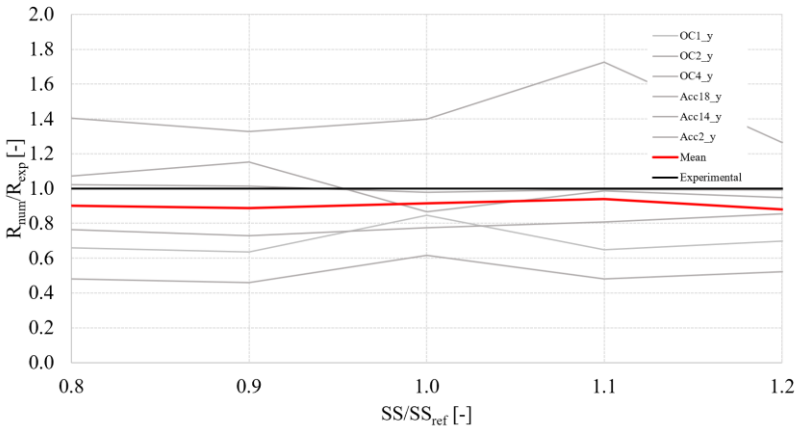

Figure 5.3 Local sensitivity of the numerical response to the separation strain (SS)

This outcome confirms that, for realistic perturbations of the separation strain, the model response is remarkably stable and accurate, with minimal sensitivity in both displacement and acceleration fields.

In summary, the quantitative evaluation confirms that the Separation Strain parameter primarily controls the transition between bonded and detached states in the masonry interfaces. Within the physically meaningful range ($0.08 \leq SS \leq 0.12$), the model reproduces the experimental behaviour with excellent accuracy and only marginal sensitivity, ensuring both numerical stability and physical realism. Conversely, excessively low values (e.g., SS = 0.05) lead to premature detachment and unrealistic amplification of the response, demonstrating that the parameter must be properly calibrated to preserve model robustness.

Overall, the separation strain can thus be regarded as a global calibration factor that governs the onset of cracking and the post-cracking stiffness of the vault, while guaranteeing a consistent and reliable simulation of its seismic behaviour.

5.4 DISCUSSION OF MODEL ROBUSTNESS AND PARAMETER INTERACTIONS

The discussion presented in this section aims to evaluate the overall robustness of the AEM numerical model and to identify the interdependence among the most influential mechanical parameters governing the vault behaviour. The outcomes of the sensitivity analyses on the separation strain demonstrated that the model response remains stable and consistent with the experimental observations within the physically realistic range. However, the mechanical behaviour of the vault is also influenced by a broader set of

modelling assumptions and parameters that interact nonlinearly, making the calibration process particularly complex.

To assess the robustness of the numerical model, additional sensitivity analyses were performed by varying the mesh density, the stiffness of the contact interfaces, and the material properties of the connection zones.

5.4.1 Sensitivity on mesh size

The discretisation adopted in the Applied Element Method (AEM) model has a direct impact on the predicted mechanical behaviour of the vault, as it governs the number and distribution of potential cracking interfaces. To investigate this influence, a comparative analysis was carried out using a coarser mesh configuration, the meso-modelling approach applied to the geometry, in which each eight-node element no longer represents an individual brick but a larger portion of masonry, specifically block with dimensions equal to 10 cm x 10 cm, as shown inFigure 5.4, were employed.

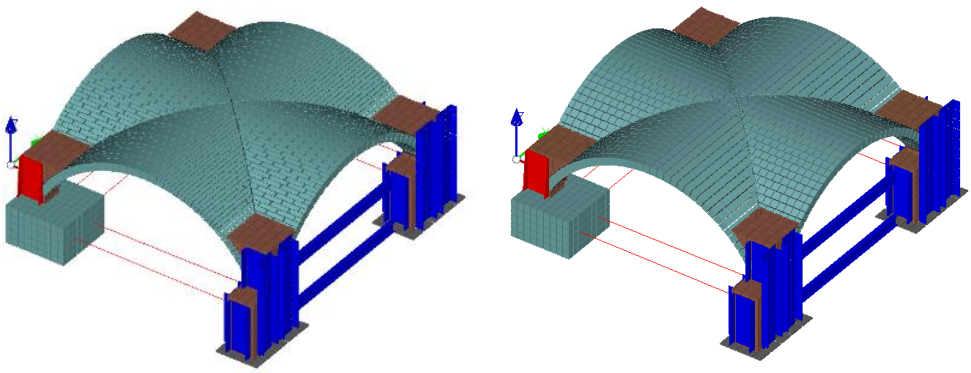

(a) (b)

Figure 5.4 Comparison of mesh sizes: simplified micro-modelling (a) and meso-modelling (b)

Figure 5.5 compares the damage distribution obtained with the coarser mesh configuration for three different separation strain values (SS = 0.1, 0.4 and 0.5) at 75 % of the AQA signal. When SS = 0.1, the vault exhibits an extensive cracking pattern and local separation along the key, indicating a premature loss of stiffness and partial instability. By contrast, for SS = 0.4 the damage is more contained and mainly localised near the vault intersections and imposts, while the remaining portions remain largely

intact. The case with SS = 0.5 shows an even more limited damage extension, with the structure behaving almost elastically under the same excitation.

This progressive reduction of cracking with increasing SS confirms that, in the coarse discretisation, higher separation strain values are required to reproduce the same deformation capacity observed in the experimental test. The reduction of potential contact interfaces limits the ability of the model to develop distributed tensile damage, leading to a stiffer and less dissipative response. Consistently, the maximum displacement amplitudes decrease while acceleration peaks increase with higher SS, quantitatively confirming the overall stiffening effect of the mesh coarsening.

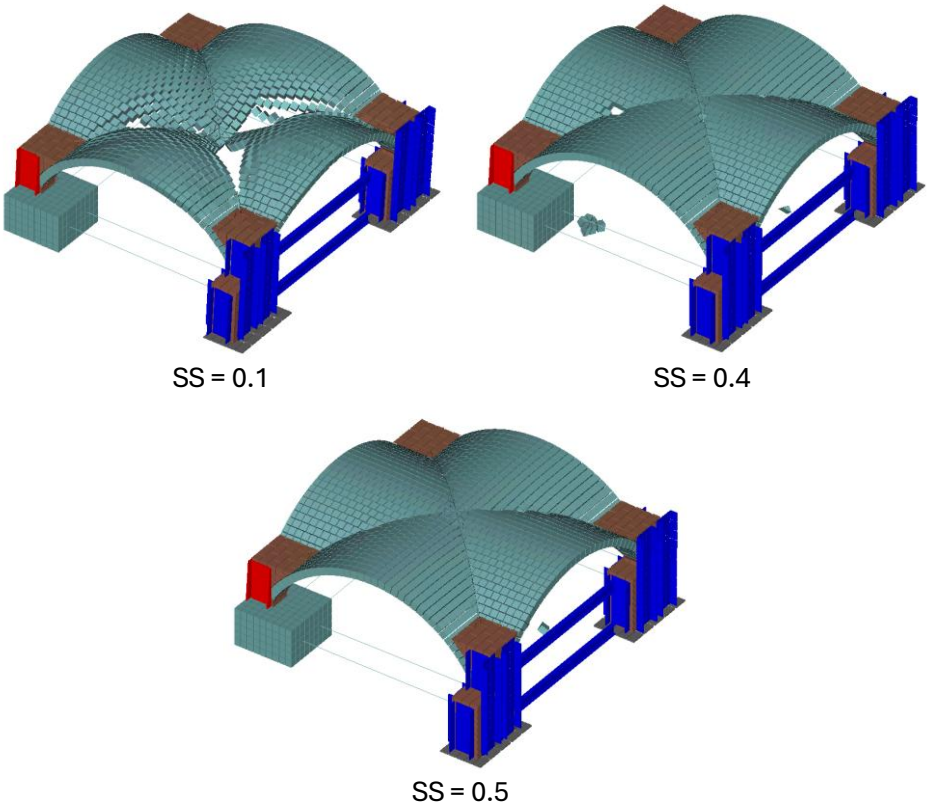

Figure 5.5 Results of the NLTHAs at the end of the 75% of AQA for different SS values with geometry meso-modelling approach

Table 5.4. Comparison of experimental and numerical absolute maximum total displacements and accelerations for the unstrengthened specimen for different mesh sizes and SS values

		SS				
		Exp.	***0.1***	***0.1c***	***0.4c***	***0.5c***
Displacement [mm]	OC1-y	30.7	25.9	25.5	26.0	25.5
	OC2-y	52.5	32.3	35.0	35.9	35.0
	OC4-y	32.1	24.9	34.1	34.9	34.1
Acceleration [m/s^2]	Acc18-y	3.5	4.9	5.8	9.98	5.8
	Acc14-y	4.5	4.4	4.5	4.56	4.5
	Acc2-y	4.5	3.9	5.1	5.57	5.1

These results highlight that the discretisation level and the separation strain parameter are closely interdependent: coarser meshes require higher SS values to compensate for the loss of potential cracking planes. Nevertheless, excessive SS values (e.g. 0.5) lead to an unrealistically elastic response, whereas SS≈0.4 provides a reasonable compromise between stiffness and damage representation, ensuring a physically consistent simulation of the vault behaviour.

5.4.2 Sensitivity on contact material

Further calibration was required for the contact stiffness between the steel boundary elements and the masonry blocks, in order to reproduce the experimental dynamic properties recorded during the dynamic identification tests.

The interface between the four vault quadrants was also adjusted: initially modelled as masonry, trying to homogenized the material, these connections were subsequently defined as mortar interfaces, which provided a more realistic representation of the actual construction details and improved the physical coherence of the simulated behaviour. As shown in Figure 5.6, masonry interface led to a more damaged final configuration with respect to the one obtained by mortar interface. The latter better represents the actual response of the specimen according to the experimental test.

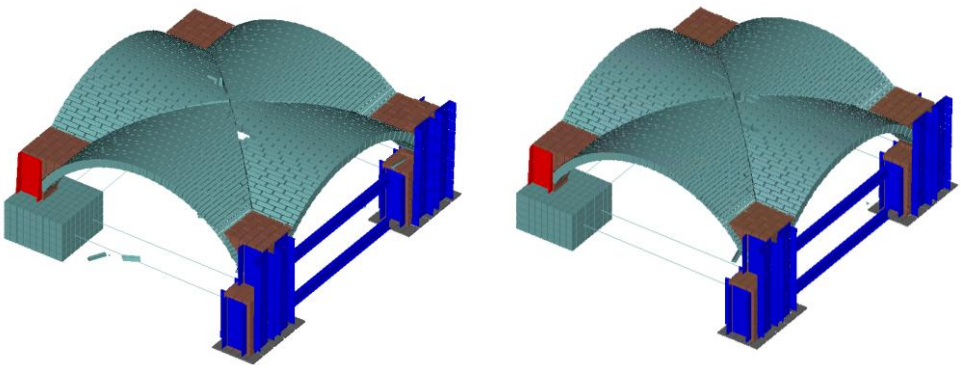

(a) (b)

Figure 5.6 Comparison of damage at the end of 75% of AQA for different interface between vault's fields: masonry (a) and mortar (b)

5.4.3 Sensitivity on higher values of SS

Complementary parametric tests were also carried out for larger SS values (0.2–0.3) as discussed in Chapter 4. These analyses resulted in a more contained damage distribution and lower deformation demand, confirming that the adopted value SS = 0.1 can be regarded as a lower bound for the realistic separation capacity of the masonry interfaces. Nonetheless, it is acknowledged that the actual value might be higher, as no experimental data on full-scale collapsing vaults are available for direct validation.

5.4.4 Conclusions

The sensitivity analyses presented in this chapter have provided a comprehensive evaluation of the robustness and reliability of the AEM numerical model adopted for the simulation of the unstrengthened masonry vault. The results demonstrated that the structural response is governed by a complex interplay among several mechanical and numerical parameters, most notably the separation strain, the discretisation level, and the stiffness of the contact interfaces, whose effects are strongly nonlinear and interdependent.

Among these, the separation strain emerged as the most influential factor, as it directly controls the onset of element detachment and the development of tensile cracking. Within the physically meaningful range ($0.08 \leq SS \leq 0.12$), the model reproduced the experimental behaviour with excellent agreement, showing minimal sensitivity in both displacement and acceleration responses. Conversely, unrealistically low values (e.g.,

SS = 0.05) led to premature detachment and an overestimation of the deformation demand, confirming the stabilising role of this parameter.

Additional analyses on mesh discretisation revealed that coarser models require proportionally higher separation strain values to reproduce equivalent damage patterns, due to the reduced number of potential cracking interfaces. Similarly, the stiffness and material type of contact interfaces were found to significantly influence the extent of damage and energy dissipation, with mortar-type interfaces providing a closer match to experimental observations than homogeneous masonry connections.

Overall, these findings confirm that the proposed modelling strategy is numerically stable and physically consistent, as moderate perturbations of the main parameters do not substantially alter the global failure mechanism or the overall seismic response. The AEM model thus proves to be a robust predictive tool for assessing the dynamic behaviour of masonry vaults, capable of capturing both global deformation and local cracking mechanisms with satisfactory accuracy.

Nevertheless, the study also highlights the need for further experimental investigations on full-scale vaults up to collapse, which would enable a more precise calibration of post-cracking and failure parameters and strengthen the general validity of the adopted numerical approach. In addition, tests on larger-span vaults would be valuable to investigate potential scale effects associated with the use of coarser mesh discretisation, helping to clarify whether the mechanical behaviour and sensitivity trends observed in small-scale models remain consistent at architectural scale. Similarly, experimental campaigns on different typologies of vaults, such as barrel, cloister, and ribbed vaults, would provide a broader validation basis and support the generalisation of the modelling strategy to a wider range of masonry configurations.

6 VAULTS SEISMIC VULNERABILITY

The study of vaults represents a crucial step in understanding the seismic and structural vulnerability of historical masonry churches. This chapter examines the mechanical behaviour and inherent weaknesses of vaulted systems, emphasizing how geometry, materials, and construction history interact to determine their stability. The discussion unfolds progressively:

- first, by framing the general principles of masonry vulnerability and the architectural role of vaults within church structures;
- then, through emblematic case studies that illustrate different sources of vulnerability, static degradation (Pavia Cathedral), seismic excitation (Basilica of St. Francis in Assisi), and induced seismicity (Groningen region);
- and finally, by synthesizing how these examples highlight the complex relationship between structural efficiency, long-term deterioration, and heritage preservation.

6.1 INTRODUCTION

Masonry architecture represents one of the most enduring and expressive forms of construction in Europe, yet it also ranks among the most vulnerable when exposed to environmental degradation, aging, or dynamic actions. Historical buildings embody centuries of cultural and technical evolution, but the intrinsic limitations of their materials, the empirical nature of their construction processes, and the cumulative impact of later modifications have often reduced their structural capacity (Croci, 1998b; Heyman, 1995).

This condition is particularly evident in churches, where architectural ambition was often expressed through large spans, slender piers, and heavy roofing systems, all built with a material fundamentally lacking tensile strength. These structures, although aesthetically magnificent, are maintained in a delicate equilibrium between thrust and resistance, where minimal distortions or differential movements may cause significant instability.

Within this architectural context, vaulted systems occupy a special position. Arches, cross vaults, and domes are not only symbols of artistic ingenuity but also essential structural components that ensure the spatial and mechanical coherence of churches by transferring forces mainly through compression. However, their stability is highly

sensitive to geometric imperfections, foundation settlements, material decay, and horizontal displacements, all of which may lead to cracking, progressive deformation, or even collapse(Block, 2009; Huerta, 2001). Vaults therefore represent both the strength and the weakness of historical churches: they contribute to overall equilibrium while remaining among the most structurally exposed components.

This duality explains why vaulted systems have become a central focus of research in seismic engineering and heritage preservation. The following sections address the vulnerability of these systems under both static and dynamic conditions through emblematic case studies, beginning with the dome of Pavia Cathedral and the collapse of the adjacent Civic Tower, continuing with the Basilica of St. Francis of Assisi, and concluding with the effects of induced seismicity on historic churches in the Groningen region.

6.1.1 Masonry churches and vaulted system

Unreinforced masonry (URM) buildings exhibit limited tensile strength and poor energy dissipation, which make them intrinsically vulnerable to both static and dynamic actions (D'Ayala & Speranza, 2003; Lourenço et al., 2013). This vulnerability is amplified in ecclesiastical architecture, where large spans, slender supports, and massive roofs were designed with little or no awareness of horizontal actions (Magenes, 2006).

Post-earthquake surveys, such as those following the 2009 L'Aquila and 2016 Central Italy earthquakes, confirmed the high damage rate in churches, with frequent façade collapses, overturning of gables, and vault failures (Canuti et al., 2021; Penna et al., 2019). Predictive studies further indicate that Renaissance and Baroque churches, with complex vaulted systems, are significantly more vulnerable than simpler medieval naves (Gianfranco De Matteis et al., 2019).

A church can be viewed as an assemblage of macro-elements—façade, nave, transept, apse, bell tower, and dome, interconnected by arches and vaults. These components ensure spatial unity but also introduce horizontal thrusts that must be restrained by tie-rods, buttresses, or thick supporting walls. When these restraints are insufficient or deteriorated, local mechanisms such as façade overturning or vault collapse easily develop. Similar weaknesses have been documented in territorial studies: vulnerability mapping in Coimbra (Portugal) and Vittorio Veneto (northeastern Italy) linked deformable diaphragms, irregular aggregations, and poor masonry quality to higher seismic susceptibility (Bernardini et al., 2008; Vicente et al., 2011).

Within this framework, vaulted systems play a decisive structural role. Arches, cross vaults, and domes ensure the transfer of vertical loads by compression but rely on precise geometric balance and consistent boundary conditions. In real constructions, irregular geometry, differential settlements, and heterogeneous materials frequently disturb this equilibrium, promoting cracking, joint opening, and progressive deformation (Block, 2009; Huerta, 2001).

Vaults thus embody both the continuity and the vulnerability of historical churches. Their geometry favours stability under gravity loads but makes them extremely sensitive to imposed displacements and dynamic excitation. Over time, creep and material decay can reduce curvature and increase horizontal thrusts, further compromising their safety. Recent research, including discontinuum approaches such as the Distinct Element Method, has improved the understanding of local instability mechanisms and of the role played by frictional contact and block separation (Furiosi et al., 2024).

In parallel, strengthening techniques with limited architectural impact, such as thin extrados coatings, fibre-reinforced polymers, or compatible composite systems, have gained importance as viable solutions to enhance structural safety without altering the artistic or symbolic identity of the monuments.

Taken together, these findings depict a structural typology where mechanical efficiency and cultural significance coexist in delicate equilibrium, a balance that, when altered, exposes churches to progressive and often unpredictable forms of vulnerability. Such intrinsic conditions explain why severe damage or even collapse may occur without any seismic excitation, as a result of accumulated material decay, geometric distortion, and the absence of effective restraint systems.

A paradigmatic example of this phenomenon is offered by the Cathedral of Pavia, where the collapse of the adjacent Civic Tower in 1989 unexpectedly revealed the hidden vulnerability of the dome and its supporting structures.

6.1.2 The case of dome of Pavia Cathedral and the 1989 Civic Tower collapse

The Cathedral of Pavia proves how critical structural conditions can develop in large masonry vaults solely due to long-term degradation, construction heterogeneity, and cumulative static effects, even in the absence of seismic excitation. Built over more than five centuries, the Cathedral evolved through successive and discontinuous construction phases, marked by long interruptions, changes in designers, and the use of

materials with significantly different mechanical characteristics. As a result, the structural behaviour of the central octagon progressively diverged from any coherent or unified conception originally intended for the monument.

(a) (b)

Figure 6.1 Cathedral of Pavia (Italy) external view (a), internal view of the dome (b) (Calvi & Palenzona, 2013)

On 17 March 1989, the Civic Tower adjacent to the Cathedral suddenly collapsed, causing casualties and severe damage to the northern nave (Figure 1.2). Although the dome was not directly impacted by the falling debris, the event triggered a comprehensive programme of inspections that exposed a widespread and pre-existing condition of structural distress involving the piers, the drum, and the dome itself. The piers, which carried the entire load of the dome, displayed through-cracks up to 60 mm wide on the western side, while the marble facing showed significant detachment and local failures. These deficiencies were particularly critical because the octagonal piers, constructed over more than a century and subsequently loaded by the nineteenth-century drum and dome, adding approximately 20,000 tons to the structure, were never designed as a unified system but rather as the product of fragmented construction phases, variable workmanship and incompatible materials.

The drum had been structurally weakened by the insertion of sixteen monofora windows, which considerably reduced its effective resisting section. Moreover, the nineteenth-century dome designed by Maciachini (1882–1885) was added without a comprehensive analytical evaluation of its effects on the existing structure. Archival evidence indicates that the rupture of a tension chain observed at the time already reflected excessive stresses induced by the gradual settlement of one of the main piers. Subsequent modifications further altered the global equilibrium: the demolition of two massive masonry walls that originally closed the north and south sides of the octagon,

and effectively acted as internal buttresses contributing to the lateral containment of the dome, introduced a further imbalance in the horizontal thrust system.

Beyond these issues affecting the supporting elements, the dome itself exhibited a severe and well-developed cracking pattern, characterized by continuous subvertical fissures along its primary meridians. In several locations, these cracks extended through the full thickness of the masonry, indicating a loss of continuity of the meridional compression-ring mechanism and the inability of the dome to withstand the excessive tensile stresses generated by centuries of differential settlement, deformation incompatibilities among structural components, and alterations of the original static scheme. This progressive loss of cooperation between the concentric masonry rings significantly reduced the dome's ability to redistribute meridional compressive forces, marking a condition of advanced structural vulnerability.

(a) (b)

Figure 6.2 Cathedral of Pavia (Italy): debris-removal operations following the collapse of the Civic Tower (a), and base of the Civic Tower after the clearing operations (b) (Calvi & Palenzona, 2013)

(a) (b)

Figure 6.3 Cathedral of Pavia (Italy) cracking pattern on triangular vault adjacent to the central octagon (a) and on the major arch of the octagon (b) (Calvi & Palenzona, 2013)

6.1.2.1 Monitoring, emergency measures and early diagnosis (1989-1996)

Concerns regarding the safety of the Cathedral and the potential risk of a progressive collapse raised after the collapse of the Civic Tower. A commission were named by the Ministry of Civil Protection to investigate the causes of the failure and to assess the structural condition of the Cathedral. The Commission implemented a continuous, real-time monitoring programme to detect any signs of accelerated deformation or crack propagation, given the extensive fissuring already present in the octagon and the dome.

Highly sensitive instruments recorded structural deformations and crack evolution around the clock, transmitting data via radio to a dedicated processing centre at the Department of Structural Mechanics of the University of Pavia. This unprecedented monitoring campaign made it possible to identify the most active deformation mechanisms, to quantify the sensitivity of the structure to environmental and loading variations, and to design subsequent strengthening solutions based on quantitative evidence. The system ensured safe use of the Cathedral until 1996, while providing early-warning capability and supporting the preventive conservation strategy.

6.1.2.2 Social perception and impact on the local community

In 1996, the Cathedral was closed to the public due to the detachment of marble fragments from considerable height, an event perceived by the population as a sign of an impending collapse spreading anxiety among the citizens of Pavia. The closure severely impacted the religious and civic life of the city. As (Calvi & Palenzona, 2013) note, it caused "severe discomfort for the faithful, for the Chapter, and for the entire community." Until 2011, liturgical functions were relocated and the community lost one of its most

important symbolic sites, demonstrating how this event influenced also social identity and community.

6.1.2.3 Final considerations

The collapse of the Civic Tower reveals a latent condition of structural fragility that had developed over centuries because of cumulative degradation, incompatible construction phases, and alterations of the original static scheme.

The extensive programme of structural retrofitting that involved the octagonal piers, the drum, and the dome, will be discussed in Chapter 7, where strengthening measures of the Cathedral are examined in detail.

6.1.3 Seismic vulnerability of masonry vaults

The seismic assessment of masonry vaults represents one of the most critical issues in the preservation of historic churches. Vaults behave primarily in compression, and their stability is strongly dependent by geometry, boundary conditions, and construction details. Post-earthquake surveys have shown that vaults often activate independent collapse mechanisms, behaving as macro elements whose response is only partially influenced by the global structural system (Lagomarsino, 1998).

Typical seismic damage includes longitudinal and transversal cracking of the vault surfaces, detachment from stiffening arches, and progressive hinge formation at the springers, which may culminate in the sudden collapse of entire bays. Such mechanisms were systematically codified in the methodology proposed by (Lagomarsino & Podestà, 2004a), where vaults of the nave, transept, apse, and presbytery were explicitly listed among the eighteen most recurrent collapse mechanisms in churches. The accompanying statistical study, based on more than 3,000 churches damaged in the 1997 Umbria–Marche earthquake, confirmed that vaults rank among the most frequently and severely damaged macro elements, with a significant proportion of failures observed even at moderate macro seismic intensities (Lagomarsino & Podestà, 2004b).

Several intrinsic weaknesses aggravate this vulnerability. Thin or lowered vault geometries, the presence of lunettes and large openings, and additional concentrated loads from the roof covering increase the probability of instability. The lack of transverse and longitudinal tie-rods is particularly detrimental, as their absence correlates with a dramatic increase in the incidence of vault failures under seismic excitation. The effectiveness of such devices was statistically demonstrated in the Umbria–Marche

database, where the presence of tie-rods significantly reduced the damage in both façade overturning mechanisms and in the transversal vibration of naves, which directly affects the vaults (Lagomarsino & Podestà, 2004b).

International case studies corroborate these findings: in the 2003 Bam earthquake, for instance, the collapse of vaults and domes was widespread, often leaving the vertical walls still standing, thus underlining their role as structurally vulnerable elements under dynamic actions (Mahdi, 2017). he importance of vaults within the overall vulnerability of churches is further highlighted in (National Civil Protection Service, 2013), , which identifies 28 typical seismic collapse mechanisms, of which as many as seven are directly related to vaulted systems, including those of the nave, side aisles, transept, presbytery, and chapels. This disproportionate representation underlines the structural centrality and susceptibility of vaults, whose failure often triggers severe local collapses with catastrophic cultural consequences. The presence of large spans and heavy masses, and the lack of effective confinement make vaults and domes considered intrinsically vulnerable, (ICOMOS-ISCS, 2023). Pavia Cathedral is an example of geometric and material vulnerability, while the Basilica of San Francis of Assisi demonstrates the seismic vulnerability of vaulted systems, when frescoed vaulted collapsed during the earthquake occurred in 1997.

Masonry vaults represent one of the most vulnerable components when an earthquake occurs. Their vulnerability is also affected by geometry of the structure, construction techniques, boundary conditions and mechanical properties of masonry itself (lack of tensile strength, heterogeneity). Any comprehensive seismic assessment of historic churches must give specific attention to the history of structure and construction phases, combining detailed survey data with vulnerability indicators, in order to develop strengthening interventions which are reversable and compatible from the architectural point of view and structurally efficient.

6.1.4 The case of the Basilica of St. Francis of Assisi

On 26 September 1997, two strong earthquakes struck central Italy, with magnitudes of M_w 5.7 and M_w 6.0, occurring at 02:33 a.m. and 11:40 a.m., respectively. Both events were located near Colfiorito, along the Umbria–Marche boundary, where two normal faults with opposite directivity were activated (Istituto Nazionale di Geofisica e Vulcanologia – INGV, 2017). The 1997 Umbria–Marche sequence represented a turning point for Italian seismology: it was the first seismic crisis for which high-quality ground-based and satellite data were available, allowing for an unprecedented definition of fault

geometry and rupture mechanisms. Over the following months, more than 6,000 aftershocks were recorded, including seven main events of magnitude between M_w 5.0 and M_w 6.0, which activated a fault system extending roughly 45 km along the Apennine chain (Antonioli et al., 2005; Miller et al., 2004).

(a) (b)

Figure 6.4 Basilica of St. Francis of Assisi (Italy) external view (a), internal view of the vaults (b)

The second shock (M_w 6.0) severely affected the town of Assisi and caused the collapse of two frescoed cross-vaults in the Upper Basilica of San Francesco. Two Franciscan friars and two technicians of the Superintendency were killed instantly while performing post-event inspections. The dramatic collapse, captured on video and broadcast worldwide, exposed both the human and cultural dimension of the disaster and soon became a symbol of the seismic fragility of Italy's architectural heritage (Dipartimento della Protezione Civile, 2023).

Figure 6.5 Basilica of St. Francis of Assisi collapse of masonry frescoed vaults

The seismic sequence left the remaining vaults in a highly compromised state, characterized by widespread cracking, permanent deformations, and a marked loss of curvature (Croci, 1998a, 1998b). Structurally, the failures occurred in two critical areas, near the façade and at the transept crossing, where the nave behaved as a horizontally restrained beam, Figure 6.6 (Croci, 2001). Under the combined effects of self-weight and horizontal acceleration, bending and shear stresses concentrated at the springing zones. Numerical analyses showed that, under accelerations close to 0.2 g, tensile stresses in the ribs exceeded the masonry's limited tensile capacity, and the reduced curvature could no longer ensure equilibrium (Croci, 1998b).

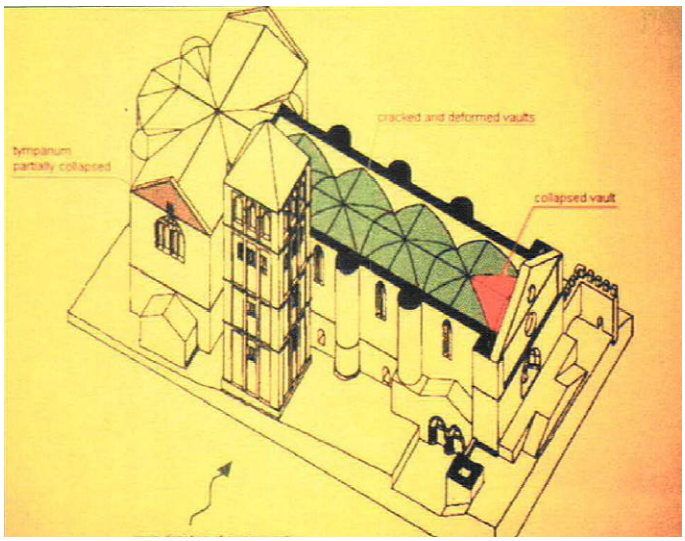

Figure 6.6 The collapsed vaults (one is hidden behind the bell tower) and the damaged tympanum of the Basilica of St. Francis of Assisi

A decisive factor contributing to the collapse was the presence of a large volume of incoherent fill material, rubble and fragments from centuries of roof repairs, accumulated above the vault springers. This material not only increased vertical loads but also behaved unfavorably during seismic shaking, amplifying deformations and promoting the formation of hinges and rib failures (Croci, 1998a). Emergency stabilization was carried out immediately after the event. The operations included the removal of the fill, injection of salt-free mortars into cracks, application of synthetic-fibre bands on the extrados, and suspension of the vaults from the roof structure using steel tie-bars equipped with springs to maintain constant tension and avoid over-stressing the frescoes. Later, light Kevlar composite ribs were added to the extrados to enhance stiffness while preserving reversibility and compatibility with the historic materials.

Subsequent analyses placed the collapse within the broader structural evolution of the Basilica.

The interventions on roof in 1958, during which the original timber elements were replaced with reinforced concrete purlins, and ring beams and rigid slabs were added, altered the dynamic behaviour of the structure increasing both stiffness and mass, shortening the fundamental period by more than 60 % and amplifying seismic demand on the façade and transept, precisely where the collapses occurred (Arcidiacono et al., 2016). The intrinsic Gothic vaults vulnerability and the incompatible retrofitting measures resulted in a dramatic failure in 1997.

Figure 6.7 Cracks and deformations in the vaults with relative displacements till 30 cm *(Croci, 2000)*

After this significant seismic event, the Dipartimento della Protezione Civile established a special commissioner for cultural assets and introduced new operational protocols for post-earthquake heritage management. The subsequent restoration involved the recovery of approximately 300,000 fragments of frescoed plaster, requiring eight years, 160,000 working hours, and an investment of about € 6.5 million. Completed in April 2006, the restoration became a benchmark for the integration of structural safety and artistic conservation (FireRiskHeritage Project, 2010; OFMConv – Order of Friars Minor Conventual, 2022).

The 1997 Assisi earthquake highlighted how vulnerability of masonry vaults is governed by geometric irregularities, cumulative cracking, added mass, and inappropriate strengthening choices. It also demonstrates the need of reversible, lightweight, and compatible interventions to respect both the structural integrity and the artistic value.

6.2 INDUCED SEISMICITY AND MASONRY VAULTS: THE GRONINGEN CASE

The region of Groningen, in the northern Netherlands, is not considered as a seismic prone area; in spite of that, the effects of induced seismicity on unreinforced masonry churches are of comparable significance. For centuries constructions were not designed accounting for seismic action. Architectural and structural traditions therefore evolved with no awareness of horizontal forces or ductile detailing requirements, resulting in buildings designed solely for vertical loads.

Seismicity in the Netherlands arose from gas extraction from the Groningen field in the early 1960s. Since then, more than 1,400 earthquakes have been recorded, most of them characterized by magnitudes below M_w 3.6 and low focal depths of about 3-5 km (Muntendam-Bos et al., 2022). Despite their limited magnitudes, these shallow events have produced strong surface accelerations, often exceeding 0.1-0.2 g. The result has been unexpectedly severe damage to historic unreinforced masonry buildings. These structures are often composed by slender walls, cavity walls with insufficient number of connectors, thin vaulted ceilings, without any tie-rods or ring beams which could have absorb vaults thrust. Recurrent low-intensity shaking caused cracks along the vault haunches and lunettes, detachment between ribs and supporting arches, and the gradual flattening of vaults geometry, damaging walls and promoting progressive instability (Van Elk et al., 2017).

After the Huizinge earthquake of 16th August 2012 (ML 3.6), extensive field surveys and tests investigations confirmed the vulnerability to cumulative low-amplitude shaking. Shake-table tests and numerical analyses on representative Groningen buildings showed that even peak ground accelerations of 0.1-0.2 g, when repeated over time, can cause stiffness degradation, permanent deformation, and local collapse of vault elements (Van Elk et al., 2017).

From a seismological perspective, gas withdrawal causes reservoir compaction and redistribution of stresses, progressively reactivating faults within the overburden. Statistical–geomechanical models developed by (Bourne & Oates, 2017) established an exponential correlation between cumulative reservoir strain and seismic activity rate, consistent with the progressive failure of a heterogeneous fault network. These models underpin the Probabilistic Seismic Hazard and Risk Assessments (PSHRA) conducted under the NAM research programme, which quantified expected peak ground accelerations up to 0.2 g for exceedance probabilities of 0.2 % per year (Van Elk et al., 2017).

Complementary work by (Bommer et al., 2016) developed a ground-motion prediction model tailored to Groningen, based on over eighty local accelerometric recordings. The study showed that the combination of very soft soils (Vs_{30}≈180-210 m/s) and shallow focal depths produces both high spectral amplifications and long shaking durations. These site effects notably increase the dynamic demand on non-ductile masonry systems such as vaults, where low-frequency resonance may amplify out-of-plane displacements and contribute to local collapse mechanisms.

To address these risks, the Nederlandse Aardolie Maatschappij (NAM) and the Dutch government established extensive research and mitigation programme, including the Earthquake Damage Centre (EDC) and the Knowledge Platform for Structural Safety (KPST) (Van Elk et al., 2017). These initiatives integrate continuous structural monitoring, digital surveying, and experimental testing on representative vault typologies to calibrate numerical models and refine fragility assessments.

The need for an interdisciplinary approach in risk management is clear and needs a combination of engineering, conservation, and social acceptance. The restoration of historic churches in Groningen has triggered broad discussions among engineers, heritage authorities, and local communities on how to reconcile safety requirements with cultural identity, an issue that mirrors the debates long familiar in seismic regions such as central Italy.

6.3 CONCLUSIONS

Vulnerability of vaulted system arises from the same intrinsic characteristics: compressive behaviour, geometric sensitivity, and the absence of tensile resistance. All the case studies analysed, Pavia, Assisi and Groningen, show that masonry vaults are susceptible to both static degradation and dynamic excitation, whether natural or induced. Their preservation requires a holistic approach, which should integrate material knowledge, continuous monitoring, and preventive conservation, while respecting their artistic and symbolic significance. Any intervention must therefore pursue compatibility, reversibility, and minimal visual impact, ensuring that mechanical efficiency is enhanced without compromising authenticity or aesthetic value.

These principles furnish the foundation for the contemporary approach to strengthening historical vaults, which will be examined in detail in Chapter 7, where advanced retrofitting techniques and performance assessment methods are presented as part of a broader strategy aimed at safeguarding the architectural and cultural identity of Europe's masonry heritage.

7 MASONRY VAULTS: RETROFITTING SOLUTIONS

Masonry vaults represent some of the most emblematic and structurally vulnerable components of historic buildings. Their preservation requires strengthening strategies that reconcile mechanical effectiveness with material compatibility, reversibility, and architectural integrity. Building upon the vulnerability assessment developed in the previous chapter, this chapter examines the evolution, application, and experimental validation of retrofitting solutions for masonry vaults, with the overarching aim of aligning structural safety with conservation principles.

Section 7.1 provides an in-depth examination of strengthening approaches developed from the Middle Ages to contemporary conservation engineering. Traditional measures, such as iron tie rods, reinforced concrete overlays or ring beams, and steel frames, are discussed in terms of their structural role, mechanical performance, conservation compatibility, and limitations. Particular emphasis is placed on how these techniques interact with the funicular behaviour of masonry and with the boundary conditions that control thrust distribution. This historical overview sets the stage for the introduction of composite materials (FRP, FRCM/TRM, SRG), whose development marks a paradigm shift from strengthening by stiffness and added mass toward strengthening by compatibility and distributed tensile capacity. The section concludes with an assessment of numerical modelling strategies used to simulate the behaviour of both unreinforced and strengthened vaults, highlighting the central role of interface modelling and experimentally validated approaches.

Section 7.2 applies this theoretical framework to two monumental structures that exemplify distinct strengthening philosophies. The Cathedral of Pavia illustrates a preventive, long-term consolidation strategy addressing cumulative damage, material degradation, and evolving boundary conditions in a non-seismic context. In contrast, the Basilica of St. Francis of Assisi represents a corrective, post-seismic intervention following the 1997 Umbria–Marche earthquake. Here, the integration of advanced composite ribs, prestressed steel belts, and smart devices demonstrates how structural safety, artistic preservation, and reversibility can be pursued simultaneously. Together, these two case studies offer complementary perspectives on how modern strengthening principles are adapted to different structural conditions, levels of urgency, and conservation constraints, with particular attention to the rehabilitation of boundary conditions and the preservation of thrust-based load transfer.

Section 7.3 introduces the numerical validation of TRM/FRCM strengthening measures at the component scale. This section consolidates the experimental and numerical evidence obtained from reinforced masonry walls and arches, providing a physically grounded calibration of material properties, interface behaviour, and modelling assumptions. These intermediate validations demonstrate the capability of the Applied Element Method to reproduce bond-dependent mechanisms and to capture the transition from local interaction between textile and substrate to global structural response. As such, they establish the methodological basis for extending the modelling framework to full-scale vaulted systems.

Section 7.4 shifts the focus from in-situ applications to controlled experimental validation. It examines the seismic behaviour of a full-scale masonry cross vault strengthened with a TRM system and tested at the Laboratório Nacional de Engenharia Civil (LNEC) within the SERA project. After a brief recall of the unreinforced configuration, modelled and validated in Chapter 4, the analysis concentrates on the retrofitted specimen. The section presents the modelling assumptions, dynamic response, crack evolution, and comparison with experimental data, demonstrating the capacity of the Applied Element Method (AEM) to reproduce the enhanced performance induced by the strengthening system. A final comparative discussion situates AEM within the broader landscape of FEM and DEM formulations that have simulated the same benchmark experiment, emphasising the trade-offs between physical fidelity, computational efficiency, and the representation of cracking and interface behaviour.

Overall, the chapter provides a comprehensive exploration of strengthening solutions for masonry vaults, bridging historical practice, real-world interventions, and advanced numerical–experimental validation. This multi-scale perspective establishes the methodological foundation for assessing the seismic performance of retrofitted vaulted systems and for guiding future conservation-oriented engineering applications.

7.1 LITERATURE REVIEW

7.1.1 Traditional strengthening methods before composite materials

Before the widespread use of advanced composite systems such as FRP and FRCM, the strengthening of masonry vaults relied on a limited set of conventional solutions developed through empirical knowledge and practical experience. These interventions, tie rods and chains, reinforced concrete overlays or ring beams, and steel frames or trusses represent important stages in the historical evolution of consolidation practice.

They also reflect different conceptual models of masonry behaviour, ranging from passive thrust containment to enforced monolithic action. However, their effectiveness has often been compromised by issues of compatibility, reversibility, and long-term durability, as well as by their tendency to disrupt the funicular, compression-dominated behaviour of masonry. These limitations progressively motivated a shift toward lighter, more deformable, and mechanically compatible materials.

7.1.1.1 Iron tie rods and chains

Among the earliest and most widespread strengthening measures, iron tie rods were employed to counteract the horizontal thrusts produced by arches and vaults, as illustrates in Figure 4.2. Acting as tensile elements, they close the structural ring, maintaining the line of thrust within the masonry thickness and thus preventing the formation of plastic hinges at the supports (Heyman, 1995; Huerta, 2001).

7.1.1.1.1 Structural role and historical development

Tie rods operate as passive tensile members that close the structural ring of arches and vaults, counteracting horizontal thrusts that would otherwise induce rotation at the supports or the opening of hinges. The practice dates back to the late Middle Ages and became particularly widespread in the Renaissance and Baroque periods, especially in large-span churches where the lateral containment offered by walls was insufficient.

In their simplest form, tie rods are forged iron bars anchored at both springing points and occasionally connected through visible plates or decorative devices. Chains, often embedded within the masonry or located at attic level, provide a similar function on a larger scale, tying together multiple arches or an entire bay system.

(a) (b)

Figure 7.1 Example of ties at the intrados of the vaults (a) and an anchorage detail (b) (Santa Monica, Cremona – Italy, project by Studio Calvi)

(Heyman, 1995) demonstrated that the introduction of tie rods allows an arch to achieve static equilibrium with reduced horizontal thrusts, keeping the internal forces fully compressive. This “closed arch” configuration is the geometric and mechanical foundation for the stability of many historical vaults.

7.1.1.1.2 Mechanical behaviour and performance

From a structural standpoint, tie rods act in tension while the masonry remains in compression. When properly tensioned, they compensate for the lack of tensile strength of the masonry and limit horizontal displacements at the imposts. Their function is purely kinematic containment, without significantly altering the internal stress distribution of the vault. However, their performance depends on several factors:

- Anchorage conditions, which must ensure effective transfer of tensile forces without damaging the surrounding masonry;
- Material properties and corrosion: loss of cross-section over time reduces tensile capacity;
- Prestress and monitoring: loss of tension due to thermal or long-term effects can compromise their efficiency.

(Croci, 1998b) emphasized that tie rods should always be installed in correspondence with the line of thrust to minimize secondary bending. When positioned too high or too low, they may induce eccentric loads and cause local cracking.

From a seismic perspective, however, their contribution is inherently directional and limited. Tie rods primarily restrain horizontal spreading along their axis and do not, by themselves, provide significant energy dissipation or control of out-of-plane mechanisms. Their effectiveness therefore depends not only on correct positioning with respect to the thrust line but also on the overall three-dimensional behaviour of the vault system and its supports. In buildings with complex geometries or irregular boundary conditions, tie rods may stabilise selected thrust directions while leaving other potential mechanisms essentially unrestrained.

7.1.1.1.3 Variant and construction practice

Historically, several configurations were developed to adapt to different architectural needs:

- Single tie rods aligned with the impost level, directly connecting the springing points of arches;

- Continuous chains linking successive arches along a nave, forming a horizontal restraining network;
- Braced systems where rods were combined with wooden or steel elements to counter both thrust and torsion;
- Hidden ties embedded within attics or masonry, used where visible elements were unacceptable for aesthetic reasons.

These systems were often combined with masonry reinforcements or metallic anchors to improve the overall box behaviour of the structure.

7.1.1.1.4 Seismic and conservation aspects

Under seismic actions, tie rods can limit the opening of cracks and control relative displacements between structural parts, but they are not designed for energy dissipation or to counter out-of-plane mechanisms. (D'Ayala & Speranza, 2003) showed that while tie rods can delay collapse by restraining lateral thrusts, their contribution to seismic safety remains marginal unless integrated with global strengthening strategies.

Tie rods represent a compatible and reversible reinforcement solution. Their installation typically requires minimal alteration to the historic structure, and they can be removed or re-tensioned without irreversible interventions. Nonetheless, an improper installation or an excessive tension may cause localized crushing at anchorage points; furthermore, their visible aesthetic intrusion, particularly in decorated interiors, is not always accepted.

Nowadays, the use of stainless steel or composite tie system is recommended, combining traditional mechanical principles with improved durability.

7.1.1.1.5 Considerations

Iron tie rods and chains represent a flexible solution which closely follows the structural logic of masonry: equilibrium through compression and confinement rather than stiffness. Their advantages include simplicity, reversibility, and mechanical compatibility, making them a reference model for later tensile-based reinforcements such as FRP or FRCM strips.

However, their effectiveness is limited to a single thrust direction, makes them inadequate in complex vault geometries or under dynamic excitation, where multi-axial restraint and ductile behaviour are needed. As a result, while they remain an essential component of heritage strengthening strategies, they are now complemented or

replaced by more versatile composite systems capable of providing continuous and distributed tensile reinforcement.

It is worth it to underline that loss of tension due to creep, relaxation, thermal cycles, or construction inaccuracies can significantly reduce their effectiveness over time. In many heritage structures, the absence of systematic monitoring makes it difficult to quantify their actual contribution to safety.

7.1.1.2 Reinforced concrete overlays and ring beams

During the 20th century, reinforced concrete (RC) started to be employed for the strengthening of masonry vaults and domes, particularly in Italy following the major earthquakes of Friuli (1976), Irpinia (1980), and Umbria-Marche (1997). The main retrofitting idea was that by increasing stiffness and guaranteeing a monolithic behaviour, the structure would be able to sustain higher loads and limit deformations. In practice, this philosophy often led to a radical modification of the original structural behaviour of masonry vaults.

Within the RC strengthening measures, the RC overlays and RC ring beams were the most widespread.

7.1.1.2.1 Reinforced concrete overlays (rigid crowns)

In many post-war restorations, RC overlays, thin slabs or shells, were cast directly on the extrados of vaults or domes. The aim was to stiffen the structure, improving its flexural resistance and preventing deformation at the haunches.

Such overlays typically consisted of a 4-8 cm thick RC layer, often with light steel reinforcement, bonded to the masonry surface and connected through metallic dowels.

(a) (b)

Figure 7.2 Example of RC overlay: reinforcement grid (a) and concrete pouring (b) (San Tommaso, University of Pavia, Pavia – Italy, supervision of works by Studio Calvi)

Mechanically, these interventions transformed the vault from a compressive structure governed by thrust-line equilibrium into a composite plate subjected to bending moments. Although they provided a short-term increase in load-bearing capacity, several studies and post-seismic assessments (Doglioni et al., 1994) revealed that:

- The added mass increased the seismic demand;
- The rigid diaphragm disrupted the natural thrust distribution;
- Incompatibility in stiffness, moisture absorption, and thermal expansion caused cracking and detachment.

This type of interventions is now considered rigid, irreversible, and mechanically incompatible with both the behaviour of masonry and the conservation principles of reversibility, compatibility, and minimal intervention, now codified in modern guidelines (Lagomarsino & Podestà, 2004a, 2004b).

7.1.1.2.2 Reinforced concrete ring beams

A second and equally widespread practice involved the insertion of reinforced concrete ring beams, linear RC elements placed at the top of masonry walls or at the springing of vaults. These RC beams were intended to act as continuous ties, counteracting the horizontal thrust of vaults and improving the box behaviour of the building (Giuffrè, 1993). Structurally, the RC ring beam behaves as a rigid tensile-flexural member that confines the walls and redistributes local thrusts. It serves three main functions:

- Containment of thrusts: acting as a rigid chain that closes the vault's springing line;
- Horizontal connection: linking parallel walls and tying the structure transversely;
- Load distribution: providing a uniform support for roofs or floors above the vaults.

Although conceptually similar to iron tie rods, ring beams differ profoundly in behaviour. Their high stiffness alters the deformation pattern of the vault and can generate stress concentrations or out-of-plane bending in the supporting walls.

Several post-earthquake investigations (Doglioni et al., 1994) have shown that massive or poorly connected RC ring beams often caused cracking and separation between the concrete and the masonry substrate. In seismic events, they sometimes amplified the overturning of walls rather than preventing it.

From a conservation standpoint, ring beams suffer from the same drawbacks as overlays: excessive rigidity, chemical and thermal incompatibility, and irreversibility.

Their use is now discouraged in heritage structures, where lighter and more compatible solutions, such as steel, FRP, or FRCM ring systems, can achieve the same confining effect without altering the original mechanical behaviour.

7.1.1.2.3 Considerations

Both types of RC intervention, overlays and ring beams, belong to the category of rigid strengthening systems. They pursue safety through stiffness and additional mass rather than compatibility and ductility. While they can be effective for short-term static strengthening, they are fundamentally inconsistent with the funicular and deformable nature of masonry vaults, which rely on compressive equilibrium and controlled deformation rather than flexural strength and forced monolithic action. In dynamic conditions, the increase in mass amplifies seismic demand, and the stiffness contrast with the underlying masonry gives rise to stress concentrations and interface damage.

For these reasons modern restoration approaches deem RC solutions suitable only for temporary stabilisation or for exceptional cases where no alternative can ensure safety. Its historical use marked anyway an important point in the evolution of strengthening techniques, because it created the base for more compatible materials, such as fibre-reinforced composites, which aim to supply tensile capacity without neglecting the geometric and compressive logic of masonry.

7.1.1.3 Steel frames

In parallel with the diffusion of reinforced concrete, the mid-twentieth century also witnessed extensive use of steel frameworks as a means to support, stabilize, or replace damaged masonry vaults and domes. Steel was considered a rational and technologically advanced material, lightweight, strong in tension, and easy to assemble, and therefore appeared well suited for the consolidation of historic structures that exhibited extensive cracking or partial collapse.

Early examples include the insertion of steel ribs at the intrados following the geometry of the vault, or trusses anchored to the surrounding walls at the extrados, designed to share or entirely carry the loads previously resisted by the masonry (Croci, 1998b; Giuffrè, 1993). In some cases, these frameworks were conceived as reversible external skeletons, while in others they were integrated into the masonry mass, effectively creating hybrid composite systems.

7.1.1.3.1 Structural function and configurations

The primary objective of steel interventions was to restore load paths and restrain thrusts where the masonry had lost its integrity. Three categories can be identified:

- Steel ribs or arches, placed at the intrados of the vault, acting as a secondary supporting structure, intended to relieve the masonry from tension.
- Trusses or frames, positioned above the vault, at the extrados, connecting the springing points and often coupled with tie rods, these systems confined spreading and provided a pseudo-thrust-resistant mechanism.
- Perimetral steel frames, installed at the impost or along the façade walls, aiming to restore the box-like behaviour of the building by tying together the vertical and curved elements.

Figure 7.3 Example of perimetral steel frame (Santa Monica, Cremona – Italy, project by Studio Calvi)

7.1.1.3.2 Performance and long-term issues

Despite their apparent effectiveness, many applications revealed serious limitations in the long term. The difference in stiffness between steel, which is ductile, and masonry, which is brittle, often induced uneven stress distributions and local cracks, particularly where rigid steel members were rigidly connected to uneven masonry substrates. (Croci, 1998b).

The corrosion of steel elements became a recurrent problem, in particular when moisture was present in the vault or dome. Where the steel frame carried a significant portion of the load, the masonry often experienced progressive detachment and loss of function, turning the vault into a passive shell. From the seismic perspective, partial or

non-symmetric connections sometimes introduced torsional effects and secondary mechanisms, rather than improving global stability. The resulting systems often lacked the flexibility required under dynamic loading, leading to brittle damage of the surrounding masonry.

7.1.1.3.3 Conservation and compatibility issues

Steel frame strengthening measures raised several concerns: on one hand their visual impact may not be accepted, especially where decorated and frescoed interiors are present; on the other hand, their mechanical properties are not fully compliant with the criteria of reversibility and material coherence (Croci, 1998b; Giuffrè, 1993). When dealing with steel elements maintenance is always an important issue: once integrated within the structure, steel frames may be difficult to inspect and maintain, often leading to hidden corrosion and progressive loss of performance.

Nevertheless, steel frames can provide valuable temporary shoring and emergency stabilization, offering non-invasive support during restoration works. In such cases, the metallic system acts as a temporary carrier, aligning more closely with conservation principles.

7.1.1.3.4 Conclusions

Steel frames and metallic trusses represent a transitional phase between traditional and modern strengthening techniques: an attempt to combine the tensile capacity of iron tie rods with the global stiffening effect of reinforced concrete, yet without the excessive weight of the latter. In practice, however, their long-term compatibility and aesthetic impact have limited their acceptance in conservation engineering.

These systems can be classified as semi-rigid strengthening measures, offering high tensile capacity but insufficient adaptability to the deformable behaviour of masonry vaults.

7.1.1.4 Critical assessment and lessons learned

The analysis of traditional strengthening techniques, tie rods, reinforced concrete overlays and ring beams, and steel frameworks, highlights a progressive evolution in the understanding of masonry behaviour, from empirical restraint toward engineered reinforcement.

Each method reflects the prevailing technological context and the conceptual model of the time: from the passive containment of iron elements to the rigid monolithic

behaviour introduced by concrete, and finally to the mechanical hybridization with steel frameworks. Traditional reinforcements therefore cover a spectrum from flexibility and reversibility to rigidity and intrusion. While iron tie rods embody the structural logic of masonry, strength through geometry and compression, reinforced concrete overlays and ring beams often disrupted this logic, replacing the thrust-based equilibrium with an artificial bending system. Steel frames represented a compromise, offering tensile capacity without the mass of concrete, yet introducing material incompatibilities and visual intrusion.

In historic vaults, strengthening is often less about reinforcing the curved surface than about restoring the boundary conditions that enable membrane action. The structural performance of arches, domes, and cross vaults is governed primarily by the ability of the supports, connections, and adjacent walls to constrain horizontal spreading and to preserve the geometry necessary for thrust-line equilibrium. For this reason, when dealing with vaults retrofit, the whole structure and how different elements interact with each other must be evaluated Traditional strengthening systems frequently underestimated this aspect, focusing on increasing local capacity rather than recovering global equilibrium. Modern conservation engineering recognises instead that the stability of a vault derives not only from the qualities of its curved geometry but from the integrity of the entire structural chain that contains and directs its thrusts.

7.1.1.4.1 Evolution of the design philosophy

The shift from empirical practice to analytical design during the twentieth century brought advances in safety but also new challenges. Early interventions sought to suppress deformation through rigid connections; later, attention moved toward controlling deformation while preserving the intrinsic compressive behaviour of masonry. This conceptual change parallels the growing awareness within conservation engineering that:

- An increase of the stiffness does not necessarily mean higher safety, especially under seismic loading conditions, where ductility and energy dissipation are critical.
- Compatibility and reversibility should be considered as fundamental design requirements.
- The structural autonomy of masonry, its capacity to carry loads through geometry, should be maintained rather than overridden by foreign materials.

7.1.1.4.2 Toward a new generation of reinforcements

The limitations of traditional techniques prompted the development of composite materials capable of reproducing the effects of tensile restraint while avoiding mass, rigidity, and incompatibility. Fibre-reinforced polymers (FRP), fabric-reinforced cementitious matrices (FRCM), and steel-reinforced grouts (SRG) emerged from this search for a middle ground: materials that can interact mechanically with masonry, remaining light, breathable, and reversible.

7.1.1.4.3 Concluding remarks

Traditional strengthening measures provided empirical solutions that ensured the survival of countless vaulted structures, and they remain invaluable for understanding the mechanics of heritage architecture. Their mechanical and material limitations, mainly excessive rigidity, added mass, and poor compatibility, have driven the search for innovative materials that align more closely with conservation principles.

The next section will therefore focus on composite strengthening techniques (FRP, FRCM, and SRG), which represent the contemporary stage of this evolution. These systems embody the same fundamental goal as tie rods, tensile reinforcement for thrust control, but achieve it through materials and methods fully compatible with the preservation of historic masonry.

7.1.2 Composite strengthening techniques

Fibre-reinforced composite materials marked a shift in the philosophy of strengthening historic masonry structures. Rather than imposing rigidity and mass, modern composites aim to supplement the deficient tensile capacity of masonry while preserving its compressive, thrust-based behaviour. These systems can be grouped as: Fibre-Reinforced Polymers (FRP), Fabric/Fibre-Reinforced Cementitious Matrix (FRCM or TRM), and Steel-Reinforced Grout (SRG). The main goal of these new retrofit measures is to provide a lightweight, distributed, and mechanically compatible reinforcement for arches, vaults, and walls, with minimal impact on architectural and physical integrity.

7.1.2.1 Fibre-Reinforced Polymers (FRP)

FRP systems were introduced in the late 1990s and consist of carbon, glass, aramid, or basalt fibres embedded in an epoxy resin matrix and externally bonded to the masonry substrate. Different studies (Anania et al., 2017; Basilio Sanchez, 2007; Valluzzi et al., 2013) demonstrated their ability to delay hinge formation and increase load-bearing

capacity, particularly when applied along the intrados or extrados of arches. Analytical and experimental research confirmed that FRPs can significantly enhance tensile strength and ductility, transforming the collapse mechanism from a four-hinge failure to a mixed flexural-debonding mode.

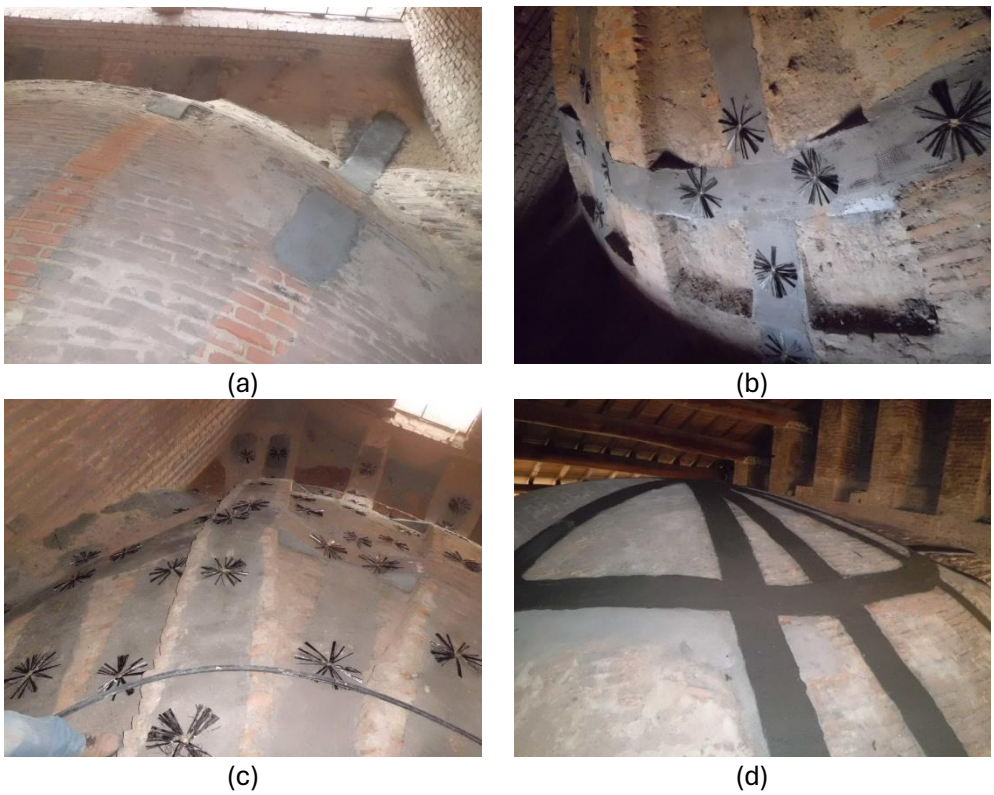

Figure 7.4 FRP application: preparation of the surface (a), application of mortar and net (b), connection with wraps (c), second layer of mortar (d), (Pavia Cathedral, Pavia – Italy, project by Studio Calvi)

However, the epoxy matrix presented serious drawbacks for cultural-heritage applications:

- lack of vapor permeability;
- incompatibility with humid or salt-contaminated substrates;
- limited reversibility and thermal resistance;
- risk of debonding under temperature or moisture variations (Carozzi & Poggi, 2015).

For these reasons, despite their mechanical efficiency, FRPs are now used mainly in non-decorated or non-heritage masonry.

7.1.2.2 Fibre-Reinforced Cementitious Matrix (FRCM/TRM)

The limitations observed in FRP systems, mainly related to the use of epoxy resins, led to the development of a second generation of composite materials known as Fabric- or Fibre-Reinforced Cementitious Matrix (FRCM or TRM) systems. In these solutions, the synthetic resin is replaced by a cement- or lime-based mortar, in which an open-mesh textile, typically made of carbon, basalt, glass, PBO, or steel fibres, is embedded.

This configuration produces a fully inorganic composite that is far more compatible with historic masonry, not only from a mechanical but also from a physical and chemical standpoint (Bellini et al., 2022; Cucuzza et al., 2022; Garmendia et al., 2015).

From a mechanical perspective, FRCM systems enhance the tensile strength of the vault while preserving its intrinsic deformability and funicular behaviour. Numerous experimental campaigns on arches and small-scale vaults (De Santis et al., 2019; Garmendia et al., 2015; Zampieri et al., 2018) have consistently demonstrated that the application of these reinforcements leads to a clear improvement in strength and ductility, with higher ultimate loads, delayed hinge formation, and a more progressive damage evolution compared to unreinforced specimens.

The typical collapse mechanism is no longer brittle, as in unreinforced masonry, but governed by controlled debonding or slippage at the interface between the textile and the mortar matrix.

(a)

(b)

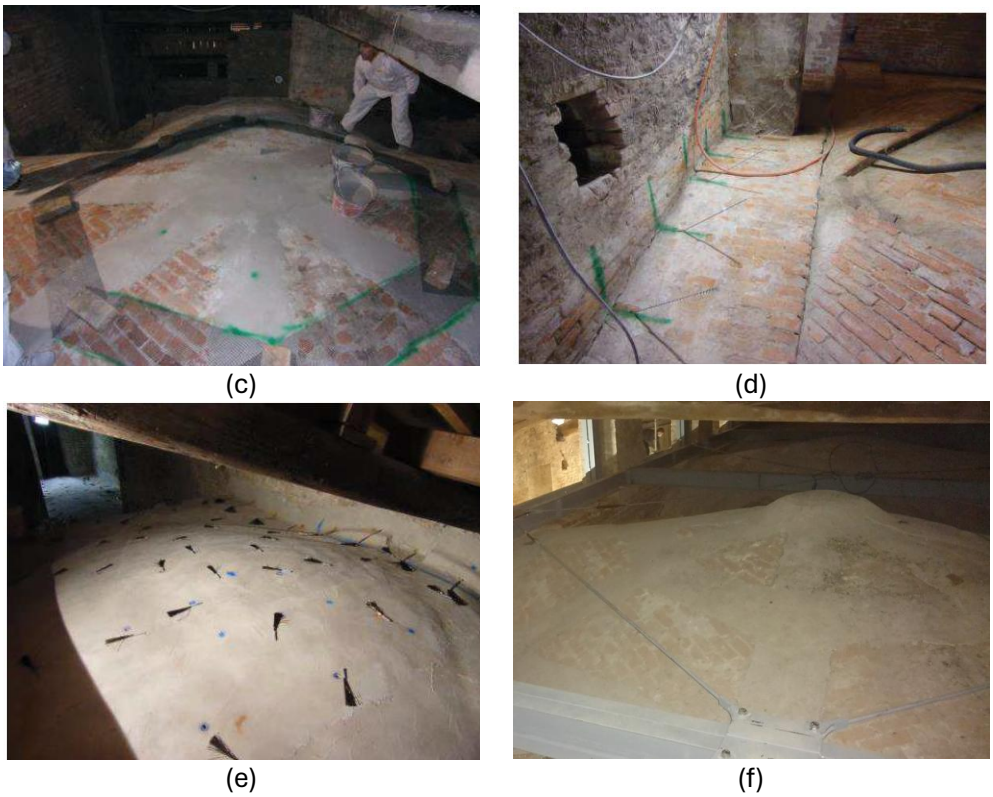

Figure 7.5 FRCM application: preparation of the surface (a), disposition of basalt fibres (b), first mortar layer (c), perimetral connection with helicoidal bars (d), basalt connetors (e) and final configuration (f) (Santa Monica, Cremona – Italy, project by Studio Calvi)

Tests on full-scale cross vaults and inter-storey vaults with backfill (De Santis et al., 2019) have also confirmed that FRCM layers, applied either at the intrados or extrados, contribute to both increase capacity and larger deflection at failure. The extrados configuration is generally preferred for architectural and conservation reasons, as it avoids direct contact with decorated surfaces while still providing effective confinement.

The bond behaviour of FRCM differs significantly from that of FRPs. The interaction between textile, matrix, and masonry substrate typically follows a nonlinear tri-linear stress–slip relationship, characterised by an initial elastic phase, a progressive cracking stage, and a final frictional regime governed by fibre pull-out (Focacci et al., 2017; Zampieri et al., 2018). This behaviour gives rise to a pseudo-ductile response, allowing the structure to dissipate energy without sudden loss of strength, and has motivated the formulation of dedicated cohesive-zone and interface models in numerical analyses

(Scacco et al., 2020). This bond–slip behaviour is strongly substrate-dependent: surface roughness, masonry quality, and curing conditions can significantly affect the effective stiffness, strength, and dissipative capacity of the system. As a consequence, FRCM performance cannot be regarded as an intrinsic material property but must be interpreted as a coupled response of textile, mortar, and substrate. This aspect has direct implications for both design and modelling, since interface parameters often govern the global effectiveness of the intervention as much as the nominal tensile capacity of the textile.

Beyond their mechanical efficiency, FRCM systems offer a series of practical advantages that make them particularly suitable for heritage applications: they are breathable, chemically compatible, and, to some extent, reversible, allowing future interventions or removals. Few limitations should be mentioned, such as the variability of bond performance depending on substrate roughness and curing conditions, and the uncertainties regarding long-term durability and environmental resistance (Cucuzza et al., 2022).

7.1.2.3 Steel-Reinforced Grout (SRG)

A further development is the use of unidirectional steel cords or strips embedded in inorganic grout, known as SRG systems. These materials combine the ductility of steel with the compatibility of mineral matrices, offering a hybrid solution for retrofitting vaults and arches.

Research by (Carozzi & Poggi, 2015; De Santis et al., 2019) demonstrated that SRGs provide higher ultimate capacity and improved bond performance compared to carbon or basalt FRCMs, although with increased weight and potential corrosion risk. Their behaviour under cyclic loading is particularly favourable, showing stable hysteretic response and limited degradation of bond stiffness. SRGs are especially suited for hidden or extradosal applications, where visual impact is not a concern but high tensile strength and fatigue resistance are required.

Despite these advantages, SRG systems also present potential drawbacks, including their greater weight compared with organic-matrix composites and the need to ensure long-term protection of the steel cords against corrosion. Their use is therefore most appropriate in hidden or extradosal applications, where visual impact is not a concern and where environmental conditions can be controlled or adequately mitigated.

7.1.2.4 Failure modes and design implications

Across all composite systems, the main failure modes include:

- debonding at the matrix–masonry interface;
- fibre slippage within the mortar;
- textile rupture or mortar cracking in the tensile zone;
- shear sliding near the supports under combined loading.

These mechanisms are a combination of shear, deboning, and tensile failure, which are governed by the quality of the bond and the orientation of fibre (Valluzzi et al., 2013; Zampieri et al., 2018). During the design process, particular attention should be put on anchorage length, matrix composition, and textile configuration in order to ensure a controlled and ductile response.

7.1.3 Numerical modelling approaches

Advanced numerical studies have increasingly focused on reproducing the mechanical response of both unreinforced and TRM-strengthened masonry vaults through meso- and macro-scale modelling techniques.

Continuum-based formulations and discrete-element approaches have been used to capture the nonlinear behaviour of masonry, including distributed cracking, joint opening, and interfacial slip, while maintaining computational efficiency and compatibility with large-scale geometries such as cross vaults and domes (Basilio Sanchez, 2007; Scacco et al., 2020).

In recent years, particular attention has been devoted to reproducing the shaking-table tests carried out at the Laboratório Nacional de Engenharia Civil (LNEC) on full-scale masonry cross vaults, both unreinforced and strengthened with TRM systems, (Bianchini et al., 2023, 2024). Among these, (Oktiovan et al., 2023) applied a distinct element micro-modelling approach to simulate the LNEC vault under dynamic loading, accurately reproducing the hinge formation and the stabilising contribution of the TRM reinforcement. Similarly, (Ferrante et al., 2024) conducted a comparative analysis between continuous and discrete strategies, confirming that both FEM and DEM frameworks can capture the beneficial effect of TRM overlays in limiting damage propagation and enhancing energy dissipation. Finally, (Kesavan et al., 2024) performed a detailed finite element micro-modelling of the same LNEC specimens within the SERA blind-prediction campaign, further validating the numerical representation of the TRM retrofitted configuration.

Together, these studies provide a comprehensive numerical benchmark for the dynamic assessment of TRM-strengthened vaults, demonstrating the ability of advanced models to capture the essential features observed experimentally, namely, the delay in hinge formation, reduction in residual displacements, and preservation of the masonry-like behaviour even after reinforcement. These findings form the basis for the dedicated discussion presented later in section7.4.

7.1.4 Heritage applications and conservations compatibility

The application of these solutions in several historic churches, including the Basilica of St. Francis of Assisi and the Cathedral of Pavia, highlighted that composite system are able to achieve the structural safety, while preserving their artistic value. Post-earthquake studies

7.1.5 Considerations

Composite materials represent a turning point in the strengthening of masonry vaults. They provide a direct continuation of the tensile-restraint philosophy introduced by iron tie rods but with a distributed, adaptive form of reinforcement. Their main achievements include:

- lightweight, non-invasive application;
- compatibility with masonry substrates;
- high tensile performance and crack control;
- potential for reversibility and aesthetic preservation.

Remaining challenges concern long-term durability, standardization of design procedures, and scale-dependent validation for large or ribbed vaults.

The stability of historic vaults is governed by thrust-line equilibrium, which can only be preserved if piers, walls, and connections retain adequate stiffness and continuity. This principle is central to both interventions discussed below, where the recovery of global boundary conditions proved as essential as the application of local reinforcement systems.

The principles emerging form the basis for interpreting real-world applications in the following case studies.

7.2 STRENGTHENING OF MASONRY VAULTS: CASE STUDIES

Starting from the vulnerability analysis presented in the previous chapter and on the different strengthening techniques shown in the previous section, the focus is now moved on two case studies, which are representative of all the critical aspects discussed so far: the Cathedral of Pavia, representing a case of progressive structural distress in large-span vaults affected by long-term deformation but not by seismic action; and the Basilica of St. Francis of Assisi, which embodies the challenges of post-seismic reconstruction following the 1997 Umbria–Marche earthquake.

Together, these monuments provide complementary perspectives on the strengthening of historic vaults. Pavia exemplifies preventive reinforcement aimed at stabilising an ageing structure through the rehabilitation of boundary conditions and minimally invasive, extradosal measures. Assisi, conversely, demonstrates corrective intervention after catastrophic seismic failure, combining modern composite materials and smart devices with strict conservation requirements.

The description of the diagnostic investigations, intervention strategies, and strengthening techniques adopted in each structure are herein analysed, focusing on their structural performance and compliance with cultural heritage preservation.

7.2.1 The case of dome of Pavia Cathedral

All the information of Pavia Cathedral, including its history, analyses of structural condition and the strengthening interventions undertaken after the collapse of the Civic Tower, is derived from (Calvi & Palenzona, 2013), unless otherwise indicated.

The structural restoration of the dome of Pavia Cathedral represents one of the most significant and technically sophisticated consolidation campaigns ever undertaken on a large historic masonry vault in Italy. As discussed in Chapter 6, the Cathedral had developed a critical state of structural vulnerability well before the collapse of the adjacent Civic Tower in 1989, primarily due to construction discontinuities, long-term material degradation, and complex load redistributions accumulated over five centuries of building history.

7.2.1.1 Preliminary investigations and long-term monitoring

Following the collapse of the Civic Tower in 1989, emergency stabilisation measures were immediately implemented along the northern nave. A governmental commission was appointed to investigate the causes of the collapse and the structural condition of

the Cathedral. The presence of widespread cracking affecting the dome, the drum, and the octagonal piers led to the installation of a permanent monitoring system, which recorded deformation, crack opening, and relative displacements in real time, with continuous transmission of data to the Department of Structural Mechanics of the University of Pavia.

The monitoring confirmed progressive differential settlements of the piers, increasing distortion of the central octagon, and the widening of through-cracks visible even from the exterior. Fragments of marble started to detach from a dangerous height in 1996; consequently, the Cathedral was immediately closed until 2011. This event was interpreted as a sign of impeding collapse of the structure and caused significant impact of the religious and community life of the city.

This experience made it clear that monitoring the structure to study its behaviour and how this evolves over time was as important as defining an adequate and effective structural strengthening programme.

Beyond its practical role in risk management, the monitoring campaign also marked a conceptual turning point. The cathedral evolved from a structure occasionally inspected after visible damage into a continuously observed system, where decision-making on strengthening was informed by quantitative evidence of deformation trends and boundary-condition deterioration. This shift anticipates current approaches to preventive conservation of large masonry domes.

7.2.1.2 Global shoring strategy

Before any strengthening work on the dome or the vault system could be undertaken, a large-scale provisional structure was installed between 1996 and 1998 to ensure absolute safety during interventions.

This temporary steel framework consisted of centering arches and vertical steel towers founded on reinforced-concrete plinths supported by micropiles. It was dimensioned to carry up to 20,000 tons, the total weight of the drum, dome, and lantern, in the hypothetical case of a sudden collapse of one or more piers.

Although never required to operate under such extreme conditions, the structure guaranteed full geometric stability during all subsequent strengthening activities, particularly those involving the upper vaults.

Figure 7.6 Centering and shoring frames used to support the arches bearing the octagonal drum (Cathedral of Pavia, Pavia – Italy)

7.2.1.3 Strengthening of the supporting system and its effects on the vaults

Investigations revealed severe deficiencies in both the octagonal piers and the drum, conditions that were critical primarily because they altered the boundary conditions and the load-transfer mechanisms of the dome. The stability of a large masonry vault is strongly dependent on the integrity and stiffness of its supports; in Pavia, the poor interaction between the marble facing and the heterogeneous masonry core in the piers caused significant vertical stress concentrations, local crushing, and through-cracks up to 60 mm on the western side. These mechanisms resulted in non-uniform load transfer to the drum and significantly modified the thrust paths acting at the base of the dome.

The drum, weakened by the insertion of sixteen monofora windows and characterised by heterogeneous construction phases, displayed widespread cracking and detachment of masonry leaves. A major through-crack extended from the arch below the drum to its upper portion. Such deformations directly influenced the dome, inducing differential movements and tension states incompatible with its compressive behaviour.

To restore adequate support conditions for the dome and the surrounding vaults, interventions included:

- re-compression of the piers through stainless-steel bars with expandable anchorage;
- replacement of weak mortars with compatible mixtures;
- selective reconstruction of damaged blocks;
- extensive lime-based grout injections across the drum;
- installation of stainless-steel ties;
- reconstruction of the most compromised masonry portions.

Sonic tests confirmed improved material homogeneity after injections.

These interventions, although not acting directly the dome, were necessary to create the boundary conditions for the dome itself to have adequate support, allowing the transfer of loads into the pillars and drum.

7.2.1.4 Structural condition and strengthening of the dome

The double-shell masonry dome was the most critically affected component of the Cathedral's central octagon. Due to long-term settlements, loss of material cohesion, and deformation incompatibilities with the supporting structures, the dome had progressively lost its original membrane behaviour and entered a stress regime dominated by tension and bending, conditions for which masonry vaults have intrinsically limited capacity.

7.2.1.5 Damage pattern

Both shells exhibited extensive subvertical cracks along the meridians, indicating insufficient tensile capacity to resist horizontal thrusts, thermal variations, and differential movements from the drum and piers. The principal ribs showed reduced continuity and local detachment, while further evidence of decay confirmed the loss of structural integration. This damage significantly reduced the global stiffness of the dome and compromised its safety.

7.2.1.6 CFRP reinforcement of the shells

To address the limited tensile capacity and restore structural continuity, carbon-fibre reinforced polymer (CFRP) strips were applied along the extrados of both masonry shells using structural bonding adhesives. The main advantages are that CFRP is a lightweight material, minimally invasive and reversible. This allows the repairing of cracks, increasing of the tensile strength and the ductility while maintaining structure's mass and aesthetic appearance virtually unchanged.

Figure 7.7 Application of FRP at the extrados of the dome's shells (Cathedral of Pavia, Pavia – Italy)

7.2.1.7 CFRP reinforcement of the ribs and worksite configuration

In addition to strengthening the shells, CFRP bands were placed along the main meridional ribs to reinforce these critical load-carrying elements and improve their interaction with the surrounding masonry. This measure counteracted the tendency of the ribs to open under horizontal thrusts and differential deformations, thereby restoring their role in distributing stresses across the dome. Access to the extrados required the construction of an 80-metre-high internal scaffolding tower reaching the intrados of the dome, complemented by an external tubular framework aligned with the ribs. This configuration enabled safe execution of the strengthening works on both shells and the subsequent interventions on the lantern.

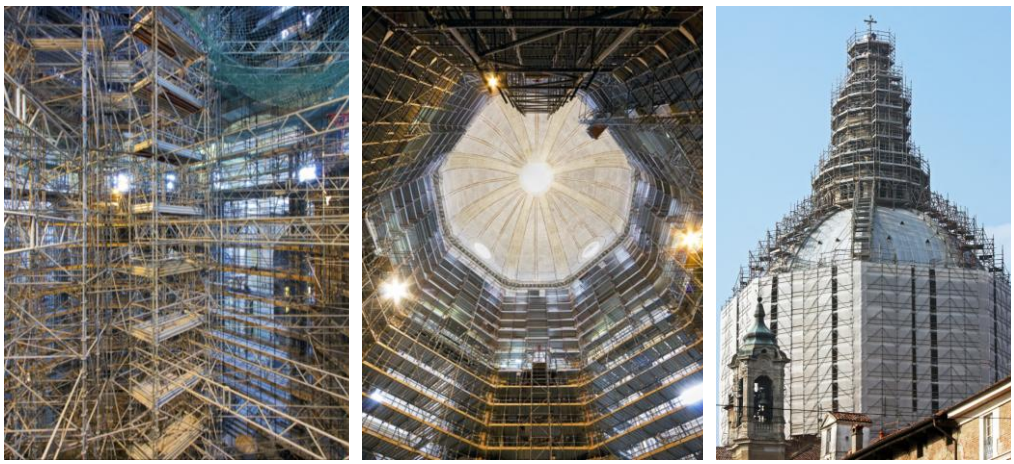

(a) (b)

Figure 7.8 Internal scaffolding in the centre of the octagon (a) and external framework (Cathedral of Pavia, Pavia – Italy)

7.2.1.8 Integrated structural response and conservation philosophy

The strengthening programme implemented on the Cathedral of Pavia was conceived as a multi-scale intervention aimed at restoring the structural coherence of the entire vaulting system. At the global level, the consolidation re-established the load paths through the octagonal piers and reinstated the stiffness and continuity of the drum, both of which had been compromised by centuries of differential settlement and construction heterogeneity. The application of CFRP strips locally restored structural continuity, increased the dome's tensile strength, and increased its deformation

capacity. The effectiveness of these interventions was also demonstrated by the continuous monitoring system. This case study clearly demonstrates how the stability of a dome, especially a large one, is strongly influenced by the surrounding conditions, and therefore by the rest of the structure.

The coordinated intervention on piers, drum, and dome not only reinstated equilibrium within the central octagon but also provided a methodological reference for the strengthening of historic masonry vaults affected by cumulative degradation, long-term differential movements, and material inconsistency.

Beyond its engineering significance, the rehabilitation of the Cathedral stands as an exemplary synthesis of structural innovation and conservation ethics. Rather than imposing a new resistant system, the intervention sought to recover the original compressive behaviour of the vaults while improving the material continuity of the historic fabric. As highlighted by (Calvi & Palenzona, 2013), the strengthening was conceived "not as a replacement of history, but as a means to allow history to endure." By integrating traditional knowledge of masonry vault behaviour with advanced composite materials and real-time monitoring technologies, the project demonstrated that scientific rigour and cultural sensitivity can coexist in the preservation of monumental architecture, offering a robust and respectful approach to safeguarding complex vaulted systems.

7.2.2 The case of the Basilica of St. Francis of Assisi

The collapse of the frescoed vaults of the Upper Basilica of St. Francis of Assisi during the 1997 Umbria, Marche earthquake, discussed in the previous chapter, revealed both the structural vulnerability of medieval ribbed vaults and the dramatic consequences of incompatible past interventions. Beyond its symbolic and artistic significance, the event represented a decisive moment for Italian seismic engineering, prompting the development of a new methodological framework in which safety, compatibility, and reversibility became inseparable objectives (Croci, 1998a).

7.2.2.1 Emergency measures

In the immediate aftermath of the earthquake, emergency measures were implemented to prevent any further collapse and to secure the frescoes.

The provisional works, coordinated by the Istituto Centrale per il Restauro and the Department of Structural Engineering of La Sapienza University, comprised:

- removal of incoherent fill accumulated over centuries;
- injection of salt-free lime mortars to restore continuity;
- application of synthetic-fibre bands on the extrados;
- and temporary suspension of the vaults from the roof employing steel tie-bars equipped with pre-tensioned springs to maintain constant tension and avoid overstressing the frescoed surfaces (Croci, 2000).

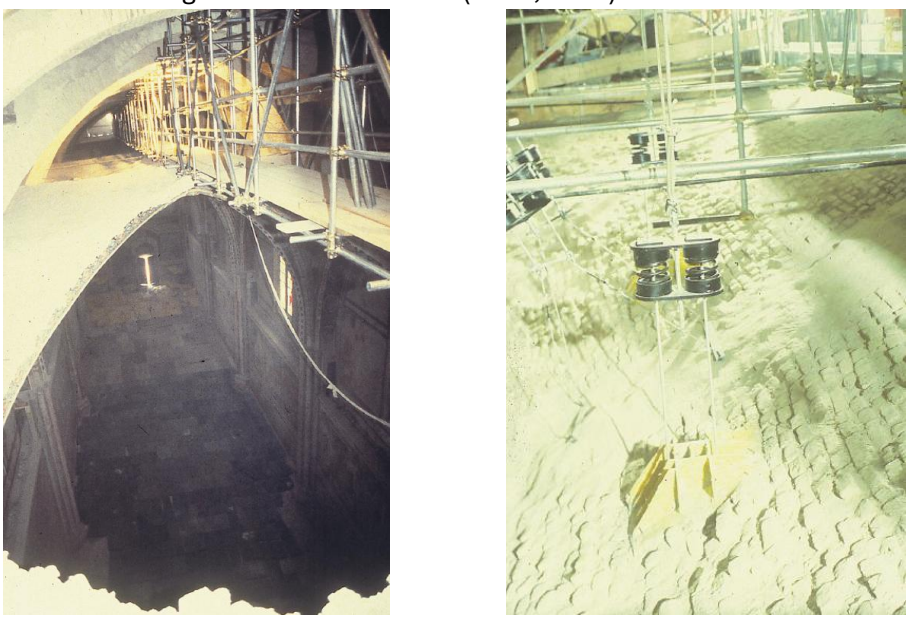

(a) (b)

Figure 7.9 The little flying bridge suspended to the roof to inspect and strengthen the vaults (a) and the system of provisional wires and springs to suspend the vaults to the roof (b) *(Croci, 2000)*

From a structural standpoint, these provisional systems are particularly significant because they introduced controlled, elastic suspension devices capable of maintaining approximately constant tension despite geometric changes and thermal variations. This approach foreshadowed later developments in the use of semi-active and passive control devices in heritage structures, while remaining fully reversible and minimally intrusive to the decorated intrados.

7.2.2.2 Definitive strengthening

The definitive consolidation, designed and directed by (Croci, 2001), embodied a pioneering application of advanced composite and smart materials in the conservation

of monumental masonry. The design objective was clear: to restore structural integrity while preserving the painted intrados and the original Gothic identity of the vaults.

Since reinstating the pristine geometry would have required unacceptable interventions on the frescoes, the adopted solution followed the deformed configuration of the surviving structure. A network of lightweight composite ribs, constructed directly on the extrados, was installed to replicate the mechanical action of the original Gothic ribs. Each rib was composed of a mahogany-plywood core wrapped in aramid (Kevlar) fibres and epoxy resin, providing high tensile capacity, ductility, and durability while remaining invisible from the interior (Croci, 2001).

These composite elements were arranged in a hierarchical pattern:

- major ribs along the diagonals;
- paired ribs over the transverse arches;
- smaller ribs reinforcing the vault webs and crowns.

This configuration provided distributed tensile reinforcement and improved energy dissipation under dynamic loading.

Additional structural measures complemented the rib system:

- lime-based injections were completed to reconnect cracked masonry and improve load transfer;
- prestressed steel belts were installed at the impost level to improve the global box behaviour;
- and a perimeter trussed beam, equipped with shock transmitter and shape-memory alloy (SMA) devices, was introduced along the nave to mitigate horizontal acceleration and protect the frescoed walls.

Figure 7.10 The new ribs, made of a central timber nucleus and external aramidic fibres. In the background, the steel belt to anchor the base of the arches which sustain the roof is visible *(Croci, 2000)*

(a) (b)

Figure 7.11 Shock Transmitter Unit and Shape Memory Alloy devices *(Martelli, 2011)*

In the reconstructed bays, fragments of fallen ribs were reassembled as voussoir-like elements, re-integrated with new bricks fabricated from the same clay mixture as the originals. Hydraulic jacks were used during reassembly to control stress transfer between old and new fabric and to avoid rigid interfaces between materials of differing stiffness. The new composite ribs replace the structural role originally played by the Gothic ribs, with the advantage of greater tensile strength.

The application of these ribs follows the deformed shape of the vaults that withstood the earthquake, simultaneously increasing their seismic behaviour.

7.2.2.3 Philosophy and significance

As (Croci, 1998a) points out, the guiding principle of the restoration and reinforcement of the Basilica of San Francesco was to achieve structural safety without modifying the structure, restoring its functionality while preserving its historical and artistic value. This approach embodies the philosophy of "minimum intervention and maximum compatibility", in which strengthening is conceived as a reversible act integrated into the life of the monument rather than imposed upon it.

From a broader perspective, the Assisi project anticipated modern trends in heritage engineering, demonstrating how composite materials and intelligent devices can be applied with sensitivity and precision to monumental masonry. The combination of experimental verification, numerical analysis, and continuous monitoring transformed the Basilica into a benchmark for post-seismic restoration, where scientific methodology and conservation ethics converge. As emphasized by (Modena et al., 2011), it remains one of the first examples where advanced engineering served not merely to rebuild but to preserve the cultural identity embodied in structure itself.

7.2.3 Comparative discussion

The cases of Pavia Cathedral and the Basilica of St. Francis of Assisi demonstrate two completely different situations, but the underlying philosophy remains the same: to define an appropriate structural reinforcement intervention while seeking to preserve and avoid damaging the artistic heritage they represent.

In Pavia, the intervention was preventive and long-term oriented. It addressed a condition of progressive deformation caused by material decay, differential settlements, and thrust redistribution in a non-seismic environment. Here, the priority was to stabilise an existing equilibrium, preserving the dome's original compressive behaviour and preventing the slow evolution of cracks into collapse mechanisms. The solution relied on distributed reinforcement, steel ties, localized injections, embedded carbon-fibre strips, and on the implementation of a permanent monitoring system capable of tracking the structure's performance over decades.

In Assisi, on the other hand, the intervention involved a partial reconstruction of the collapsed vaults and the strengthening of the ones that withstood the earthquake. This strengthening was based on the use of innovative materials, aramid composites,

prestressed steel belts, and viscous damping systems, while preserving the frescoed surfaces intact.

Despite their differences, both interventions share a key methodological principle: the respect for the original structural logic of masonry. From the maintenance of equilibrium in the static case to the re-establishment of equilibrium after collapse in the seismic case, both illustrate the growing integration between engineering analysis, material science, and conservation ethics. They also demonstrate the progressive convergence between research and practice: in Pavia through the use of monitoring and modelling for predictive maintenance, and in Assisi through experimental validation and the use of composite prototypes under real seismic constraints.

Taken together, the two case studies provide both the conceptual and practical framework for interpreting the behaviour of strengthened masonry vaults. They clarify how the recovery of boundary conditions, the choice of compatible materials, and the geometry of the reinforcement influence global stability and local damage evolution. These insights form the basis for the numerical modelling and experimental validation discussed in the following sections.

7.3 NUMERICAL MODELLING OF FRCM STRENGTHENING MEASURES

Before examining the numerical simulation of the full-scale LNEC vault, it is necessary to outline the intermediate experimental and numerical evidence that supports the modelling strategy adopted in this study. The behaviour of TRM-strengthened masonry cannot be inferred solely from large-scale tests or from isolated numerical assumptions; instead, it emerges from a multi-level chain of validation that includes component-scale experiments, reduced-scale structural tests, and dedicated numerical models capable of reproducing both bond mechanisms and failure evolution.

In this context, two studies have contributed to the calibration and verification of the modelling approach used here. Within the research group, numerical simulations were carried out on TRM-strengthened masonry wallets tested under monotonic and cyclic loading. Parallel analyses performed by (Calò et al., 2025) extended this validation to two TRM-strengthened arches, allowing a direct assessment of the modelling accuracy in curved geometries.

These intermediate studies serve two essential purposes. First, they establish a validated set of material and interface parameters for the simulation of TRM systems, ensuring that the response of the composite layer is not prescribed a priori but emerges

from physically grounded constitutive assumptions. Second, they confirm that the adopted numerical framework is capable of reproducing the transition from local bond phenomena to global structural behaviour, a prerequisite for interpreting the seismic performance of the full-scale LNEC vault. The following subsections summarise the main findings of these component-scale investigations, which collectively underpin the modelling decisions applied in the subsequent simulation of the strengthened cross vault.

7.3.1 Validation on FRCM-strengthened masonry walls

A first level of validation concerned the out-of-plane behaviour of TRM/FRCM-strengthened masonry walls, for which both experimental tests and numerical simulations were available within the project. The experimental programme, (D'Ambra et al., 2019), consisted of two clay-brick masonry walls restrained along one vertical and one horizontal edge and loaded out of plane through a displacement-controlled actuator applied at the upper corner. One wall was tested in its as-built (unreinforced) condition, while the other was retrofitted on one side with a basalt-grid FRCM system composed of a thin inorganic mortar matrix and an embedded fibre mesh. These tests provide an essential intermediate scale of observation between material-level characterisation and full structural behaviour.

The test setup allowed both out-of-plane and vertical loads; however, only a monotonically increasing out-of-plane load was applied. The test was conducted under displacement control at a constant rate of 1 mm/min, using a manually operated jack. The loading continued until the wall reached partial failure that compromised the stability or even total failure.

(a)

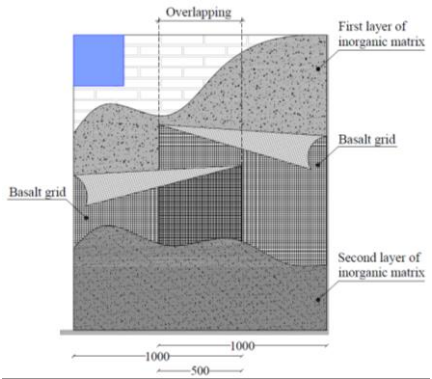

(b)

Figure 7.12 General view of tested specimens: (a) unreinforced wall and (b) FRCM reinforced wall (units: mm)

The numerical simulations were carried out using the Applied Element Method (AEM) implemented in Extreme Loading for Structures (ELS), adopting a simplified micro-modelling strategy in which each brick is represented by a rigid element connected through nonlinear cohesive-frictional interfaces. The FRCM layer was modelled through an equivalent reinforcement net using RFT elements, which generate axial and shear springs at the interface with the bricks, thus reproducing the interaction between textile and substrate, Figure 7.13.

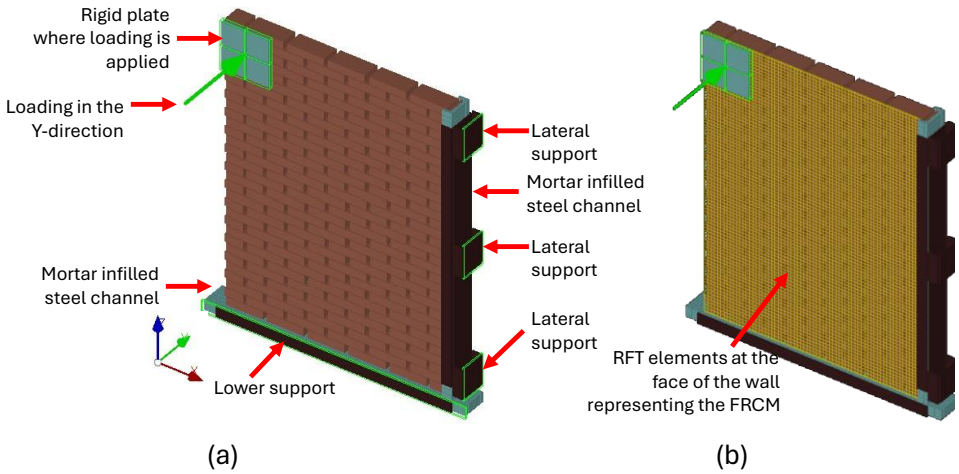

Figure 7.13 Characteristics of the numerical models in ELS: (a) unreinforced model (as-built configuration) and (b) FRCM-reinforced model

7.3.1.1 Equivalent modelling strategy

The FRCM reinforcement applied to the experimental specimens is represented through an equivalent reinforcement-net strategy. The entire composite layer, comprising both the mortar matrix and the embedded fibres, is idealised as a mesh with homogenised mechanical properties. This mesh is positioned close to the external surface of the wall, shifted 0.1 mm towards the interior along the y-direction, and generated through the RFT element tool previously described in Chapter 4. The net consists of 0.8 mm^2 bars arranged at 20 mm spacing in both principal directions. The mechanical parameters assigned to the RFTs correspond to those reported in Table 1 under the “FRCM Basalt Fibre” column.

Figure 7.14 illustrates the configuration of the numerical model implemented in ELS. In Figure 7.14(a), the equivalent fibre grid is visualised as yellow line elements, whereas

Figure 7.14(b) depicts the longitudinal and transverse springs used in the analysis to represent the interaction of the reinforcement with the masonry substrate, shown in light purple.

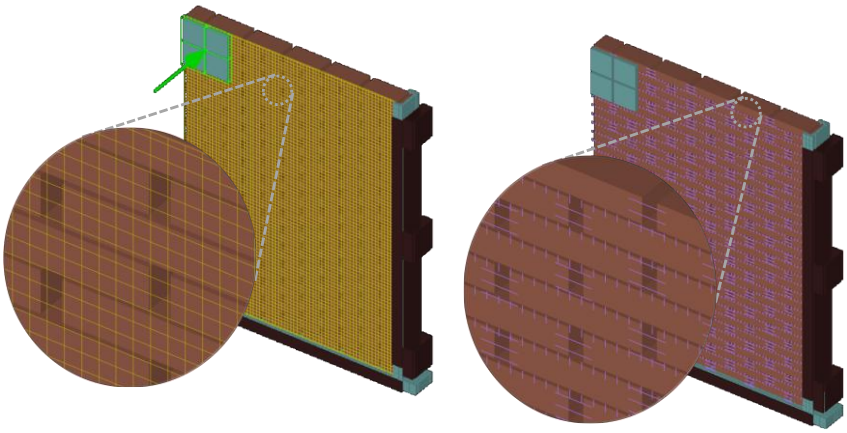

(a) (b)

Figure 7.14 Details of the FRCM-reinforced model on the strengthened side: (a) grid representing the fibres, and (b) longitudinal and transverse springs associated with the fibres

Although this reinforcement-net approach does not increase the total number of elements, and therefore does not enlarge the global stiffness matrix, it significantly increases the computational effort due to the numerous additional springs introduced at the brick–reinforcement interface.

7.3.1.2 Summary of the results

For the unreinforced wall, the AEM model accurately reproduced the initial stiffness, peak force and post-peak softening observed in the experiments, including the formation of a sub-horizontal crack at the upper third of the wall and the onset of localised out-of-plane deformation.

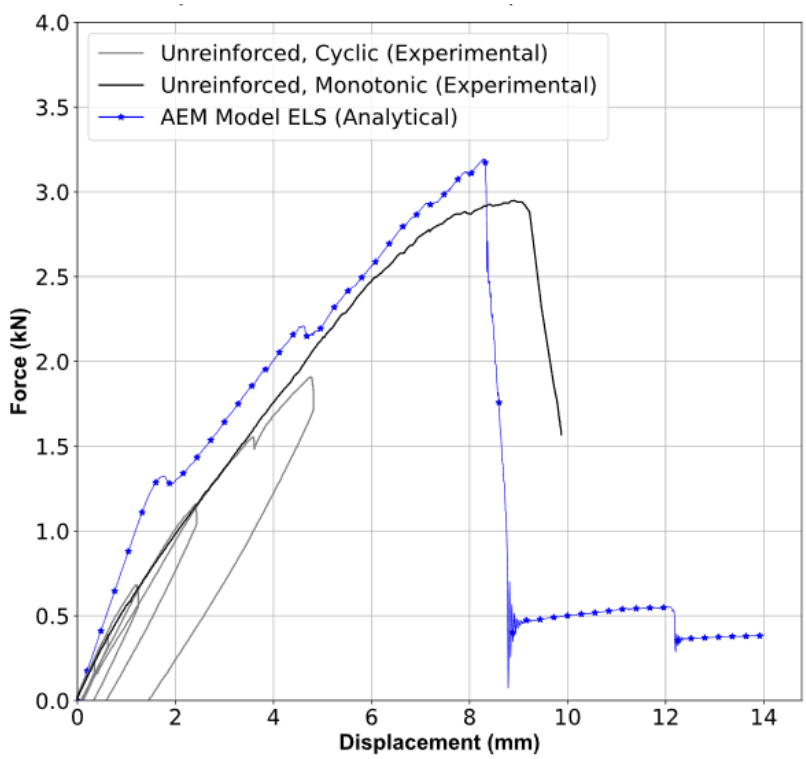

Figure 7.15 Comparison of experimental and analytical force–displacement curves for the unreinforced masonry wall (as-built model)

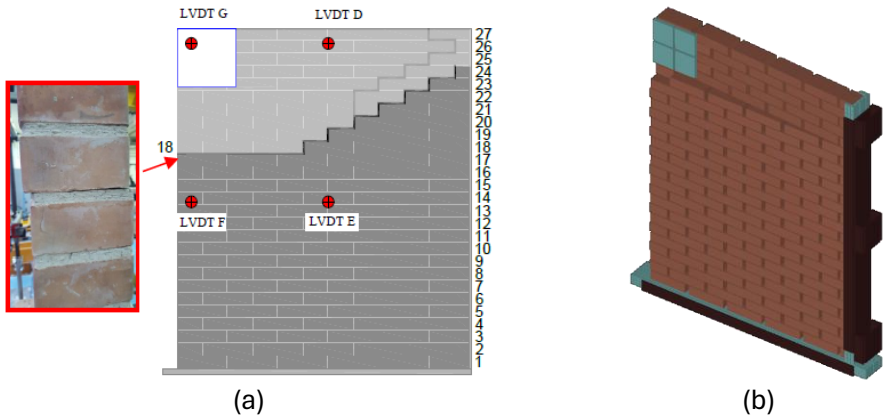

Figure 7.16 Characteristics of the failure in out-of-plane testing of the unreinforced wall (as-built model): (a) schematic of the failure mode on the rear side, and (b) isometric view of the analytical model in the deformed configuration, with deformations magnified by a factor of five

For the reinforced specimen, the model captured the multilinear force–displacement response, the gradual mobilisation of the FRCM layer, and the frictional plateau at large displacements. Although the model slightly underestimated the peak strength of the strengthened wall, it reproduced the ductile post-peak response and the characteristic staggered cracking pattern observed experimentally, Figure 7.17.

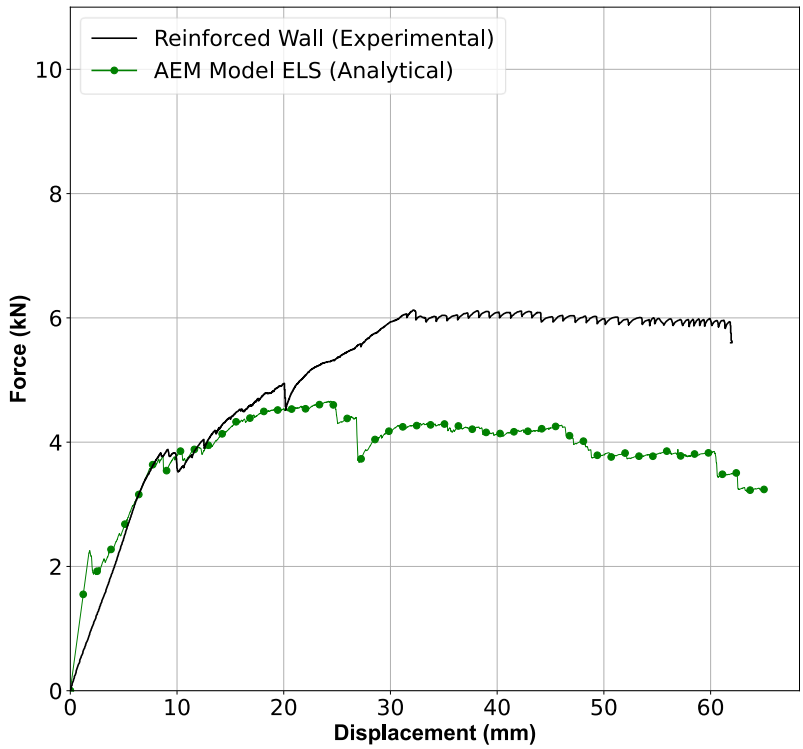

Figure 7.17 Comparison of experimental and analytical force–displacement curves for the FRCM-reinforced masonry wall

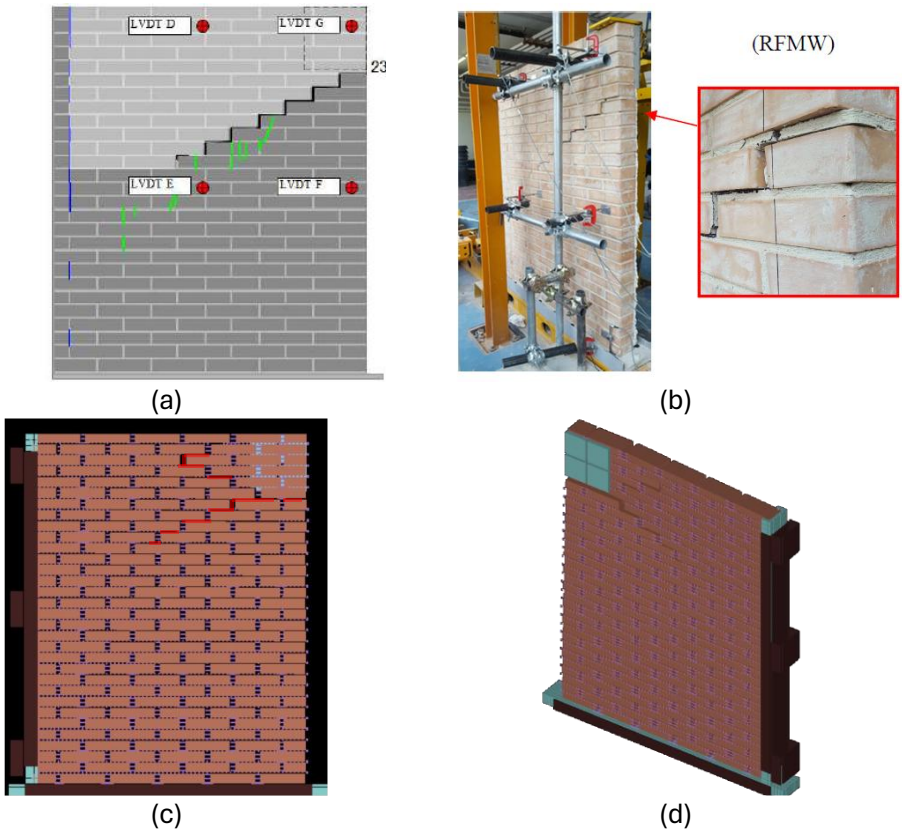

Figure 7.18 Characteristics of the failure in the out-of-plane response of the FRCM-reinforced wall obtained from: experimental rear side (a) and isometric view (b); numerical rear side (c) and isometric view (d)

7.3.1.3 Conclusions

Overall, these results demonstrate that the adopted modelling strategy is capable of reproducing both global and local response mechanisms of FRCM-strengthened masonry components. The tests confirm the suitability of the AEM framework for capturing out-of-plane behaviour governed by interface mechanisms, thus providing a physically grounded calibration baseline for the subsequent numerical simulation of the TRM-strengthened vault tested at LNEC.

The author gratefully acknowledges Studio Calvi Beam S.r.l. for providing the numerical models used for the validation of the FRCM-strengthened masonry walls. Their contribution formed an essential basis for the component-scale calibration adopted in this study.

7.3.2 Validation on FRCM-strengthened masonry arches

A further level of validation concerned the behaviour of masonry arches retrofitted with FRCM composites, for which both experimental evidence and AEM-based numerical simulations were available. The reference experimental campaign, carried out (Alecci et al., 2016), tested ten 1:2-scale clay brick arches under displacement-controlled loading, including two unreinforced specimens and several arches strengthened with PBO-FRCM and CFRP systems, applied either on the extrados or on the intrados. The unreinforced arches displayed a brittle four-hinge mechanism, whereas the FRCM-strengthened specimens exhibited improved load-bearing capacity and enhanced post-peak behaviour, particularly when the reinforcement was placed on the extrados.

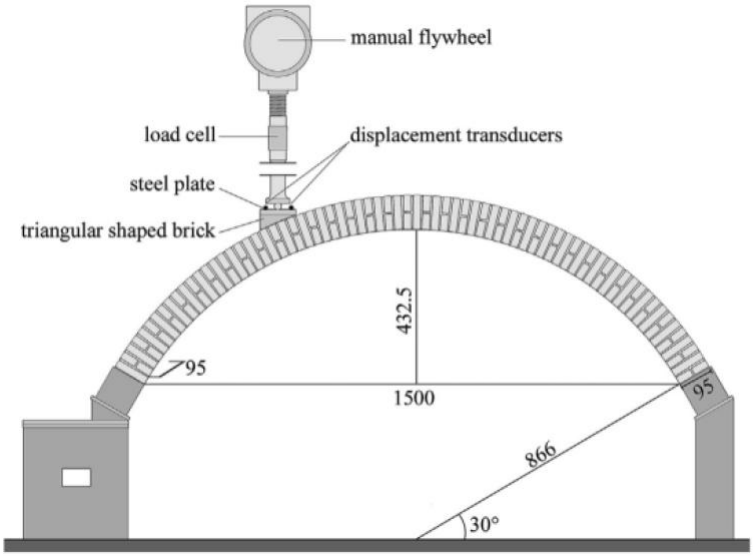

Figure 7.19 Test set up *(Alecci et al., 2016)*

Building on this campaign, (Calò et al., 2025) developed a numerical reproduction of the tests using the Applied Element Method. Two distinct modelling strategies were implemented:

- an explicit representation of the FRCM layer, in which the mortar and fibre mesh were modelled as rigid units connected to the masonry substrate through cohesive–frictional interfaces; and
- an equivalent "grid" approach, where the composite is idealised as a single layer of distributed springs positioned at the extrados of the arch.

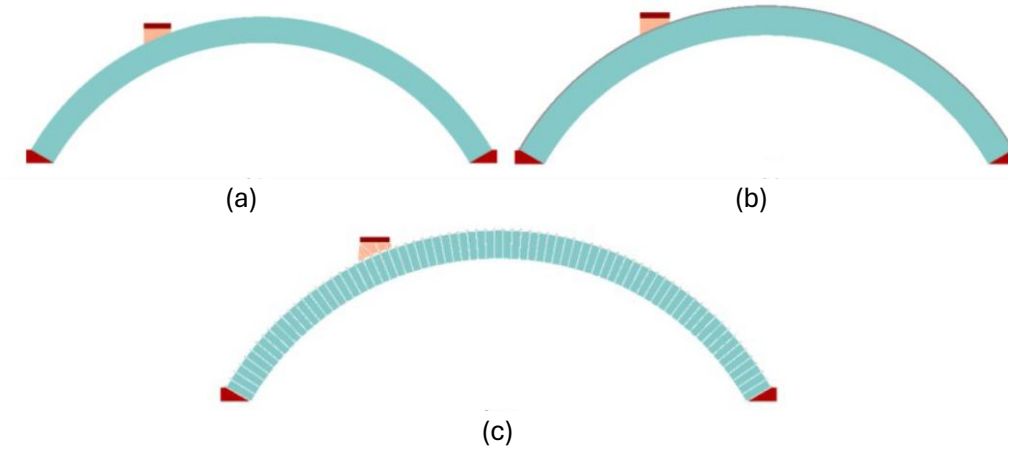

Figure 7.20 AEM-based numerical models: (a) as-built configuration, (b) explicit modelling approach of the reinforcement layer and (c) equivalent modelling by means of a grid layer from *(Calò et al., 2025)*

While the explicit method provides a detailed description of the reinforcement–masonry interaction, including bond degradation and local slip, it entails a higher computational cost. Conversely, the equivalent grid approach significantly reduces analysis time by avoiding the introduction of additional elements, while preserving the essential mechanical interaction.

7.3.2.1 Summary of the results

The numerical simulations are capable to reproduce the experimental response. For the unreinforced arch, the AEM model captured the correct initial stiffness, the sequence of hinge formation and their final positions, and the brittle four-hinge collapse mechanism. In the strengthened condition, both modelling approaches accurately reproduced the increased load-bearing capacity, the stabilised post-peak response, and the transition to a failure mechanism driven by debonding of the composite followed by shear slip at the abutments. Minor discrepancies in post-hinge stiffness and residual strength were observed, but the overall agreement with experimental trends was strong for both modelling strategies.

7.3.2.2 Conclusions

These component-scale results confirm the suitability of AEM for simulating complex failure mechanisms in both unreinforced and FRCM-strengthened masonry arches. Moreover, the comparison between explicit and equivalent modelling highlights the trade-off between accuracy and computational efficiency. This insight is particularly

relevant for the present study, where the explicit modelling of reinforcement, consistent with the approach adopted for the LNEC vault, is necessary to capture the bond-dependent mechanisms governing the seismic behaviour of TRM-strengthened curved structures.

7.3.3 Final remarks

Taken together, the wall and arch validations provide a robust and experimentally grounded basis for the modelling assumptions adopted in this work. They confirm that the AEM framework and the explicit representation of the TRM layer are capable of reproducing the bond-dependent mechanisms governing the behaviour of strengthened masonry components. Building on this foundation, the next section extends the modelling strategy to the full-scale cross vault tested at LNEC, where the same mechanisms interact within a three-dimensional geometry and under dynamic loading conditions.

7.4 SIMULATION OF LNEC SHAKING TABLE TEST

Chapter 4 validated the proposed AEM meso-modelling strategy through comparison with the unstrengthened configuration of the full-scale masonry cross vault tested on the shaking table at the Laboratório Nacional de Engenharia Civil (LNEC) in Lisbon. In addition to the validation of the unstrengthened configuration, the modelling of the TRM strengthening adopted here is supported by the component-scale validations presented in Section 7.3, which demonstrated the ability of the AEM framework to reproduce the bond-dependent behaviour of FRCM/TRM systems on walls and arches. That analysis focused on the mechanical characterisation, numerical calibration, and dynamic response of the original vault, providing the reference condition for assessing the effectiveness of strengthening measures and for understanding the role of boundary conditions and in-plane shear mechanisms. The present section concentrates on the retrofitted configuration, where the same vault was repaired and reinforced with Textile Reinforced Mortar (TRM) layers applied at the extrados, and subsequently re-tested under the same input protocol.

After completing the shaking-table sequence on the unstrengthened configuration (10%, 25%, 50%, and 75% of the AQA input), the vault specimen underwent a repair and strengthening intervention before the subsequent test campaign. The procedure, illustrated in Figure 7.21, followed a multi-step approach. First, the existing cracks were injected with *GeoCalce Antisismico FL*, a highly fluid mortar used to restore continuity

and improve the mechanical integrity of the damaged masonry. Following the crack injection phase, a geosteel G200 composite grid was applied over the extrados and embedded within a layer of *GeoCalce Antisismico F* mortar. An additional geosteel G600 mesh was installed at the corners to ensure a good anchorage. The mortar layer was finally applied to fully incorporate the textile reinforcement. The final appearance of the strengthened vault is shown in Figure 7.21(f), highlighting the continuous TRM layer distributed across the entire extrados.

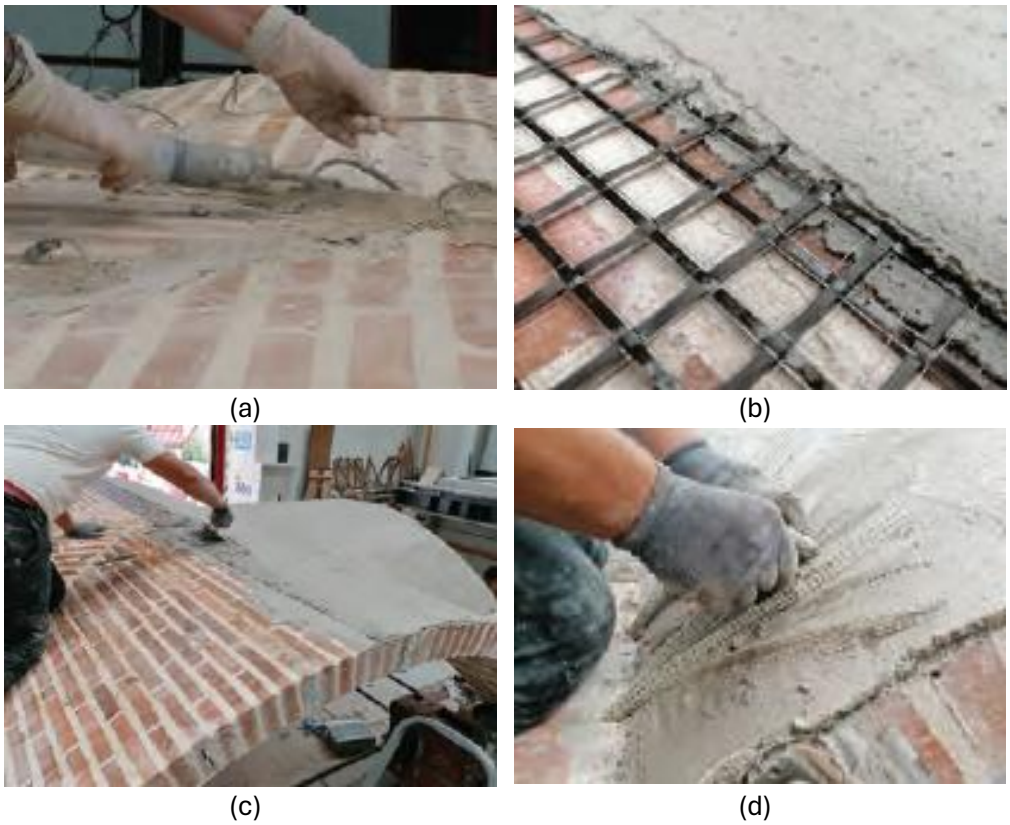

(a) (b)

(c) (d)

(e) (f)

Figure 7.21 Application of the strengthening TRM system: (a) injecting fluid mortar GeoCalce antisismico FL in the cracks, (b) detail of the geosteel grid 200 embedded in GeoCalce antisismico F, (c) application process, (d) detail of the corners close to the infill with geosteel grid 600, (e) injecting the fluid mortar GeoCalce antisismico FL, (f) final appearance of the strengthened model *(Bianchini et al., 2024)*

In dynamic terms, the intervention produced a measurable increase in the initial stiffness and fundamental frequency of the vault, reflecting the contribution of the TRM layer to the in-plane tensile capacity of the webs. Despite this increase in global stiffness, the overall deformation pattern remained consistent with a shear-dominated mechanism, indicating that the strengthening enhanced, rather than altered, the original masonry-like behaviour of the system. It is important to note that the repair phase preceding the TRM application modified the mechanical baseline of the specimen by reducing residual cracking and partially restoring stiffness, an aspect that must be considered when interpreting both the experimental response and the numerical simulations.

Overall, the intervention allowed the previously damaged specimen to recover structural integrity and provided an externally bonded reinforcement system tailored to improve its seismic performance during the second series of shaking-table tests. The strengthened vault successfully withstood the full sequence up to 150% AQA, exhibiting distributed damage but no global collapse. The composite layer effectively limited crack opening along the groins and crowns, enhanced tensile capacity, and promoted a more uniform stress redistribution across the webs, while preserving the characteristic in-plane shear mechanism. These results confirm the efficiency of TRM systems in increasing both strength and ductility, fully aligning with the conservation-oriented principles illustrated in the previous case studies, namely, achieving greater seismic safety through lightweight, reversible, and materially compatible reinforcement.

In the numerical phase, the same AEM meso-modelling framework was extended to include the TRM layer as a discrete reinforcement grid coupled to the masonry substrate through cohesive interfaces. This approach allowed simulation of debonding, sliding, and partial delamination phenomena, enabling a realistic reproduction of the experimental behaviour. The model captured the delayed onset of cracking, reduced deformation amplitudes, and higher acceleration peaks, signatures of the enhanced stiffness induced by the composite layer.

Overall, the LNEC strengthened vault provides a controlled experimental validation of the strengthening principles applied in real heritage structures such as Pavia and Assisi. Whereas the former adopted embedded carbon-fibre strips and the latter employed aramid-composite ribs, the LNEC experiment isolates and quantifies the mechanical contribution of composite reinforcement under cyclic seismic loading. In this sense, it constitutes a bridge between laboratory testing and monumental-scale application, offering a reproducible reference for numerical benchmarking and for parametric studies on composite-based strengthening strategies.

The LNEC campaign also fills a critical gap in the experimental literature, which is largely dominated by small-scale or simplified specimens that cannot fully reproduce the mechanics of large masonry vaults subjected to distributed inertia. At the same time, it is important to recognise the intrinsic limitations of the benchmark: it represents a single geometry, a specific boundary configuration, and one particular TRM layout. Additional tests on different vault typologies, support conditions, and reinforcement arrangements would therefore be necessary to broaden the generality of the conclusions drawn from this experiment.

7.4.1 Numerical modelling and preliminary validations

The numerical analyses presented in this section refer to the study by (Cogliano et al., 2025b), where the Applied Element Method (AEM) was employed to reproduce the experimental response of the TRM-strengthened LNEC cross vault under dynamic excitation. The same meso-modelling approach validated in Chapter 4 for the unreinforced configuration was extended to include the reinforcing layer, enabling a direct comparison between the two structural conditions.

The masonry vault was modelled using 8-node elements discretized through a fine mesh of equivalent bricks and mortar joints, adopting nonlinear normal and shear springs to represent tensile cracking, crushing, and sliding. Mechanical parameters were calibrated against the material properties reported in the experimental campaign, with

slight adjustments to capture the stiffness measured during the dynamic identification of the strengthened specimen, as shown in Chapter 4.

The TRM was introduced as a reinforcement grid applied at the extrados surface together with the mortar layer, representative of *Geosteel grid 200* embedded in the *Geocalce Antisismico F* provided by Kerakoll, Figure 4.7. This system was coupled to the masonry through cohesive interface capable of simulating debonding and frictional sliding. The grid spacing and fibre orientation were defined according to the geometry of the basalt textile used in the test (20 × 20 mm), while the cohesive parameters were determined from pull-off tests and calibrated to reproduce the observed bond-slip behaviour. This simplified yet physically consistent representation allowed the AEM to capture both the distributed tensile contribution of the reinforcement and the localised detachment phenomena occurring under large displacements. However, it also highlights a key aspect of composite-based retrofitting: the global response of the strengthened vault is governed not only by the nominal properties of the textile and mortar but also, and often predominantly, by the constitutive law adopted for the TRM–masonry interface. Cohesion, friction, and separation strain at this interface control the onset of debonding and sliding, and thus strongly influence both stiffness evolution and damage distribution.

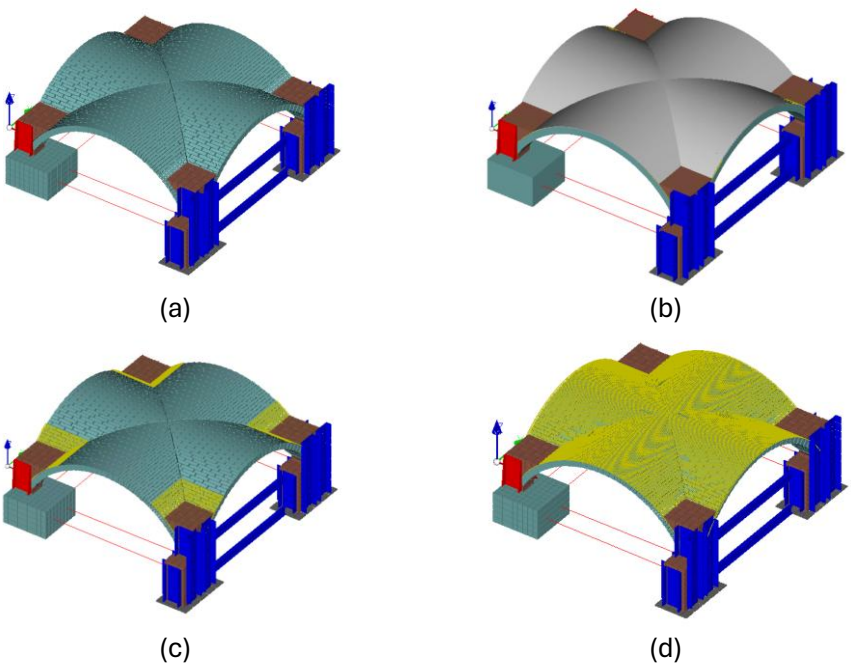

(a) (b)

(c) (d)

Figure 7.22 Numerical model developed within ELS software: (a) unstrengthened, (b) strengthened specimens, and detailing of reinforcement grid (c) Geosteel 600 at the corner and (d) Geosteel 200 uniformly distributed

The experimental sequence consisted of successive shaking-table tests, each performed with incrementally higher input amplitudes according to Table 4.2.

Table 7.1. Summary of the sequential seismic test

Specimen	***% AQA Earthquake***						
Strengthened	-	25%	50%	75%	100%	125%	150%

The numerical configuration was thus able to replicate both the global response and the local damage evolution observed during the shaking-table campaign.

Because TRM systems rely on bond-dependent tensile transfer, the interface may govern retrofit effectiveness more than the textile or mortar properties themselves. This aspect remains underexplored in both experiments and numerical studies.

7.4.2 Nonlinear time history analyses results

The damage patterns observed in the strengthened configuration reveal a substantially different distribution of cracking compared with the unreinforced vault. The webs of the vault, which in the original specimen displayed extended diagonal cracking and early hinge formation along the groins, appear markedly less damaged after strengthening.

Both the experimental and numerical results (Figure 4.14) confirm the expected effect of the TRM layer: by providing additional tensile capacity and limiting crack opening, the reinforcement stabilises the vault panels and delays the activation of the primary collapse mechanisms typically associated with cross-vault behaviour under seismic loading.

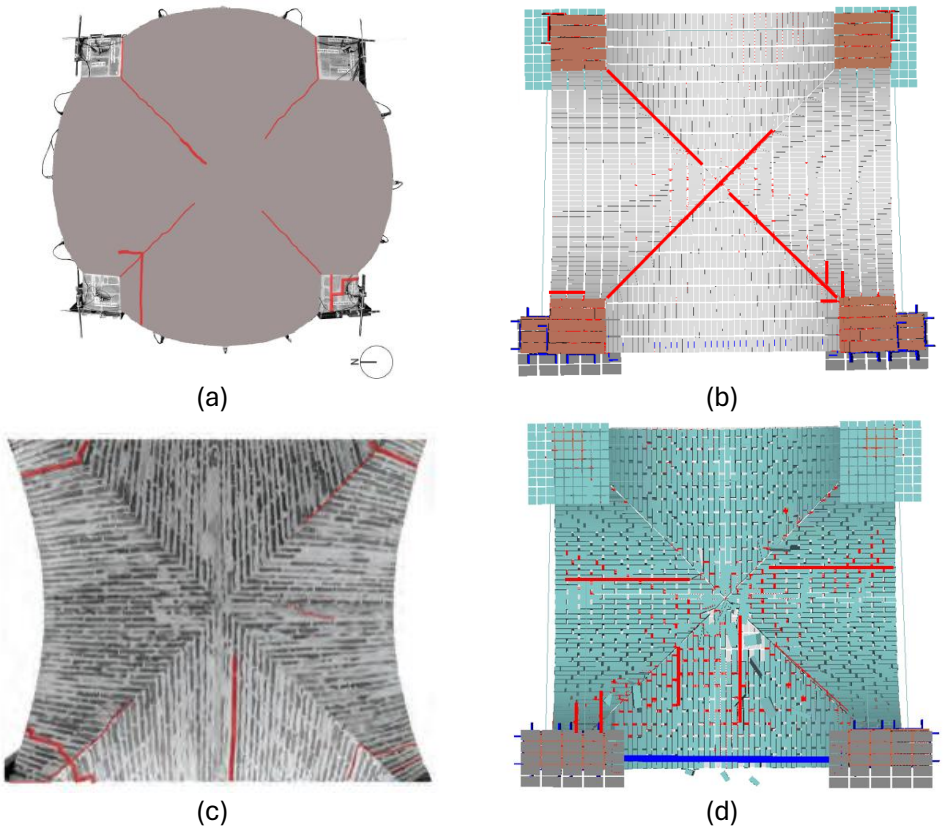

Figure 7.23 Comparison of experimental** (Bianchini et al., 2023) **(a) and numerical (b) at the extrados and (c) and (d) at the intrados crack patterns at the end of 150% of AQA signal

At the same time, the introduction of the TRM system leads to a more pronounced concentration of damage at the supports, particularly near the springing zones and along the interface between the vault and its boundary arches. This shift is clearly visible in the extradosal experimental pattern, where cracking tends to cluster around the imposts, while the webs remain largely intact. The numerical model is able to reproduce this behaviour, capturing both the diagonal shear mechanism and the support-dominated cracking, which becomes more pronounced as the strengthened panels restrain in-plane deformations and transfer a larger portion of the seismic demand to the supports.

At the intrados, the experimental pattern is characterised by substantially reduced and more diffuse cracking compared with the unreinforced vault, reflecting the effectiveness of the TRM layer in suppressing major hinge formation and mitigating diagonal tensile damage. The AEM simulation captures this global trend; however, it predicts a denser

intradosal crack network than observed experimentally, particularly near the crown and the transitional regions between adjacent vault panels. This overestimation suggests that, although the model effectively simulates the redistribution of internal forces induced by the reinforcement, it may overpredict tension transfer through the thickness of the vault. In other words, the adopted interface law between the TRM layer and the masonry substrate tends to maintain a stronger mechanical coupling than that effectively mobilised in the test, thereby propagating tensile stresses more deeply into the section and triggering additional cracking at the intrados. Overall, the comparison demonstrates that the TRM strengthening significantly enhances the seismic performance of the vault: damage in the web regions is reduced, collapse mechanisms are delayed, and cracking becomes concentrated at the supports, behaviours captured consistently in both the experimental and numerical records.

These observations indicate that the mechanical interaction between the TRM layer and the masonry substrate is not fully constrained in the present model, and that the predicted crack distribution and global response are strongly influenced by the assumed interface properties. A dedicated calibration of cohesion, friction and separation strain would be required to refine the accuracy of the strengthened configuration.

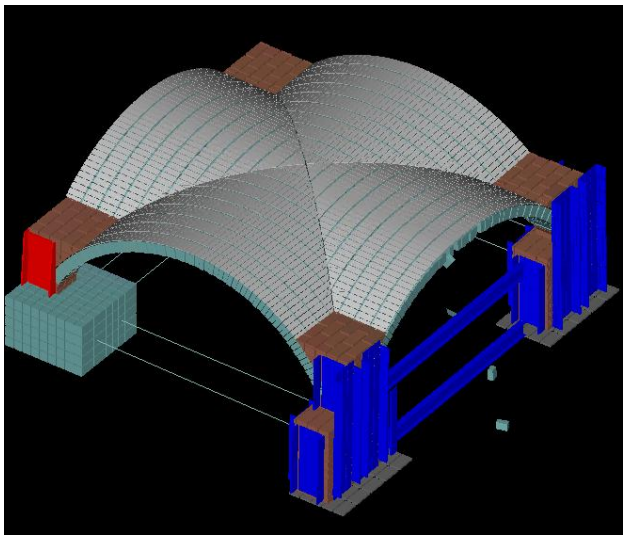

Figure 7.24 Vault damage at the end of the 150% of the AQA

The comparison between experimental and numerical results for the strengthened configuration, Table 4.5, shows a generally coherent trend, with accuracy levels that vary depending on the monitored point and response quantity. Since the shaking-table test

was performed under unidirectional excitation along the y-axis, and the analysis of the unstrengthened specimen demonstrated that the y-components provide the most meaningful representation of the vault's dynamic response, only OC*-y and Acc*-y values are reported here.

For the displacement response, the numerical model exhibits a balanced performance, with relative errors ranging approximately between −11.7% and +11%. These values indicate a satisfactory agreement, especially considering the nonlinear behaviour of the TRM-reinforced system under cyclic loading. The model tends to slightly overestimate displacements at OC1–y and OC4–y, while underestimating them at OC2–y, suggesting that local stiffness variations introduced by cracking and partial debonding may influence the precision of the numerical predictions at specific locations.

The correlation of the acceleration response is overall acceptable, with most relative errors falling within ±20%. The model overestimates the peak values at Acc18–y (+18.7%) and Acc14–y (+11%), while underestimating the response at Acc2–y (−18.3%). These discrepancies point to the model's inherent limitations in fully capturing localized dynamic effects, likely associated with the interaction between the TRM layer and the underlying masonry, as well as with the boundary conditions imposed at the vault supports.

Table 7.2. Comparison of experimental and numerical absolute maximum total displacements and accelerations for the strengthened specimen

		Experimental	*Numerical*	*Relative Error [%]*
Displacement [mm]	OC1-y	57.2	62.8	9.8
	OC2-y	64	56.6	-11.7
	OC4-y	62.9	69.5	11
Acceleration [m/s²]	Acc18-y	7.6	9.1	18.7
	Acc14-y	10.5	11.7	11
	Acc2-y	9.4	7.8	-18.3

The comparison between experimental and numerical displacement time histories at 150% AQA, Figure 4.16, shows a generally consistent response across all monitored nodes (OC1, OC2, OC4). In all three cases, the initial transient phase is reproduced with acceptable accuracy, with the numerical model capturing both the amplitude and the

phase of the primary displacement cycles. The AEM simulation tends to slightly overestimate peak displacements during the early seconds, particularly at OC1 and OC4, whereas at OC2 the numerical trace remains marginally lower than the experimental one. These trends are consistent with the relative error distribution previously discussed and reflect localized stiffness variations that the model approximates only partially.

Despite minor discrepancies, the overall agreement is satisfactory, confirming that the model reproduces the essential features of the nonlinear displacement history under severe seismic demand.

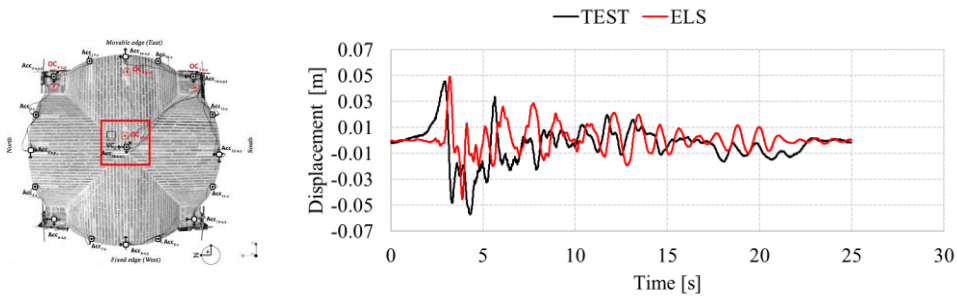

(a)

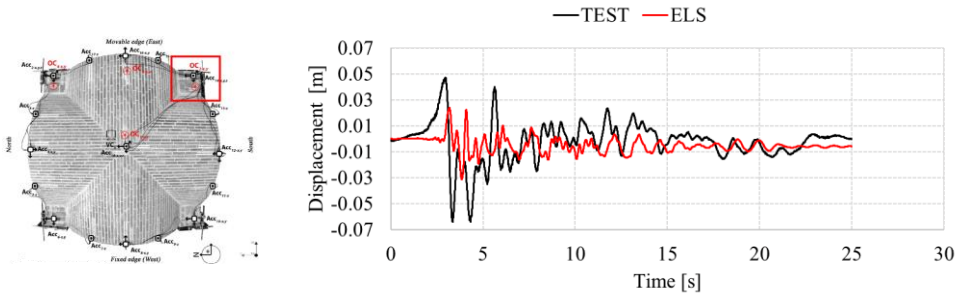

(b)

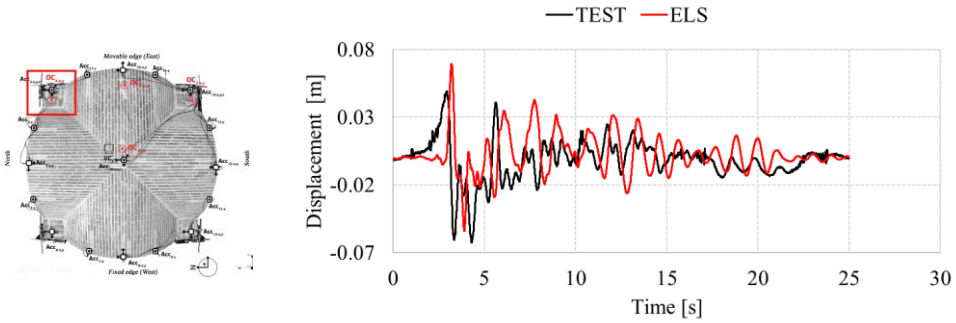

(c)

Figure 7.25 Displacement time histories along N-S direction for OC1 (a), OC2 (b), and OC4 (c) node during 150% of the AQA

The comparison of the acceleration time histories in Figure 4.17 highlights the model's ability to reproduce the dynamic content of the motion with notable fidelity. Across all monitored nodes (Acc18, Acc14, Acc2), the numerical traces closely follow the experimental records during the strong-motion phase, capturing both the intensity and the temporal evolution of the input-induced pulses. Peak accelerations show moderate deviations, with slight overestimation at Acc18 and Acc14 and underestimation at Acc2, but the overall waveform agreement remains robust throughout the duration of the record.

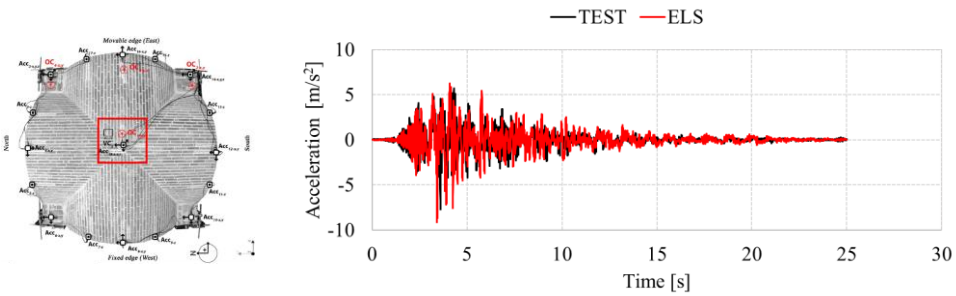

(a)

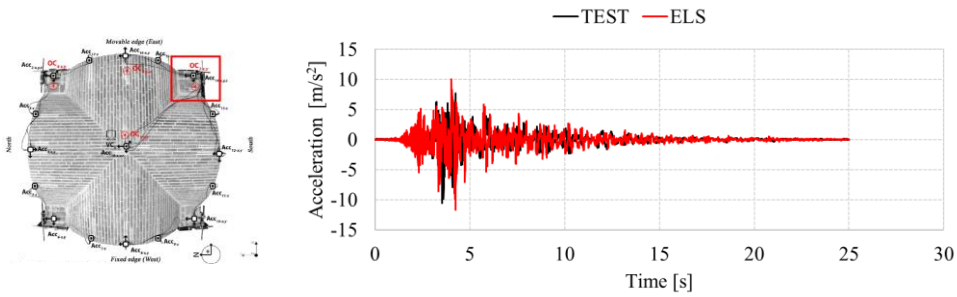

(b)

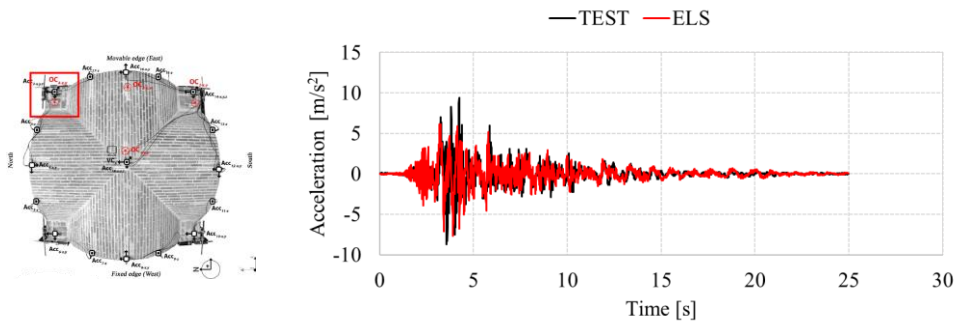

(c)

Figure 7.26 Acceleration time histories along N-S direction for Acc18 (a), Acc14 (b), and Acc2 (c) node during 150% of the AQA

7.4.3 Conclusions on LNEC test simulation using AEM

The AEM-based simulation of the TRM-strengthened LNEC vault achieved a close correspondence with the experimental findings, validating the method's capacity to model composite–masonry interaction under cyclic dynamic loading.

The analyses demonstrated that a simplified representation of the reinforcement through discrete cohesive links is sufficient to reproduce the essential phenomena observed during testing, namely:

- the increase in initial stiffness and frequency due to the composite layer;
- the delayed onset of major cracking and reduced deformation amplitudes;
- the distributed damage pattern consistent with the experimental crack maps; and
- the enhanced energy dissipation and ductility without altering the vault's thrust-based behaviour.

Some discrepancies were observed in the predicted damage at the intrados, where the numerical model tended to overestimate cracking due to the limited capacity of the cohesive formulation to represent out-of-plane tension-compression coupling. Nevertheless, the overall correlation between simulation and experiment is strong, both qualitatively and quantitatively.

The study confirms that the AEM meso-modelling strategy constitutes a reliable and computationally efficient tool for assessing the seismic response of TRM-strengthened masonry vaults, bridging the gap between laboratory experimentation and real-scale applications such as those presented in Pavia and Assisi. The insights derived from this validation serve as the basis for the comparative analyses discussed in the next section, where alternative modelling strategies, FEM, DEM, and hybrid approaches, are compared against the AEM framework.

7.4.4 Numerical modelling of the LNEC vault: comparative approaches

The shaking-table test conducted at LNEC on the unreinforced and TRM-strengthened masonry cross vault has served as a reference benchmark for several numerical investigations. Alongside the AEM analyses presented in this study (Cogliano et al., 2025b), the same experiment was simulated using finite element (FEM) and discrete element (DEM) formulations (Ferrante et al., 2024; Kesavan et al., 2024; Oktiovan et al., 2023). This provides a unique opportunity to compare distinct computational frameworks against an identical experimental dataset.

Table 4.6 reports the comparison between experimental and numerical first-mode frequencies. All modelling strategies achieved results consistent with experimental ones, with few differences. FEM (Kesavan et al., 2024) provided the closest frequency value to the experimental one (0.33% deviation), while both AEM and DEM slightly overestimated the global stiffness of the retrofitted, with relative deviations of 19.0% and 23.4%, respectively. Indeed, discontinuum-based approaches require the calibration of interface properties to accurately reproduce the deformability of the strengthened vault.

Table 7.3. Comparison of experimental and numerical first mode frequencies

Model	*f [Hz]*	*Absolute Error [Hz]*	*Relative Error [%]*

(Kesavan et al., 2024) - FEM	6.13	0.02	0.33
(Cogliano et al., 2025) – AEM (present work)	7.32	1.17	19.02
(Oktiovan et al., 2023) - DEM	7.59	1.44	23.41
Experimental test frequency [Hz]	6.15		
Numerical mean frequency [Hz]	7.01		
Standard Deviation σ [Hz]	0.78		
Coefficient of Variation CV [%]	11.1		

FEM micro-models discretised individual bricks and mortar joints and represented the TRM layer using orthotropic shells bonded to the extrados. They reproduced modal frequencies and global stiffness with high accuracy. However, capturing discrete cracking, debonding or delamination required complex nonlinear laws and fine meshes, resulting in high computational cost.

DEM represented the masonry as rigid blocks interacting through nonlinear contacts. It successfully reproduced hinge formation, joint opening, and shear mechanisms, especially along the webs and groins. Nevertheless, DEM tended to underestimate small-displacement stiffness and slightly overpredict energy dissipation, due to idealised contact mechanics.

Finally, the AEM adopts a hybrid continuum–discontinuum formulation: cracks form spontaneously, elements separate and reclose, and stiffness is preserved until failure. The AEM simulations reproduced both the global dynamic response and the local cracking evolution observed experimentally, including delayed hinge formation and distributed damage across the webs.

The comparison among the three methods highlights that FEM predicts stress and strain with great accuracy but requires complex numerical calibration to catch cracking. DEM offers the most intuitive representation of fracture propagation but struggles with elastic stiffness. AEM provides a balanced compromise, reliably capturing both global response and localised failure at a moderate computational cost. All methods confirm the

experimental trends: increased stiffness, delayed cracking, enhanced energy dissipation, and no collapse after TRM strengthening.

While the LNEC vault offers an exceptional benchmark, it represents a single geometry, boundary configuration, and TRM layout. Moreover, the simulations highlight the need for improved modelling of the TRM–masonry interface. No sensitivity analyses on interface parameters (cohesion, friction, separation strain) were performed in the present study; dedicated calibration could enhance the accuracy of predicted cracking patterns and overall response.

From a comparative standpoint, no modelling strategy is universally superior. FEM is most accurate for modal identification, DEM best reproduces collapse mechanisms, and AEM provides the most balanced and operationally effective framework for simulating nonlinear seismic behaviour in TRM-strengthened masonry vaults.

7.5 CONCLUDING REMARKS

This chapter has explored the evolution of strengthening measures applied on masonry vaults starting from experience-based solutions to most innovative ones. The result of this rational analysis shows that the assessment of vaulted systems cannot be approached through a single technical solution or material choice; rather, it requires a complete understanding of the structure, the evolution of boundary conditions, and the interaction between reinforcement and the existing fabric.

The review has started from the traditional strengthening methods (tie rods, reinforced concrete overlays and ring beams, steel frames), which mainly stiffen the structure and suppress deformations, with an higher seismic demand as a consequence.

Subsequent research and post-earthquake evidence progressively revealed the limitations of such rigidity-based approaches, especially in seismic conditions. Composite materials, and in particular TRM/FRCM systems, emerged as a response to these shortcomings, offering lightweight, breathable, and mechanically compatible reinforcement capable of enhancing the tensile behaviour of masonry without overriding its compressive, funicular nature.

The case studies of Pavia Cathedral and the Basilica of St. Francis of Assisi have shown how this philosophy is implemented in practice. In Pavia, where long-term deformation and boundary condition degradation threatened the equilibrium of a monumental dome, the intervention focused on restoring the load paths through the piers and drum while

introducing minimally invasive extradosal CFRP strips. In Assisi, conversely, the sudden collapse of entire portions of vaults required a strategy based on innovative composite ribs, prestressed belts, and smart devices, designed to restore seismic resilience while protecting an exceptional artistic heritage. Although the two case studies were completely different, they had in common the same goal: strengthening measures must respect the original structural behaviour.

The full-scale shaking-table tests carried out at LNEC provided an essential bridge between conservation practice and scientific validation. The experimental results on the TRM-strengthened cross vault demonstrate how composite systems improve stiffness, delay hinge formation, reduce deformation demands, and modify damage distribution from the webs toward the supports. The AEM simulations reproduced these effects, capturing both global dynamic behaviour and local cracking evolution. The comparative analysis with FEM and DEM strategies further revealed the complementary strengths of different modelling frameworks: FEM excels in stiffness and modal prediction, DEM in reproducing collapse mechanisms, and AEM in balancing continuum fidelity with discrete cracking at a moderate computational cost. The most critical aspect of each modelling strategy is represented by the TRM-masonry interface, which affect the retrofit effectiveness.

Overall, the seismic assessment of strengthened masonry vaults should always take into account the geometry, material degradation, changes in boundary conditions and construction history. The lessons derived here provide the basis for the analyses developed in the following chapter, where the performance of retrofitted vaulted systems is examined in greater depth and used to inform broader conservation-oriented engineering strategies.

8 CASE STUDIES

8.1 BACKGROUND: THE SMAC MULTILEVEL ASSESSMENT FRAMEWORK

The three case studies presented in this chapter are part of a much larger portfolio of 226 churches, which began in 2015. As a result of induced seismicity in Groningen, the need to rapidly assess large inventories of unreinforced masonry churches has arisen in order to: estimate the level of risk; develop retrofit strategies; optimise the use of resources.

The Seismic Multilevel Assessment of Churches (SMAC) had been developed by (Moratti et al., 2019) .It consists of five data collection phases (G.1, G.2, H.1, V.1, V.2) and three analysis levels (O.0, O.1, O.2), each characterised by increasing accuracy and decreasing epistemic uncertainty.

- Level O.0 provides a statistical, portfolio-wide estimate of global and local performance using an equivalent pier model and Monte Carlo simulations based on demographic distributions.
- Level O.1 extends the assessment to each individual wall of each church, combining deterministic geometric data from V.1 inspections with stochastic variables and simplified NLPO/NLKA simulations.
- Level O.2 incorporates detailed measurements from V.2 inspections to generate deterministic pushover analyses and refined kinematic checks, enabling church-specific safety evaluations.

This multilevel approach enables robust prioritisation: only a limited number of churches display structural configurations, typically involving large or geometrically complex vaulted systems, for which simplified analyses cannot ensure reliable safety evaluation. These structures progress to Level 3, where advanced nonlinear 3D AEM simulations are carried out, and, when required, to Level 4, where strengthening measures are designed and validated. The three churches presented in this chapter belong to this restricted subset. Their analysis therefore represents the final stage of the SMAC methodology.

8.2 INTRODUCTION

The advanced assessment and retrofitting procedures presented in the previous chapters are here applied to three representative Dutch churches, referred to as Church 1, Church 2, and Church 3. These structures belong to the limited group of buildings

identified as requiring more refined analyses within the SMAC framework. As explained in (Moratti et al., 2019) and summarised in Chapter 1, the SMAC framework was developed to manage large portfolios of unreinforced masonry churches exposed to induced seismicity through a systematic, multi-level procedure based on progressive refinement of knowledge and modelling complexity.

The transition from portfolio-wide, simplified evaluations (Levels 0–2) to building-specific numerical analyses (Levels 3–4) is a defining feature of the SMAC methodology. Starting from an initial inventory of 226 churches, the results of Levels 0–2 progressively narrowed the portfolio by identifying those structures for which simplified NPR-based checks could not deliver a sufficiently reliable safety evaluation.

The development of the modelling structures within the Extreme Loading for Structures (ELS) software, (Applied Science International, 2024a), were facilitated by the Building Information Modelling (BIM) framework. First, a point cloud of the whole church is obtained during inspections using a laser scan; the geometrical model is then built within a BIM-based software; and lastly, it is converted into the structural model within ELS software.

From the original portfolio, fifteen churches were passed to Level 3. What these churches have in common is the presence of vaulted ceilings, some with very complex geometries, significant geometric irregularities, pre-existing crack patterns, and reinforcement strengthening measures.

Each church, however, has its own unique characteristics; the three selected churches, in fact, feature significantly different geometries, vault types, and construction characteristics. Dutch masonry vaults differ substantially from the classical Mediterranean cross-vault typologies commonly addressed in research and experimental campaigns: examples include ribbed vaults, melon-shaped vaults, and distinctive brick arrangements such as fish-bond patterns. These vaults often reach spans of 8–9 metres, far exceeding the scale of existing experimental tests. As no dedicated full-scale experimental benchmarks exist for such configurations, numerical predictions must be interpreted as lower-bound estimates, driven by conservative modelling assumptions rather than calibration against physical tests. This conservative interpretation is reinforced by three factors:

- Material prescriptions in the NPR: Dutch guidelines for existing masonry require using 40% of the nominal mechanical properties for historical materials,

inherently biasing the assessment toward the safe side of the structural response.

- Absence of in-situ destructive or semi-destructive testing: consistent with heritage preservation principles and client requirements, no material tests were conducted on the churches. As normative values generally reflect lower fractiles of material strength, their use inevitably reinforces the conservative nature of the analyses.
- Lack of experimental benchmarks for complex vaults: the only available benchmark is the LNEC cross-vault test, which, although scientifically relevant, features a simple geometry and significantly smaller scale compared to Dutch vaults. While its use helps validate the modelling strategy, it cannot fully represent the diverse vaulting systems considered here.

These limitations call for a modelling strategy that balances accuracy and practicality. The approach adopted in this work relies on the meso-modelling validation and sensitivity analyses presented in earlier chapters, but also incorporates pragmatic simplifications necessitated by the professional nature of the project.

This chapter presents the advanced seismic assessment conducted for Church 1, Church 2, and Church 3, following the workflow defined for Levels 3 and 4. For each case, the main geometric and architectural characteristics are analysed, along with the results of the seismic assessment of the as-built state (Level 3) and the reinforced configuration (Level 4).

Finally, a comparison between the different churches is presented, analysing the possible recurring behaviours and what causes the seismic behaviour to significantly vary.

8.3 GENERAL MODELLING STRATEGY FOR THE CASE STUDIES

The numerical analyses conducted for Church 1, Church 2, and Church 3 adopt a unified modelling framework developed within the SMAC programme to ensure a consistent, scalable, and reproducible approach for the seismic assessment of vaulted churches. Although each structure displays unique architectural features, the workflow presented in this section constitutes the shared methodological basis applied across all case studies and reflects the modelling philosophy established internally during the SMAC Level 3–4 activities.

A central objective of this thesis was to formalise this homogeneous modelling procedure, originally developed and refined within the professional practice of Studio Calvi during the assessment of the SMAC church portfolio. The strategy was conceived to be generalizable across different sizes, vault typologies, and structural complexities, enabling a uniform treatment of all churches analysed at Level 3 and preparing the ground for Level 4 retrofit design.

The modelling philosophy adopted in this thesis builds upon a coherent set of assumptions governing material behaviour, discretisation, boundary conditions, and contact mechanics, integrated within a unified workflow that has been progressively refined throughout the Level 3–4 activities. These same principles were subsequently employed and discussed in (Davis et al., 2024), where a subset of SMAC Level 3 churches was analysed as part of a peer-reviewed research dissemination of the project. That publication therefore documents and contextualises, in an academic venue, modelling assumptions that were originally developed within the SMAC engineering workflow.

Building upon this foundation, the present thesis provides a systematic and fully generalised formulation of the modelling procedure, ensuring its applicability to any vaulted church within the SMAC portfolio and enabling transparent comparison across different case studies.

All Level 3 and Level 4 analyses were performed using the set of eleven accelerograms prescribed by the NPR webtool for induced-seismicity scenarios. For each ground motion, nonlinear time-history (NLTH) analyses were performed, in full compliance with the (NEN, 2020) requirements for ground-motion characterisation.

Only structural or architectural features that demonstrably influence the global response were incorporated as case-specific refinements; all other assumptions were intentionally standardised to avoid modelling-induced variability and to ensure that differences in numerical behaviour reflect genuine physical characteristics.

The results of the nonlinear time-history analyses in terms of global response (e.g., and localised vault mechanisms) are presented separately for each church in the following sections. For clarity and comparability, the outcomes of the eleven accelerograms are synthesised using envelope and statistical measures, while case-specific behaviours are discussed in detail where relevant.

8.3.1 Modelling of walls, roof structure, and boundary conditions

Although the focus of this chapter is on the behaviour of the vaulted systems, the seismic response of the vaults cannot be understood independently from the surrounding structural context. For this reason, the numerical models include the entire church configuration using a consistent and standardised set of assumptions, in line with the SMAC Level 3 workflow.

The masonry walls are discretised using blocks of 0.30 × 0.30 × 0.30 m, unless local refinements are required near geometric discontinuities or vault springings. Wall tilting is incorporated whenever measured out-of-plumb exceeds 1%, as this condition alters the effective lateral stiffness and consequently the vault–wall interaction. The foundation level is modelled as fixed, in accordance with the modelling assumptions adopted in SMAC Level 3 studies. Soil–structure interaction was not considered, as no evidence of significant foundation deformability emerged during the inspection process and no project-specific geotechnical data were available

The roof structure is typically made of timber and includes trusses, rafters, purlins, secondary timber, and a plank. It is explicitly modelled together with connections among elements according to historical documentation and on-site survey. The in-plane stiffness provided by the timber planks nailed to the purlins is represented by an equivalent elastic membrane. The equivalent shear modulus G_{eq} is obtained through analytical formulations by (Gattesco & Macorini, 2014) for drift perpendicular to the purlins, and by (Brignola et al., 2008) for drift parallel to the purlins. Since the resulting stiffnesses are comparably low and of similar magnitude, a unique value of 2.15 MPa is adopted to represent the roof membrane in both directions.

Where a tower is present, three cases can be distinguished:

- the tower is completely detached from the church structure and it is not included in the model;
- the tower is adjacent but structurally detached from the church, in this case the tower is modelled in a simplified form to reproduce its global stiffness and mass contribution but without fine architectural details;
- the tower is structurally connected to the church and its fully included within the numerical model.

This is consistent with SMAC practice, as towers were typically analysed separately at earlier levels and, despite being heavily damaged non-structurally, generally satisfied

structural verifications. Including the tower ensures that its mass and stiffness influence on the church's dynamic behaviour is properly captured.

8.3.2 Material models

8.3.2.1 Masonry

Material properties for clay brick masonry follow Section F.4.6 (Table F.2) of (NEN, 2020). In accordance with footnote (d), which recommends property reduction when pre-1945 clay brickwork shows poor mortar quality, the mean values of strength and stiffness are reduced by 40%. This choice ensures a conservative representation of the masonry behaviour and aligns with the lower-bound interpretation discussed in Section 8.1. The resulting elastic and strength parameters, Table 4.1, are applied uniformly across all masonry elements to maintain consistency and provide a conservative lower-bound representation of material behaviour.

Table 8.1. Masonry material properties used in ELS

Brick Masonry Material Properties	***Good quality***	***Poor quality (reduced by 40%)***
Young's Modulus	5000 MPa	3000 MPa
Shear Modulus	2000 MPa	1200 MPa
Specific Weight	19 kN/m^3	19 kN/m^3
Compressive Strength	8.5 MPa	5.1 MPa
Tensile Strength	0.1 MPa	0.06 MPa
Cohesion	0.3 MPa	0.18 MPa

The in-plane and out-of-plane behaviour of masonry elements follows the meso-modelling framework presented in Chapter 4. Tension is represented through a bilinear law with linear softening up to ultimate strain following (Malomo et al., 2020a), while compression follows a simplified version of the elastoplastic fracture model by (El-Kashif & Maekawa, 2004). Shear springs adopt a Mohr–Coulomb yield criterion, consistent with the cyclic response of masonry joints.

8.3.2.2 Timber

Timber properties derive from (BS EN 338:2003 Structural Timber – Strength Classes, 2003). When no specific documentation is available, a default grade C14 is adopted for pre-1945 structures and C18 for post-1945 buildings. Mean material values are taken as 1.3 times the characteristic values, following (NEN, 2020).

Timber elements follow a bilinear constitutive law with a softening branch after peak stress. Shear springs follow a Mohr–Coulomb criterion, and density is assigned according to EN 338. Nail connections between planks and rafters are modelled using mean capacities derived from EC5 formulations for timber embedment and withdrawal strength.

8.3.3 Interface behaviour and friction model

In the adopted meso-scale formulation, masonry is modelled as a homogeneous continuum material discretised into elastic elements. As a consequence, no frictional interfaces are introduced between masonry elements: adjacent elements share the same material continuum and interact through the cohesive–frictional laws defined for masonry springs. This ensures that the structural behaviour of walls and vaults is governed by the constitutive law of the masonry material, rather than by artificial contact interfaces.

Contact or friction models are introduced only where different materials interact, in accordance with the modelling practice established in the SMAC Level 3 workflow. The bearing material model of ELS is used in these cases. This model:

- transmits compressive stresses through a linear elastic response up to the compressive strength of the weaker material,
- does not transmit tensile stresses, separating when the normal stress becomes negative,
- activates shear resistance according to a Mohr–Coulomb criterion, with friction coefficients taken from Table F.3 of (NEN, 2020).

This type of interface is used only for specific material-to-material interactions, such as:

- the interface between timber planks and rafters in the roof diaphragm;
- timber-to-masonry connections, such as historical nails or bearing elements;
- steel-to-masonry contacts, where plates or anchorages transfer forces into the walls;

- the roof membrane–purlin/rafter interface, where sliding and uplift may occur;

By contrast, the connection between concrete ring beams and masonry walls is modelled as a monolithic interface unless deterioration or sliding is explicitly documented in the inspection.

This approach prevents the introduction of artificial sliding or separation within the masonry body and ensures that discontinuities develop only in accordance with the constitutive laws of the masonry material itself.

8.3.4 Modelling of the vaulted system

The vaulted systems were modelled using the AEM meso-modelling approach presented in Chapter 4, where masonry is idealised as an assemblage of elastic blocks interacting through nonlinear zero-thickness interfaces. Vault discretisation followed a refined strategy informed by laser-scanning point clouds, ensuring that the numerical model accurately reproduced the as-built geometry while remaining computationally feasible for large, multi-vault churches.

The plan geometry of each vault field was constructed through a polar mesh generated by revolving polylines extracted from the point cloud, simulating the geometric curvature of the vaults. A uniform block size of 0.20 × 0.20 × 0.15 m (the last dimension corresponding to the vault thickness) was adopted across all case studies. This choice satisfies three key modelling requirements:

- capturing the primary geometric curvature of the vault;
- ensuring adequate resolution around springings, intersections, or geometric transitions;
- avoiding excessive fragmentation that would compromise computational performance.

Where structurally justified, specific architectural details, such as ribs or characteristic Dutch brick patterns (e.g., fish-bond arrangements), were included explicitly in the geometry. Ribs were modelled using an equivalent mortar-like material with elastic and strength parameters adjusted to reflect their larger effective section, ensuring correct stiffness and interaction with the adjacent vault fields. In all other cases, simplified equivalent geometries were adopted to preserve the correct global behaviour without artificially increasing the mesh density.

No additional mechanical enhancement was introduced at the material or interface level: the correct structural response arises from the explicit geometric representation,

the frictional behaviour of the interfaces, and the meso-scale formulation adopted for the masonry material. This modelling strategy, uniformly applied across Church 1, Church 2, and Church 3, ensures both consistency and robustness in the simulation of the seismic behaviour of complex vaulted systems.

8.4 CHURCH 1

8.4.1 Architectural and structural description

Church 1 is a Romano-Gothic Church built in the early 13th century. It consists of a main nave with a semi-circular apse, originally constructed with timber ties at the vault springings and later extensively modified during a major restoration in the 1960s. In particulare, from historic documentation, timber ties were replaced with the installation of reinforced concrete ring beams, vault cracks were repaired, the timber roof was rebuilt, and external buttresses, with no structural function, removed.

(a) (b)

Figure 8.1 Church 1: external view (a) and internal view of the vault (b)

The vaulted system is particularly distinctive. The nave and apse are covered by melon-shaped vaults with ribs and a herringbone brick pattern, consistent with the Dutch tradition of complex vault geometries. The vault thickness is approximately 0.15 m, and ribs are composed of trapezoidal clay blocks intended to provide continuity at the intersection between vault fields. Each vault stands on masonry arches, to which the load is transferred.

The roof structure consists of timber trusses and main purlins, which sustain the rafters and secondary purlins. Most connections rely on friction or historical nails, except where pockets or visible fixings suggest limited tensile or shear capacity. The tower was added in the 14th century and it is classified as semi-detached, consequently it was not

included in the numerical model. Furthermore, its seismic assessment was completed at Level 2 and found to be structurally verified.

Church 1 presents the typical characteristics of Groningen vaulted churches: large spans relative to the thickness, complex brickwork, and significant geometric irregularities at the springings and intersections. These attributes, combined with the removal of historical ties, made it a suitable candidate for Level 3 assessment.

8.4.2 Seismic assessment

The Level 3 seismic assessment was carried out through nonlinear time-history (NLTH) analyses using the set of eleven accelerograms prescribed by the NPR webtool for induced-seismicity scenarios. The as-built configuration revealed that Church 1 is not verified under the NC limit state.

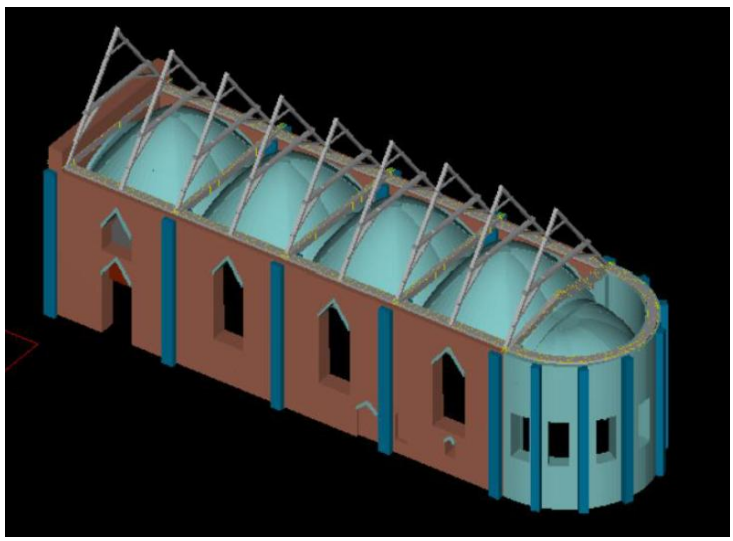

Figure 8.2 Numerical model of Church 1

The results, ***Figure 8.3***, show that the main structural problem is related to the masonry arches rather than masonry vaults. Across the most severe ground motions (e.g., signals I2, I4, I9), the lower arches between the vault fields exhibited progressive cracking, hinge formation, and in several cases full collapse. These arch failures compromise the boundary conditions of the vaults, triggering partial or complete vault collapse in some bays. Observed failure modes include:

- Collapse of the arches between the apse and Bay 4, consistently identified as the most critical zone.
- Failure of the lower arches in each bay, especially where no semi-columns are present to provide vertical confinement.
- Damage or collapse of vault fields, but only as a consequence of arch failure.
- Lintel failures at several window openings, though these did not control the overall collapse mechanism.
- Limited damage to the roof, primarily in the diagonal trusses.

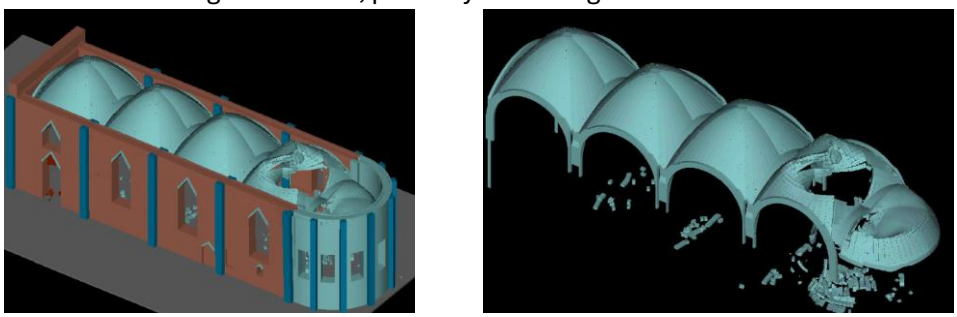

(a) (b)

Figure 8.3 Damage configuration after the application of one accelerogram: whole structure (a) and vaults detail (b) at Level 3 of Church 1

A key insight from the Level 3 analysis is that the vaults do not fail autonomously. Their seismic performance deteriorates only when the arches that establish their thrust line and load-distribution path lose stability. This confirms one of the central principles discussed in this thesis: vault behaviour cannot be assessed in isolation, and the stability of the supporting system is a prerequisite for reliable vault performance.

8.4.3 Retrofitting proposal

The Level 4 intervention strategy for Church 1 directly addresses the failure modes observed in the seismic assessment. Since the collapse sequences are initiated by the instability of the internal arches, the retrofitting measures focus on restoring an effective load path and ensuring proper interlocking between arch elements and adjacent masonry walls.

8.4.3.1 Retrofitting of arches and vault supports

Historical documentation indicated a lack of proper interlocking between the inner and outer blocks of the masonry arches. This deficiency is critical because the lower arches

act as the primary supports for the melon vaults. To re-establish structural continuity, the following interventions were implemented in the Level 4 numerical model:

- Installation of Helifix bars at the springings to connect the inner and outer arch rings.
- Restoration of effective interlocking between the arch blocks and the supporting walls.
- Modification of the arch-wall interface from a weak or frictional contact to a continuous elastic masonry interface, preventing premature sliding.

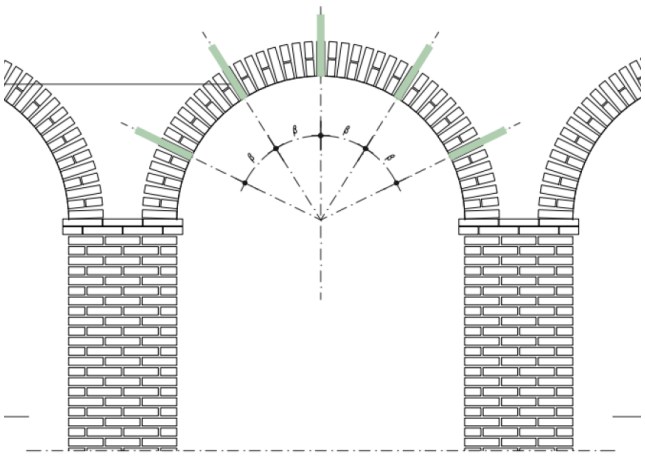

Figure 8.4 Example of arch reinforced with steel bars

These strengthening measures significantly alter the collapse mechanism: once the arches are stabilised, the vaults remain intact across all eleven input motions, confirming that their observed failure in the as-built configuration was secondary.

8.4.3.2 Roof structure adjustments

Some roof elements, primarily diagonal struts and ties, continued to experience local failures even in the retrofitted configuration. However, these failures:

- remain non-critical for overall stability,
- do not compromise the safety of occupants,
- and do not interact negatively with the vault performance.

To inform potential future detailing by the client, all normal and shear force demands for these connections were extracted and provided separately, assuming elastic behaviour.

8.4.3.3 Level 4 results

The retrofitted model withstands the full suite of eleven accelerograms without collapse of the vaults or supporting arches. Only minor, localised roof damage remains. The most severe record (signal I2) produces limited cracking but no loss of structural integrity.

This case study exemplifies how targeted reinforcement of the vault's support system, rather than of the vault itself, can be sufficient to ensure seismic safety, reinforcing the methodological principle that vaulted systems must be evaluated as part of the global structural configuration.

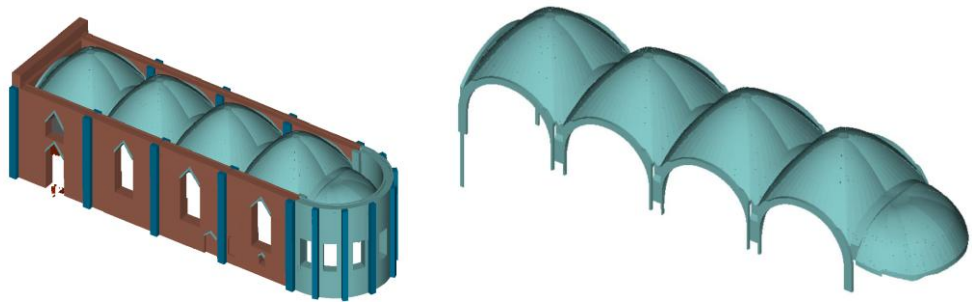

(a) (b)

Figure 8.5 Damage configuration after the application of one accelerogram: whole structure (a) and vaults detail (b) at Level 4 of Church 1

8.5 CHURCH 2

8.5.1 Architectural and structural description

Church 2 is the remains of an original late Romanesque cruciform church. In 1238 the church was damaged by a fire and it was rebuilt in 1259. A shallow transept and a new rectangular choir bay were added. At the same time, dome vaults were built, typical of late Romanesque. The transept was probably demolished in the early 16th century. Traces of the transept can still be recognized on the southern façade. During the rebuilding in 1250, a 33 m high tower was built on the west facade, which was demolished in 1808 and replaced by the current steeple. In the historical documents there is no trace of intervention with concrete beams at the attic level, while timber tie beams at the vault impost were added in the 19th century. Anchor plates connected to the attic floor joists are also visible from the outside of the church.

(a) (b)

Figure 8.6 Church 2: external view (a) and internal view of the vault (b)

The interior presents two dome vaults positioned in the eastern portion of the building, decorated with medieval painted brickwork patterns. The vaults rest on masonry arches of limited thickness, some of which are embedded into recesses and do not benefit from lateral buttressing. The western portion of the nave features a flat timber ceiling and a large pipe organ sitting on an explicitly modelled timber balcony.

The roof structure is complex and consists of multiple layers of trusses, purlins, rafters, diagonal struts, secondary bracing elements, and ties supporting the steeply pitched roof. Many connections rely solely on friction or historical nailed joints with limited tensile capacity, and several roof elements act as ties for the front and back gable walls. Local pocketing between timber elements provides partial restraint, but simultaneously introduces brittle failure mechanisms under seismic loading.

Overall, Church 2 combines complex vault geometry, geometric irregularities, weak arch supports, and a highly articulated yet fragile roof system, which together justify its selection for Level 3 modelling.

8.5.2 Seismic assessment

The Level 3 seismic assessment was carried out by performing nonlinear time-history (NLTH) analyses using the eleven accelerograms prescribed by the NPR webtool for induced-seismicity scenarios.

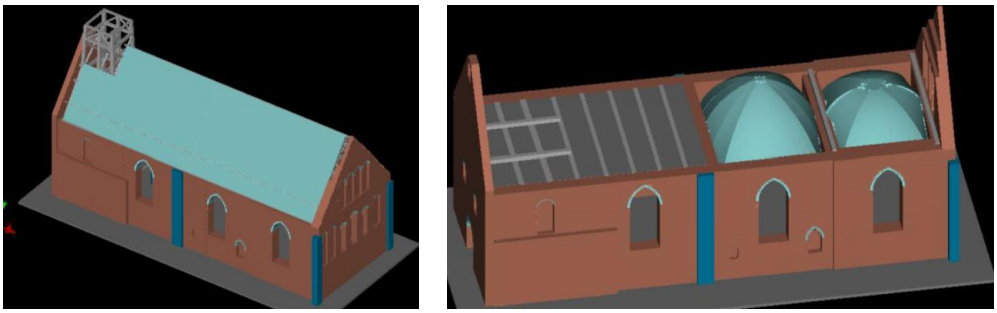

(a) (b)

Figure 8.7 Numerical model of Church 2 with (a) and without (b) the roof

The as-built configuration of Church 2 is not verified at the NC limit state, and the observed failure mechanisms reveal a multi-source vulnerability involving:

- collapse of the vault fields,
- failure of the arches between vaults,
- failure of buttresses,
- lintel failures,
- severe damage to roof connections,
- local collapse of the gable,
- sliding of the wallplate.

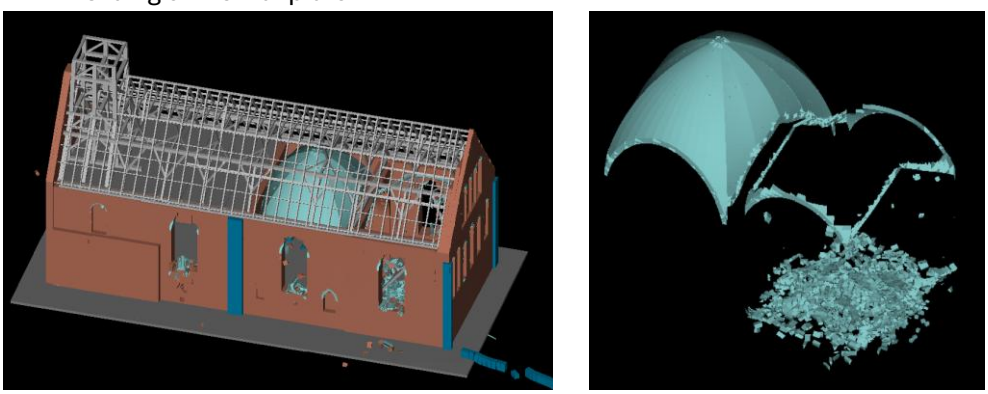

(a) (b)

Figure 8.8 Damage configuration after the application of one accelerogram: whole structure (a) and vaults detail (b) at Level 3 of Church 2

8.5.2.1 Vault behaviour

A key difference from Church 1 emerges here: the vaults of Church 2 collapse even when the arches have not completely failed, particularly for the stronger records (I1–I4, I7–

I11). The vaults near the back façade are especially vulnerable, showing early formation of tensile cracks and progressive segment separation. This indicates that the vaults possess insufficient intrinsic capacity, and that arch instability alone does not explain their collapse.

8.5.2.2 Arch behaviour

Several arches between the vaults show hinge formation, out-of-plane rotation, or sliding at the springings. In multiple signals, the arch failure precedes or triggers the collapse of the adjacent vaults. In others, arch and vault failures develop concurrently due to geometric and material weaknesses.

8.5.2.3 Other critical mechanisms

Across nearly all records:

- buttresses at the eastern end fail locally,
- lintels at all façades exhibit shear or bending failure,
- roof elements (trusses, diagonal braces, ties) fail due to shear and pull-out at connections,
- the back gable experiences local collapse or severe cracking,
- the wallplate slides on the masonry support due to lack of anchorage.

Notably, the roof behaves as a highly flexible diaphragm, amplifying out-of-plane demands.

8.5.2.4 Interpretation

Church 2 exemplifies a case where:

- arch strengthening alone (as in Church 1) is insufficient to guarantee vault stability,
- the vaults require direct strengthening,
- local geometric complexity (dome vaults, recesses, absence of laterally restraining elements) makes the vault system intrinsically vulnerable.

This supports one of the methodological conclusions of the thesis: vault safety depends simultaneously on intrinsic vault capacity and boundary conditions, and both must be addressed when deficiencies are present.

8.5.3 Retrofitting proposal

The Level 4 retrofit measures for Church 2 were designed based on the failure patterns observed in the Level 3 assessment. In contrast to Church 1, where reinforcing the arches alone was sufficient, here an effective retrofit requires combined strengthening of both the vaults and their supporting arches, complemented by selective interventions on the roof system.

8.5.3.1 Strengthening of the vaults

Two dome vaults are retrofitted using FRCM strips applied at the extrados, localised around the springings where collapse was observed during the NLTH analyses. The FRCM adopts *Geocalce F Antisismico* (mortar) and Geosteel Grid G400 (balanced bi-axial reinforcing mesh). Only the lower third of the vault is treated to respect aesthetic and heritage constraints while still restoring structural continuity. In the numerical model, the FRCM system is represented through an equivalent RFT mesh, calibrated to match the stiffness and strength of the composite system.

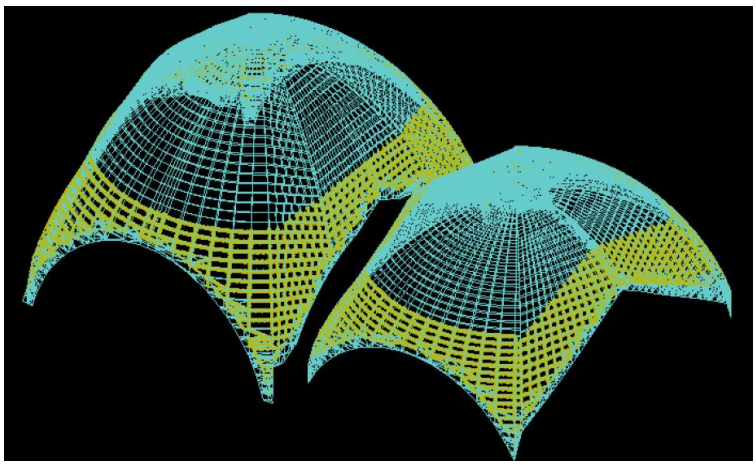

Figure 8.9 Wireframe view of the vaults with the reinforcement modelled as RFT elements of Church 2

8.5.3.2 Strengthening of arches and arch–wall interfaces

Arch failure being a primary mechanism, multiple interventions are included:

- installation of steel helical bars (Steel Dryfix) at the arch springings,
- interlocking the inner and outer arch rings,
- reinforcing the arch–wall connection to prevent sliding failures,

- out-of-plane reinforcement of the arch between vault and attic using transverse bars drilled into the wall thickness.

These measures collectively suppress both in-plane and out-of-plane mechanisms observed during Level 3.

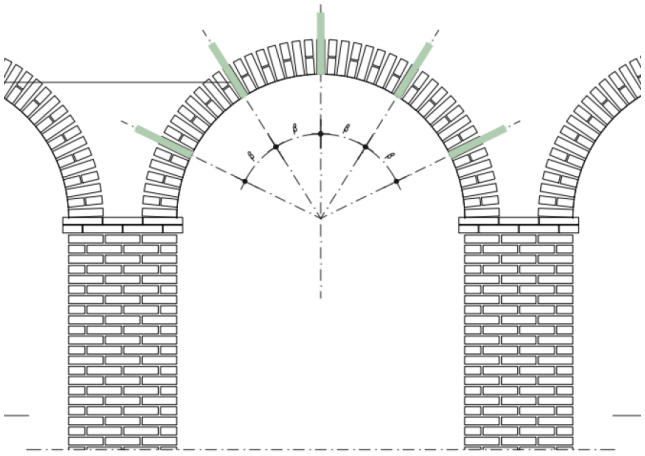

Figure 8.10 Example of arch reinforced with steel bars

8.5.3.3 Roof interventions

Given that roof fragility amplifies seismic demands, several key retrofits are implemented:

- improvement of rafter–wallplate connections,
- anchoring of the wallplate to masonry walls,
- reinforcement of truss diagonals and stiffening elements between trusses,
- retrofitting of timber ties supporting the back gable,
- application of Planitop Intonaco Armato (M15) on the upper part of the back gable,
- installation of a new roof membrane glued to the existing one, eliminating sliding mechanisms.

8.5.3.4 Level 4 results

The retrofitted configuration withstands all eleven accelerograms without collapse of the vaults or supporting arches. Damage persists only in local roof connections, which remain non-structural relative to the vaulting system. The back gable experiences cracking but does not collapse, and foundation verifications remain satisfied.

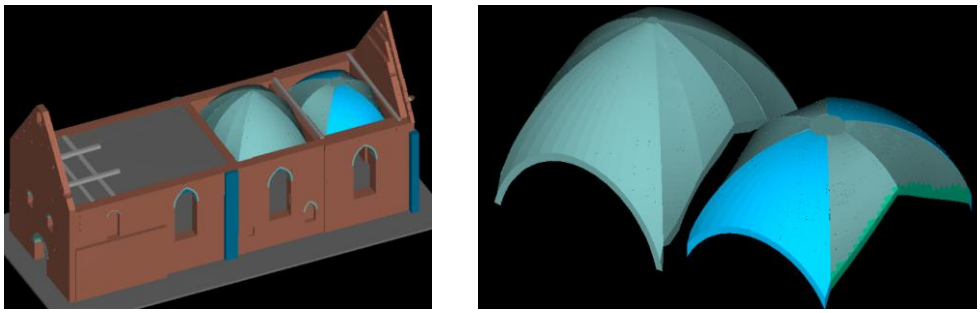

(a) (b)

Figure 8.11 Damage configuration after the application of one accelerogram: whole structure (a) and vaults detail (b) at Level 4 of Church 2

8.5.3.5 Interpretation

Church 2 demonstrates that:

- when both vaults and arches exhibit insufficient capacity,
- a combined strengthening strategy is not only appropriate but necessary,
- confirming that vault safety must be considered within the entire supporting system,
- and that interventions must ensure both intrinsic vault strength and stable boundary conditions.

8.6 CHURCH 3

8.6.1 Architectural and structural description

Church 3 was built in the second half of the 13th century. It was a simple hall church with a straight-closed choir and was dedicated to Mary. In the 16th century the nave was expanded to its current size with the five-sided closed choir and in 1705 with transepts. The old freestanding tower was demolished in 1734. On August 26, 1896, the tower burned down. In 1897, the tower was rebuilt. In 1937 a restoration took place, but no major repair was carried out on the structural elements.

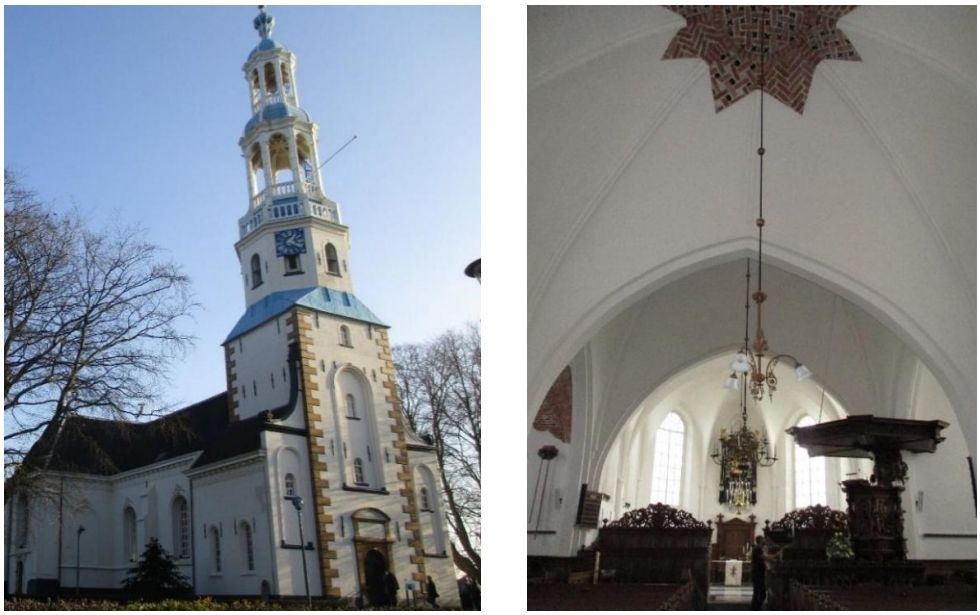

(a) (b)

Figure 8.12 Church 3: external view (a) and internal view of the vault (b)

The vaulted system is extensive and architecturally heterogeneous. From archival documentation and local inspections, the presence of an old concrete overlay applied during a past intervention came out. However, no information is available regarding its reinforcement, its thickness continuity, or its bond behaviour with the vault. As a result, its structural role is uncertain: it may function as a stiffening layer, act primarily as dead load, or behave in an intermediate condition depending on adhesion and cracking.

In addition, the point cloud survey revealed significant residual deformation in the central vault and the first bay of the nave, with an asymmetric depressions towards midspan. These deformations are likely the outcome of long-term settlement, thermal movements, or past structural interventions that modified the vault's stress state. Because these deviations from the ideal geometry can strongly influence collapse mechanisms under seismic loading, they were explicitly studied through an additional vault model incorporating the measured deformed geometry.

Overall, Church 3 is characterized by:

- heterogeneous vault typologies,
- uncertain past interventions (concrete overlay),
- geometrical irregularities,

- locally weak arch and buttress configurations,
- and a highly articulated roof system with limited tensile capacity.

These features fully justify the need for Level 3 analysis.

8.6.2 Seismic assessment

Nonlinear time-history (NLTH) analyses were performed using the eleven accelerograms prescribed by the NPR webtool for induced-seismicity scenarios.

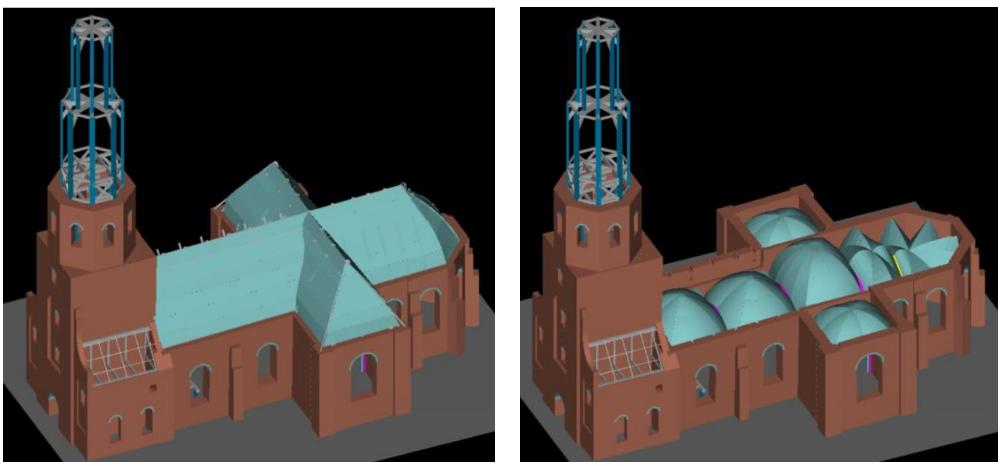

(a) (b)

Figure 8.13 Numerical model of Church 3 with (a) and without (b) the roof

The as-built configuration of Church 3 exhibits widespread collapse of the vaults, far more severe than in Church 1 and Church 2.

8.6.2.1 Vault behaviour

Across all signals (I1–I11), the following patterns are consistently observed:

- Total collapse of the apse vault, typically occurring within the first 4–5 seconds of the ground motion.
- Collapse of both transept vaults, developing shortly after the apse collapse.
- Severe damage and partial collapse of the central vault, often preceded by extensive cracking.
- Severe cracking in the nave vaults, which in some signals also progress towards collapse.

The vulnerability of the apse vault is particularly high due to its bombed geometry, where the keystone is lower than the formerets, producing an inverted curvature that facilitates early separation and sliding.

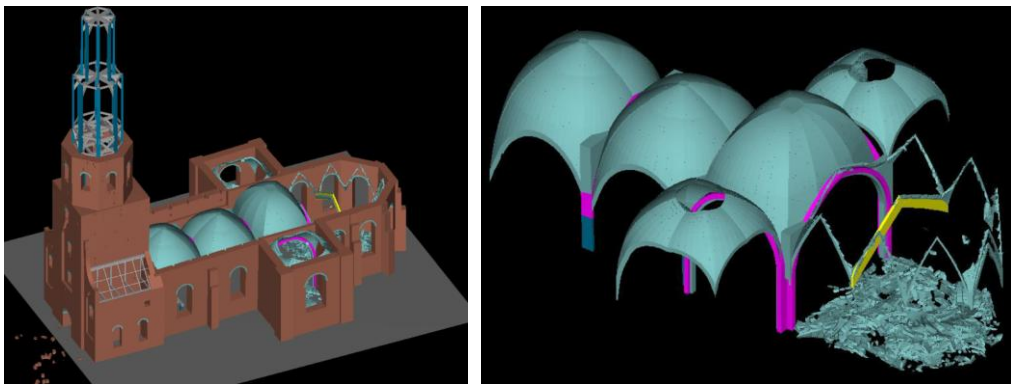

(a) (b)

Figure 8.14 Damage configuration after the application of one accelerogram: whole structure (a) and vaults detail (b) at Level 3 of Church 3

8.6.2.2 Influence of the past concrete intervention

The concrete layer applied to the apse vault behaves in an uncertain and potentially counterproductive way:

- If collaborating, it would only marginally increase capacity.
- If non-collaborating (poor bond), it acts primarily as added mass, increasing seismic demand.
- If partially cracked (likely), it may induce incompatible deformation modes.

Because of the absence of reliable historical information, the concrete layer was not assumed to provide significant structural resistance. The Level 3 analyses suggest that it did not prevent nor delay collapse, indicating that the overlay is either non-collaborating or insufficiently stiff to modify the global mechanism.

8.6.2.3 Influence of the existing vault deformations

A second vault model was created using the deformed geometry extracted directly from the point cloud. When this model is subjected to the most demanding accelerograms:

- central vault collapses,
- first vault of the nave collapses,

- collapse sequences occur earlier and more severely than in the idealized model.

The comparison shows: the deformed geometry systematically reduces vault capacity, accelerates collapse, and changes the relative timing of local mechanisms.

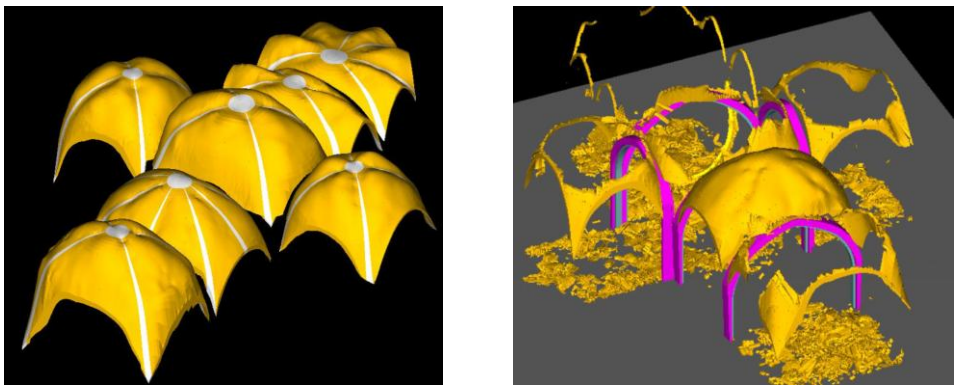

(a) (b)

Figure 8.15 Deformed vaults configuration (a) and their damaged configuration after the application of one accelerogram (b) at Level 3 of Church 3

This confirms that even moderate geometric distortions can significantly worsen the behaviour of thin, flexible Dutch vaults.

8.6.2.4 Other critical mechanisms

In addition to vault collapse, the following failures occur:

- severe cracking of tower walls,
- failure of roof truss connections,
- sliding of timber wallplates,
- collapse of timber decks inside the tower.

These failures, however, are secondary relative to the global collapse mechanism governed by the apse and transept vaults.

8.6.3 Retrofitting proposal

Given the severity of Level 3 collapse mechanisms, the retrofitting strategy for Church 3 targets:

1. strengthening of the vaults,
2. targeted reinforcement of roof connections,

3. stabilisation of critical wall-to-roof interfaces.

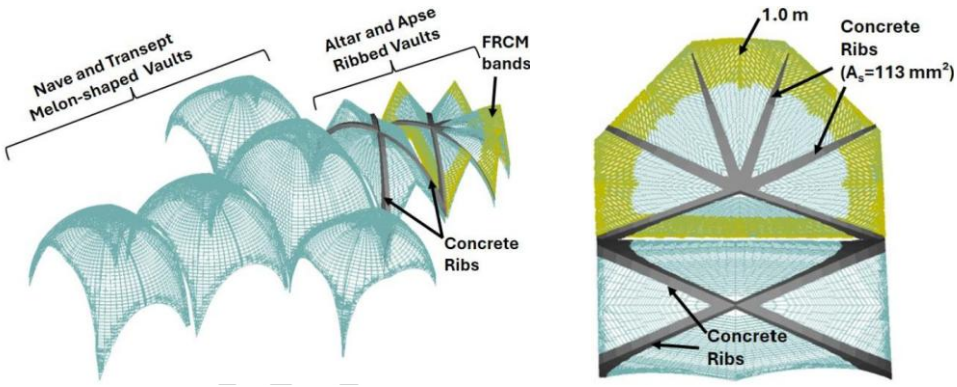

(a) (b)

Figure 8.16 Details of the reinforcement of the vaults: (a) general 3D view and (b) plan view of the vaults reinforced for Church 3

8.6.3.1 Strengthening of the vaults

The apse and transept vaults are retrofitted using FRCM bands (Geocalce F Antisismico + Geosteel Grid 600), applied along the perimeter of each ribbed vault with a minimum width of 1 m. This approach:

- restores continuity between separated vault segments,
- improves tensile capacity,
- limits early sliding at the ribs–field interface.

The FRCM system is modelled using RFT elements calibrated to match the mortar+fibre system.

8.6.3.2 Roof interventions

Given repeated failures in the roof under Level 3 signals:

- RFT connectors are added at critical roof joints,
- metallic strip connections are strengthened,
- wallplate anchorage is improved,
- upper-level ties in the transepts are reinforced.

These measures prevent progressive roof failures that could amplify vault shaking.

8.6.3.3 Performance of the retrofitted model

All eleven NPR accelerograms were applied to the retrofitted model. Results show:

- No collapse of apse, transept, central, or nave vaults,
- roof remains globally stable, though local deck failures in the tower persist (non-structural),
- tower walls remain damaged, but in a pattern consistent with Level 2 and non-critical for global stability,
- foundations satisfy capacity.

8.6.3.4 Level 4 results

All eleven NPR accelerograms were applied to the retrofitted model. Results show:

- No collapse of apse, transept, central, or nave vaults,
- roof remains globally stable, though local deck failures in the tower persist (non-structural),
- tower walls remain damaged, but in a pattern consistent with Level 2 and non-critical for global stability,
- foundations satisfy capacity.

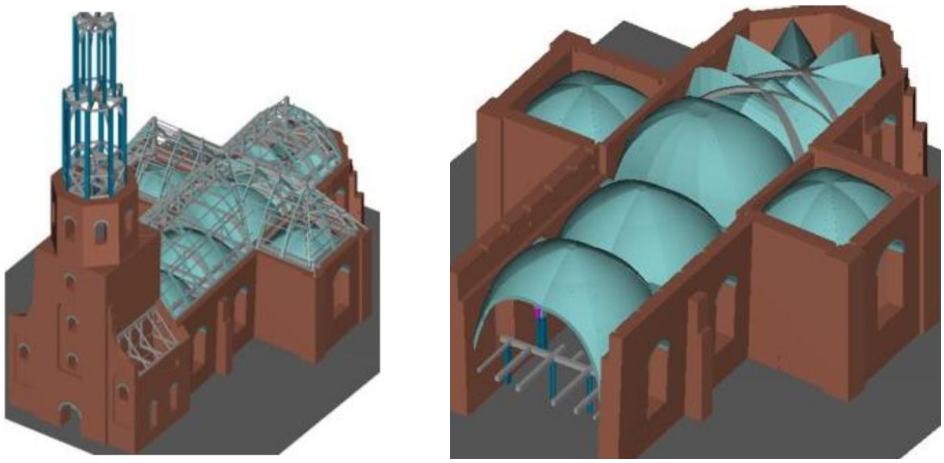

(a) (b)

Figure 8.17 Damage configuration of Church 3 after the application of one accelerogram: whole structure (a) and vaults detail (b) at Level 4

8.6.3.5 Interpretation

Church 3 demonstrates that:

- uncertainty about past interventions (e.g., concrete overlays) can significantly affect seismic behaviour;

- geometric deformations must be incorporated into the assessment, as they can meaningfully change collapse patterns;
- vault strengthening is indispensable when both material deficiencies and geometric distortions are present.

This case confirms that accurate modelling of historical vaults requires:

- correct material assumptions,
- correct geometric representation,
- and explicit consideration of past non-documented interventions.

8.7 CROSS-COMPARISON

These three case studies confirm the evaluation made in previous chapters: vaults behaviour is the results of the combination of several aspects: mechanical properties of masonry, geometry shape, boundary conditions, which include the interaction of the vaulted system with surrounding walls and roof and the presence of steel/timber ties, reinforced concrete ring beams.

Despite their differences, the analyses of these three structures (confirmed also by the results of the other Level 3 churches) show recurrent vulnerabilities: limited capacity of the supporting arches, weak vault-wall interlocking, absence of a box behaviour of the structure, and presence of geometrical and construction irregularities. The as-built configuration is different for each church and this explains how all these abovementioned aspects affect their behaviour. In Church 1, arch instability is the controlling mechanism, whereas in Church 2 the vaults themselves is characterized by insufficient intrinsic capacity. In Church 3, geometric distortions and uncertain past interventions dominate the response, demonstrating that the as-built geometry, including deformed configurations, can critically influence collapse patterns.

Starting from these evaluations performed in Level 3, the retrofit measures are designed in Level 4. In Church 1 the improvement of arches performance is sufficient to preserve the vaults system; a combined vault-and arch strengthening is necessary for Church 2 and Church 3. The last case is a clear example of how pre-existing damages and high deformations may affect the whole response of the structure, together with the interaction of previous retrofit measures.

The proposed AEM-based meso-modelling strategy proves to be robust in capturing interaction effects, progressive failure, and changes in collapse mechanisms after strengthening. At the same time, the analyses highlight the sensitivity of the results to

specific parameters identified earlier in the thesis, such as friction coefficients, tensile strength, and vault boundary conditions, reinforcing the importance of the sensitivity analyses presented in Chapter 5.

8.8 FINAL REMARKS

The three case studies presented in this chapter must also be understood within the broader framework of the SMAC multi-level methodology, which structured and guided the entire assessment process. The outlined procedure from Level 0 to Levels 3-4 allowed to analyse:

- Level 0: 226 churches;
- Level 1: 41 churches;
- Level 2: 41 churches;
- Levels 3-4: 16 churches.

A harmonised and systematic approach is used for all churches, and comparison among results of different churches can be carried out with limited source of uncertainty. Furthermore, starting from Level 2 the procedure is fully compliant with Dutch regulations (NEN, 2020).

The effort spent for Level 3, both in terms of time and cost, is limited to a small number of churches of the portfolio thanks to the ranking of the SMAC approach.

Level 3 allows to assess that among the different vaults' shapes, the most common are the ribbed shaped vaults, the so-called melon vaults. Their expected behaviour, ***Figure 8.18***, is defined based on: span, rise to span (R/L) ratio, and presence of ties. Vaults with shorter spans (L < 6 m) and higher curvature (R/L > 0.85) generally exhibit a more favourable response, if adequate ties or equivalent restraining elements are present, otherwise failure mechanisms may develop also in this case. For larger spans (L > 6 m) the vaults behaviour become more critical. Indeed, both low-curvature vaults (R/L < 0.85), and high-curvature vaults (R/L > 0.85), tend to be severely damaged. It can be noted that ties play a decisive role for all span categories, and their absence is consistently associated with an unfavourable or unsafe mechanism.

It is important to underline that ***Figure 8.18*** illustrates the expected behaviour, usefull for a first fast classification; other aspects, such as existing damages, deformations, walls' out of plumb, will strongly affect the effective behaviour of the structure.

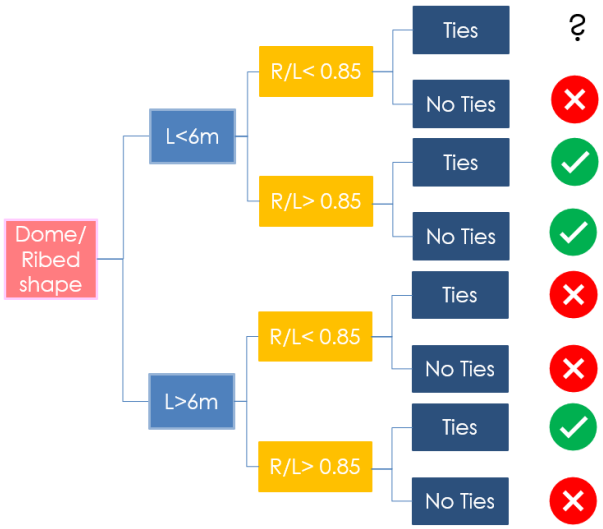

Figure 8.18 Statistical considerations of collapse or no collapse of vaults considering the 16 case studies

Building upon these portfolio-level observations, the detailed Level 3 and Level 4 analyses of the three churches confirm that vaults cannot be assessed in isolation. In Church 1, vaults possess adequate intrinsic capacity and collapse only when arch instability alters boundary conditions. In Church 2, vaults exhibit insufficient tensile capacity independently of arch behaviour. In Church 3, geometric distortions and undocumented past interventions dominate the collapse mechanism.

Overall, the case studies validate the modelling framework developed in the thesis and highlight the practical value of the SMAC approach in prioritising resources, identifying critical configurations, and defining effective, minimally invasive strengthening solutions.

9 CONCLUSIONS

9.1 KEY FINDINGS

The seismic assessment of masonry vaults, with variable geometries and tri-dimensional arrangement, has become a fundamental research area due to their vulnerability. Most of historic masonry buildings are characterized by vaulted ceiling, which were built by ancient masters following the rule of thumb and experience-based practices. Even though a modern science has been developed on the mechanical behaviour of this structural component, knowledge about the effects and potential collapse modes is still lacking, especially because of their geometric complex configuration, the unpredictable interaction with other structural elements, e.g. walls, and their sensitivity to changes in boundary conditions, e.g. settlements.

Within this context, the present study explores the chance of employing the Applied Element Method (AEM), part of discrete elements formulations, to assess the seismic behaviour of historic masonry buildings characterized by vaulted system. The AEM methodology has been demonstrated to be able to simulate the responses of masonry both at local level, considering in-plane and out-of-plane behaviours of wall components, and at the global level by modelling entire buildings. The methodology satisfactory simulates the elastic phase, initiation and propagation of cracks, up to failure and even element detachment.

The proposed meso-modelling approach built in the AEM framework was found to be able to reproduce the seismic response of masonry cross vault, compared against experimental shaking table test. The model captures the overall crack pattern, the formation of plastic hinges, and the main failure mechanism of in-plane shear. Results of simulations have been also compared with the ones obtained using other formulations, by means of Finite Element Method (FEM) and Discrete Element Method (DEM). A reliable consistent has been reach among the three methodologies, with the AEM giving the balance between accuracy and computational efforts.

The findings obtained in this work reveal that AEM method can be used for the numerical assessment of masonry vaults and historic masonry building with vaulted ceiling. Depending on the boundary conditions, material properties and pre-existing damage patterns, the method is able to capture the damage initiation, development of cracks and the failure mechanisms when subjected to ground shaking. Furthermore, the modelling

and computational efforts are relatively modest considering the high level of accuracy observed, especially when compared with other modelling approaches.

Finally, these considerations make the proposed methodology suitable for professional practice and can effectively support practitioners in real engineering applications, where the need to balance the level of accuracy of the results and the time required to obtain them is extremely important.

9.2 POTENTIAL FUTURE DEVELOPMENTS

The methodology proposed in this thesis is still in its early stage of development. Although significant progress has already been achieved, several aspects for improvement, related to the modelling choices, remains to be carried out to fully consolidate and standardize the approach.

There are very few experimental shaking table tests performed on scaled vaults, to an even lesser extent on full-scale ones; this inevitably led to limit the possibility of validating the numerical modelling approach on different vault typology, and most importantly, on different vault dimensions. The latter is a significant feature from the numerical viewpoint, because when transferring the knowledge from a small specimen to a larger one, the influence of mesh dimensions and material properties may be different. Indeed, the results obtained from the sensitivity analyses on the LNEC tests have been used as a starting point for the modelling of the bigger Dutch vaults, which consequently represent a kind of lower bound limit.

In this context, the micro-modelling of a whole Dutch vault may be of interest in order to compare its results with the one obtained using the meso-modelling approach, as it has been done for the LNEC simulation. It further allows to take into account the effective brick pattern, which can be very heterogenous even on a single vault. Because of the complexity of the configurations of the case studies presented in this thesis, and the restricted timing of the project this was not built.

An additional open point, related to modelling process, is the investigation on how other mechanical and numerical parameters (e.g. mesh sizes, residual shear strength factor, interface material between masonry and FRCM) affect the response of a vault subjected to seismic loading. Particular attention has been spent on Separation Strain parameter, because of its novelty, it in fact represents the strain corresponding to the detachment of rigid elements, influencing the post-peak behaviour of masonry.

References

A

Abrahamse, J. E., Baas, H., & Rutte, R. (2009). Dutch Heritage: Current State of Research on the History of Architecture, Urban Development and the Man-Made Landscape. In *OverHolland* (Vol. 8, pp. 87–114).

Alecci, V., Misseri, G., Rovero, L., Stipo, G., De Stefano, M., Feo, L., & Luciano, R. (2016). Experimental investigation on masonry arches strengthened with PBO-FRCM composite. *Composites Part B: Engineering*, *100*. https://doi.org/10.1016/j.compositesb.2016.05.063

Anania, L., Badalà, A., & D'agata, G. (2017). Seismic retrofitting of masonry vault using CFRP. *Alternativas*, *17*(3). https://doi.org/10.23878/alternativas.v17i3.208

Antonioli, A., Piccinini, D., Chiaraluce, L., & Cocco, M. (2005). Fluid flow and seismicity pattern: Evidence from the 1997 Umbria-Marche (central Italy) seismic sequence. *Geophysical Research Letters*, *32*(10). https://doi.org/10.1029/2004GL022256

Applied Science International, L. (2024a). *Extreme Loading ® for Structures: Theoretical Manual* (L. Applied Science International, Ed.). www.appliedscienceint.com

Applied Science International, L. (2024b). *Extreme Loading ® for Structures: Theoretical Manual* (L. Applied Science International, Ed.). www.appliedscienceint.com

Arcidiacono, V., Cimellaro, G. P., Piermarini, E., & Ochsendorf, J. (2016). The Dynamic Behavior of the Basilica of San Francesco in Assisi Using Simplified Analytical Models. *International Journal of Architectural Heritage*, *10*(7). https://doi.org/10.1080/15583058.2016.1158333

Arno, M. (2021). New functions of rural sacral buildings in the Groningen province, The Netherlands. *Architectus*, (1(65)). https://doi.org/10.37190/arc210104

B

Bacigalupo, A., Cavicchi, A., & Gambarotta, L. (2012). A simplified evaluation of the influence of the bond pattern on the brickwork limit strength. *Advanced Materials Research*, *368–373*. https://doi.org/10.4028/www.scientific.net/AMR.368-373.3495

Barends, F. B. J. (2002). A Dutch leaning tower saved in 1866 by the same method used for the Pisa tower. *Geotechnique*, *52*(2). https://doi.org/10.1680/geot.2002.52.2.141

Bartoli, G., Betti, M., & Borri, C. (2015). Numerical modeling of the structural behavior of Brunelleschi's Dome of Santa Maria del Fiore. *International Journal of Architectural Heritage*, *9*(4). https://doi.org/10.1080/15583058.2013.797038

Basilio Sanchez, I. (2007). *Strengthening of arched masonry structures with composite materials*. Guimaraes, Portugal.

Bellini, A., Incerti, A., & Mazzotti, C. (2022). Cyclic Out-of-Plane Behavior of FRCM-Strengthened Masonry Walls. *Key Engineering Materials*, *916 KEM*. https://doi.org/10.4028/p-560xb3

Benvenuto, E. (1991). An Introduction to the History of Structural Mechanics, Part I: Statics and Resistance of Solids, Part II: Vaulted Structures and Elastic Systems. *SIAM Review*, *33*(4). https://doi.org/10.1137/1033164

Bernardini, A., Valluzzi, M. R., Modena, C., D'Ayala, D., & Speranza, E. (2008). Vulnerability assessment of the historical masonry building typologies of Vittorio Veneto (NE Italy). *Bollettino Di Geofisica Teorica Ed Applicata*, *49*(3–4).

Berto, L., Saetta, A., Scotta, R., & Vitaliani, R. (2002). An orthotropic damage model for masonry structures. *International Journal for Numerical Methods in Engineering*, *55*(2). https://doi.org/10.1002/nme.495

Bertolesi, E., Adam, J. M., Rinaudo, P., & Calderón, P. A. (2019). Research and practice on masonry cross vaults – A review. In *Engineering Structures* (Vol. 180). https://doi.org/10.1016/j.engstruct.2018.10.085

Beyer, K., & Mangalathu, S. (2014). Numerical study on the peak strength of masonry spandrels with arches. *Journal of Earthquake Engineering*, *18*(2). https://doi.org/10.1080/13632469.2013.851047

Bianchini, N., Calderini, C., Mendes, N., Candeias, P., & Lourenço, P. B. (2023). *Blind prediction competition - sera.Ta - seismic response of masonry cross vaults: Shaking table tests and numerical validations*. https://doi.org/10.5281/zenodo.7624666

Bianchini, N., Mendes, N., Calderini, C., Candeias, P., & Lourenço, P. B. (2024). Shaking Table Testing of an Unstrengthened and Strengthened with Textile Reinforced Mortar (TRM) Full-Scale Masonry Cross Vault. *International Journal of Architectural Heritage*. https://doi.org/10.1080/15583058.2023.2295900

Bianchini, N., Mendes, N., Calderini, C., Candeias, P. X., Rossi, M., & Lourenço, P. B. (2022). Seismic response of a small-scale masonry groin vault: experimental investigation by performing quasi-static and shake table tests. *Bulletin of Earthquake Engineering*, *20*(3). https://doi.org/10.1007/s10518-021-01280-0

Block, P. (2009). Thrust Network Analysis: Exploring Three-dimensional Equilibrium. In *PhD thesis*.

Block, P., & Ochsendorf, J. (2007). Thrust network analysis: A new methodology for three-dimensional equilibrium. *Journal of the International Association for Shell and Spatial Structures*, *48*(155).

Block, P., & Ochsendorf, J. (2008). Lower-bound analysis of masonry vaults. *Structural Analysis of Historic Construction: Preserving Safety and Significance - Proceedings of the 6th International Conference on Structural Analysis of Historic Construction, SAHC08*, *1*. https://doi.org/10.1201/9781439828229.ch67

Bolander, J., Yoshitake, K., & Thomure, J. (1999). Stress analysis using elastically homogeneous rigid-body-spring networks. *Structural Engineering/Earthquake Engineering*, *16*(2). https://doi.org/10.2208/jscej.1999.633_25

Bommer, J. J., Dost, B., Edwards, B., Stafford, P. J., van Elk, J., Doornhof, D., & Ntinalexis, M. (2016). Developing an application-specific ground-motion model for induced seismicity. *Bulletin of the Seismological Society of America*, *106*(1). https://doi.org/10.1785/0120150184

Bommer, J. J., & van Elk, J. (2017). Comment on induced seismicity in Groningen. In *BSSA*.

Bony, J. (2023). French Gothic Architecture of the 12th and 13th Centuries. In *French Gothic Architecture of the 12th and 13th Centuries*. https://doi.org/10.2307/3332318

Bourne, S. J., & Oates, S. J. (2017). Development of statistical geomechanical models for forecasting seismicity induced by gas production from the Groningen field. *Geologie En Mijnbouw/Netherlands Journal of Geosciences*, *96*(5). https://doi.org/10.1017/njg.2017.35

Brignola, A., Podestà, S., & Pampanin, S. (2008). In-plane stiffness of wooden floor. *2008 NZSEE Conference, Paper 49*, (49).

Brown, T. M. (2013). Dutch Architecture: 1907-1917. *Netherlands Yearbook for History of Art / Nederlands Kunsthistorisch Jaarboek*, *18*(1). https://doi.org/10.1163/22145966-90000398

BS EN 338:2003 Structural Timber – Strength Classes, 3 En338:2003 (2003).

C

Calò, M., Scattarreggia, N., Monteiro, R., & Moratti, M. (2025). *Numerical-experimental validation of masonry arches strengthened with PBO-FRCM composite using the Applied Element Method*.

Calvi, G. M., Moratti, M., O'Reilly, G. J., Scattarreggia, N., Monteiro, R., Malomo, D., Calvi, P. M., & Pinho, R. (2019). Once upon a Time in Italy: The Tale of the Morandi Bridge. *Structural Engineering International*, *29*(2). https://doi.org/10.1080/10168664.2018.1558033

Calvi, G., & Palenzona, V. (2013). *La cattedrale restituita alla città* (Associazione Fabbricerie Italiane, Ed.).

Canuti, C., Carbonari, S., Dall'Asta, A., Dezi, L., Gara, F., Leoni, G., Morici, M., Petrucci, E., Prota, A., & Zona, A. (2021). Post-Earthquake Damage and Vulnerability Assessment of Churches in the Marche Region Struck by the 2016 Central Italy Seismic Sequence. *International Journal of Architectural Heritage*, *15*(7). https://doi.org/10.1080/15583058.2019.1653403

Carozzi, F. G., & Poggi, C. (2015). Mechanical properties and debonding strength of Fabric Reinforced Cementitious Matrix (FRCM) systems for masonry strengthening. *Composites Part B: Engineering*, *70*. https://doi.org/10.1016/j.compositesb.2014.10.056

Cecchi, A., & Sab, K. (2002). A multi-parameter homogenization study for modeling elastic masonry. *European Journal of Mechanics, A/Solids*, *21*(2). https://doi.org/10.1016/S0997-7538(01)01195-0

Chiozzi, A., Milani, G., & Tralli, A. (2017). Fast Kinematic Limit Analysis of FRP-Reinforced Masonry Vaults. I: General Genetic Algorithm–NURBS–Based Formulation. *Journal of Engineering Mechanics*, *143*(9). https://doi.org/10.1061/(asce)em.1943-7889.0001267

Cogliano, M., Casotto, C., Grecchi, G., Moratti, M., & Calvi, G. M. (2025a). *Seismic Assessment of a Masonry Cross-Vault Using the Applied Element Method*.

Cogliano, M., Casotto, C., Grecchi, G., Moratti, M., & Calvi, G. M. (2025b). *Seismic Assessment of an Unreinforced and Reinforced with TRM Masonry Cross-Vault using the Applied Element Method*.

Como, M. (2015). Statics of Historic Masonry Constructions: An Essay. In *Masonry Structures: Between Mechanics and Architecture*. https://doi.org/10.1007/978-3-319-13003-3_3

Cooke, J. (1903). *Wakeman's Handbook of Irish Antiquities: Third Edition*.

Creazza, G., Matteazzi, R., Saetta, A., & Vitaliani, R. (2002). Analyses of Masonry Vaults: A Macro Approach based on Three-Dimensional Damage Model. *Journal of Structural Engineering*, *128*(5). https://doi.org/10.1061/(asce)0733-9445(2002)128:5(646)

Croci, G. (1998a). The Basilica of St. Francis of Assisi after the September 1997 earthquake. *Structural Engineering International*.

Croci, G. (1998b). *The Conservation and Structural Restoration of Architectural Heritage*. Computational Mechanics Publications.

Croci, G. (2000). General methodology for the structural restoration of historic buildings: The cases of the Tower of Pisa and the Basilica of Assisi. *Journal of Cultural Heritage*, *1*(1). https://doi.org/10.1016/S1296-2074(99)00119-3

Croci, G. (2001). Strengthening the Basilica of St Francis of Assisi after the September 1997 Earthquake. *Structural Engineering International*, *11*(3). https://doi.org/10.2749/101686601780346869

Cucuzza, R., Domaneschi, M., Camata, G., Marano, G. C., Formisano, A., & Brigante, D. (2022). FRCM retrofitting techniques for masonry walls: a literature review and some laboratory tests. *Procedia Structural Integrity*, *44*. https://doi.org/10.1016/j.prostr.2023.01.280

Cundall, P. A., & Strack, O. D. L. (1979). A discrete numerical model for granular assemblies. *Geotechnique*, *29*(1). https://doi.org/10.1680/geot.1979.29.1.47

D

D'Altri, A. M., Sarhosis, V., Milani, G., Rots, J., Cattari, S., Lagomarsino, S., Sacco, E., Tralli, A., Castellazzi, G., & de Miranda, S. (2020). Modeling Strategies for the Computational Analysis of Unreinforced Masonry Structures: Review and Classification. *Archives of Computational Methods in Engineering*, *27*(4). https://doi.org/10.1007/s11831-019-09351-x

D'Ambra, C., Lignola, G. P., Prota, A., Fabbrocino, F., & Sacco, E. (2019). FRCM strengthening of clay brick walls for out of plane loads. *Composites Part B: Engineering*, *174*. https://doi.org/10.1016/j.compositesb.2019.107050

Davis, L., Cogliano, M., Casotto, C., Grecchi, G., Ozcebe, S., Tsioli, C., & Malomo, D. (2024). Pragmatic seismic collapse meso-scale analysis of old Dutch masonry churches. *Earthquake Engineering and Structural Dynamics*, *53*(2). https://doi.org/10.1002/eqe.4037

D'Ayala, D., & Casapulla, C. (2001). Limit state analysis of hemispherical domes with finite friction. *Proceedings of the III International Seminar on Structural Analysis of Historical Constructions. Guimaraes (Portugal)*. https://doi.org/972-8692-01-3

D'Ayala, D., & Speranza, E. (2003). Definition of Collapse Mechanisms and Seismic Vulnerability of Historic Masonry Buildings. *Earthquake Spectra*, *19*(3). https://doi.org/10.1193/1.1599896

DD:ENV:1996-2:2001. (2001). Eurocode 6 : Design of masonry structures — Part 2: Design, selection of materials and execution of masonry. *BSI Standards Publication*.

De Lorenzis, L., Dimitri, R., & La Tegola, A. (2007). Reduction of the lateral thrust of masonry arches and vaults with FRP composites. *Construction and Building Materials*, *21*(7). https://doi.org/10.1016/j.conbuildmat.2006.07.009

De Matteis, Gianfranco, Brando, G., & Corlito, V. (2019). Predictive model for seismic vulnerability assessment of churches based on the 2009 L'Aquila earthquake. *Bulletin of Earthquake Engineering*, *17*(9). https://doi.org/10.1007/s10518-019-00656-7

De Matteis, G, Cacace, D., & Rouhi, J. (2019). Masonry vaults: architectural evolution, structural behaviour and collapse mechanisms. *Proceedings of the Structural Engineers Word Congress*.

De Santis, S., de Felice, G., & Roscini, F. (2019). Retrofitting of Masonry Vaults by Basalt Textile-Reinforced Mortar Overlays. *International Journal of Architectural Heritage*, *13*(7). https://doi.org/10.1080/15583058.2019.1597947

Dipartimento della Protezione Civile. (2023). *Umbria–Marche: il terremoto infinito*. Presidenza del Consiglio dei Ministri.

Doglioni, F., Moretti, A., & Petrini, V. (1994). *Le Chiese e Il Terremoto*.

Domaneschi, M., Cimellaro, G. P., & Scutiero, G. (2019). A simplified method to assess generation of seismic debris for masonry structures. *Engineering Structures*, *186*. https://doi.org/10.1016/j.engstruct.2019.01.092

E

El-Kashif, K. F., & Maekawa, K. (2004). Time-dependent nonlinearity of compression softening in concrete. *Journal of Advanced Concrete Technology*, *2*(2). https://doi.org/10.3151/jact.2.233

Eogan, G. (1991). Prehistoric and Early Historic Cultural Change at Brugh na Bóinne. *Proceedings of the Royal Irish Academy 91C*, 126–132.

F

Fasolo, M., & Mancini, M. F. (2019). The 'architectural' projects for the church of st. Ignatius by Andrea Pozzo. *Disegno*, *2019*(4). https://doi.org/10.26375/disegno.4.2019.09

Ferrante, A., Dubois, F., & Morenon, P. (2024). Comparison of Continuous and Discrete Modeling Strategies for the Structural Assessment of a Masonry Vault Under Dynamic Seismic Loading. *International Journal of Architectural Heritage*, *18*(12), 1873–1885. https://doi.org/10.1080/15583058.2024.2377297

FireRiskHeritage Project. (2010). Treating debris of historical value after an earthquake. In *https://www.fireriskheritage.net/publicationsand-research-documents-of-risk-to-cultural-heritage/treating-historic-debris-after-and-earthquake/*. European Project Fire Risk Heritage – Culture 2007–2013.

Focacci, F., D'Antino, T., Carloni, C., Sneed, L. H., & Pellegrino, C. (2017). An indirect method to calibrate the interfacial cohesive material law for FRCM-concrete joints. *Materials and Design*, *128*. https://doi.org/10.1016/j.matdes.2017.04.038

Foraboschi, P. (2004). Strengthening of Masonry Arches with Fiber-Reinforced Polymer Strips. *Journal of Composites for Construction*, *8*(3). https://doi.org/10.1061/(asce)1090-0268(2004)8:3(191)

Formica, G., Sansalone, V., & Casciaro, R. (2002). A mixed solution strategy for the nonlinear analysis of brick masonry walls. *Computer Methods in Applied Mechanics and Engineering*, *191*(51–52). https://doi.org/10.1016/S0045-7825(02)00501-7

Foti, D., Vacca, V., & Facchini, I. (2018). DEM modeling and experimental analysis of the static behavior of a dry-joints masonry cross vaults. *Construction and Building Materials*, *170*. https://doi.org/10.1016/j.conbuildmat.2018.02.202

Fraternali, F. (2010). A thrust network approach to the equilibrium problem of unreinforced masonry vaults via polyhedral stress functions. *Mechanics Research Communications*, *37*(2). https://doi.org/10.1016/j.mechrescom.2009.12.010

Fraternali, F., Carpentieri, G., Modano, M., Fabbrocino, F., & Skelton, R. E. (2015). A tensegrity approach to the optimal reinforcement of masonry domes and vaults through fiber-reinforced composite materials. *Composite Structures*, *134*. https://doi.org/10.1016/j.compstruct.2015.08.087

Furiosi, A., Damiani, N., & Penna, A. (2024). Structural assessment of a masonry vault using the Distinct Element Method. In *Proceedings of the International Brick and Block Masonry Conference (IBMAC)* (pp. 1–12). Springer.

G

Gaetani, A., Monti, G., Lourenço, P. B., & Marcari, G. (2016). Design and Analysis of Cross Vaults Along History. *International Journal of Architectural Heritage*, *10*(7). https://doi.org/10.1080/15583058.2015.1132020

Garmendia, L., Larrinaga, P., San-Mateos, R., & San-José, J. T. (2015). Strengthening masonry vaults with organic and inorganic composites: An experimental approach. *Materials and Design*, *85*. https://doi.org/10.1016/j.matdes.2015.06.150

Garofano, A., & Lestuzzi, P. (2016). Seismic Assessment of a Historical Masonry Building in Switzerland: The "Ancien Hôpital De Sion." *International Journal of Architectural Heritage*, *10*(8). https://doi.org/10.1080/15583058.2016.1160303

Gattesco, N., & Macorini, L. (2014). In-plane stiffening techniques with nail plates or CFRP strips for timber floors in historical masonry buildings. *Construction and Building Materials*, *58*. https://doi.org/10.1016/j.conbuildmat.2014.02.010

Giuffrè, A. (1993). *Sicurezza e conservazione dei centri storici. Il caso Ortigia* (Laterza, Ed.).

Gregory, D. (1697). Catenaria. *Philosophical Transactions of the Royal Society of London*, *19*(231).

Guragain, R., Worakanchana, K., Mayorca, O., & Meguro, K. (2007). Simulation of Brick Masonry Wall Behavior Under Cyclic Loading Using Applied Element Method. In *BULLETIN OF EARTHQUAKE RESISTANT STRUCTURE RESEARCH CENTER, INSTITUTE OF INDUSTRIAL SCIENCE, UNIVERSITY OF TOKYO* (Vol. 40).

H

Helton, J. C., & Davis, F. J. (2003). Latin hypercube sampling and the propagation of uncertainty in analyses of complex systems. *Reliability Engineering and System Safety*, *81*(1). https://doi.org/10.1016/S0951-8320(03)00058-9

Heyman, J. (1966). The stone skeleton. *International Journal of Solids and Structures*, *2*(2). https://doi.org/10.1016/0020-7683(66)90018-7

Heyman, J. (1982). The Masonry Arch. In *Structural Analysis*. https://doi.org/10.1017/cbo9780511529580.006

Heyman, J. (1995). The stone skeleton: structural engineering of masonry architecture. *The Stone Skeleton: Structural Engineering of Masonry Architecture*. https://doi.org/10.1115/1.2787238

Heyman, J. (2008). Basic Structural Theory. In *Basic Structural Theory*. https://doi.org/10.1017/cbo9780511754487

Huerta, S. (2001). Mechanics of masonry vaults: The equilibrium approach. *3rd International Seminar in Historical Constructions, Guimarães, Portugal*, (February).

Huerta, S. (2008). The Analysis of Masonry Architecture: A Historical Approach. *Architectural Science Review*, *51*(4). https://doi.org/10.3763/asre.2008.5136

Huerta, S., & Lopez, G. (1997). Stability and consolidation of an ashlar barrel vault with great deformations: The church of Guimarei. *International Series on Advances in Architecture*, *3*.

I

ICOMOS-ISCS. (2023). *Recommendations for the Analysis, Conservation and Structural Restoration of Architectural Heritage*. 14th General Assembly, 3-6.

Istituto Nazionale di Geofisica e Vulcanologia – INGV. (2017). I terremoti del ’900: la sequenza sismica in Umbria-Marche del 1997. In *https://ingvterremoti.com/2017/09/26/i-terremoti-del-900-la-sequenza-sismica-in-umbria-marche-del-1997/*. INGVterremoti.

K

Karbassi, A., & Lestuzzi, P. (2012). Fragility Analysis of Existing Unreinforced Masonry Buildings through a Numerical-based Methodology. *The Open Civil Engineering Journal*, *6*(1). https://doi.org/10.2174/1874149501206010121

Karbassi, A., & Nollet, M. J. (2013). Performance-based seismic vulnerability evaluation of masonry buildings using applied element method in a nonlinear dynamic-based analytical procedure. *Earthquake Spectra*, *29*(2). https://doi.org/10.1193/1.4000148

Kawai, T. (1977). *A new discrete model for solid mechanics problems*.

Kawai, T. (1978). New discrete models and their application to seismic response analysis of structures. *Nuclear Engineering and Design*, *48*(1). https://doi.org/10.1016/0029-5493(78)90217-0

Kawai, T. (1980). Some consideration on the finite element method. *International Journal for Numerical Methods in Engineering*, *16*(1). https://doi.org/10.1002/nme.1620160108

Kawai, T., & Toi, Y. (1983). A discrete method of limit analysis and its application to plastic stability problems of structural members. *Engineering Structures*, *5*(1). https://doi.org/10.1016/0141-0296(83)90039-1

Kesavan, P., Petracca, M., Camata, G., Sethumadhavan, K., & Menon, A. (2024). *Discontinuum Micromodelling of Unstrengthened and FRCM-Strengthened Masonry Cross-Vaults Subjected to Seismic Excitation*.

Keys, R. A., & Clubley, S. K. (2017). Establishing a predictive method for blast induced masonry debris distribution using experimental and numerical methods. *Engineering Failure Analysis*, *82*. https://doi.org/10.1016/j.engfailanal.2017.07.017

Kikuchi, A., Kawai, T., & Suzuki, N. (1992). The rigid bodies-spring models and their applications to three-dimensional crack problems. *Computers and Structures*, *44*(1–2). https://doi.org/10.1016/0045-7949(92)90269-6

Kroesen, J. E. A. (2021). "This Is My Place". (Hi)Storytelling Churches in the Northern Netherlands. *Religions*, *12*(9). https://doi.org/10.3390/rel12090702

Kurrer, K. E. (2008). The History of the Theory of Structures. From Arc Analysis to Computational Mechanics. In *Journal of Elasticity* (Vol. 93, Number 2). https://doi.org/10.1007/s10659-008-9174-0

L

Lagomarsino, S. (1998). A new methodology for the post-earthquake investigation of ancient churches. *11th European Conference on Earthquake Engineering*, (January).

Lagomarsino, S., Penna, A., Galasco, A., & Cattari, S. (2013). TREMURI program: An equivalent frame model for the nonlinear seismic analysis of masonry buildings. *Engineering Structures*, *56*. https://doi.org/10.1016/j.engstruct.2013.08.002

Lagomarsino, S., & Podestà, S. (2004a). Seismic vulnerability of ancient churches: I. Damage assessment and emergency planning. *Earthquake Spectra*, *20*(2). https://doi.org/10.1193/1.1737735

Lagomarsino, S., & Podestà, S. (2004b). Seismic vulnerability of ancient churches: II. Statistical analysis of surveyed data and methods for risk analysis. *Earthquake Spectra*, *20*(2). https://doi.org/10.1193/1.1737736

Lengyel, G. (2017). Discrete element analysis of gothic masonry vaults for self-weight and horizontal support displacement. *Engineering Structures*, *148*. https://doi.org/10.1016/j.engstruct.2017.06.014

Lengyel, G., & Bagi, K. (2015). Numerical analysis of the mechanical role of the ribs in groin vaults. *Computers and Structures*, *158*. https://doi.org/10.1016/j.compstruc.2015.05.032

Lotfi, H. R., & Shing, P. B. (1994). Interface Model Applied to Fracture of Masonry Structures. *Journal of Structural Engineering*, *120*(1). https://doi.org/10.1061/(asce)0733-9445(1994)120:1(63)

Lourenço, P. B. (1996). Computational strategies for masonry structures. In *PhD Thesis* (Vol. 70, Number 08).

Lourenco, P. B. (1996). *Computational Strategy for Masonry Structures*. https://www.researchgate.net/publication/27344834

Lourenço, P. B., Avila, L., Vasconcelos, G., Alves, J. P. P., Mendes, N., & Costa, A. C. (2013). Experimental investigation on the seismic performance of masonry buildings using shaking table testing. *Bulletin of Earthquake Engineering*, *11*(4). https://doi.org/10.1007/s10518-012-9410-7

Lourenço, P. B., De Borst, R., & Rots, J. G. (1997). A plane stress softening plasticity model for orthotropic materials. *International Journal for Numerical Methods in Engineering*, *40*(21). https://doi.org/10.1002/(SICI)1097-0207(19971115)40:21<4033::AID-NME248>3.0.CO;2-0

Lourenço, P. B., & Rots, J. G. (1997). Multisurface Interface Model for Analysis of Masonry Structures. *Journal of Engineering Mechanics*, *123*(7). https://doi.org/10.1061/(asce)0733-9399(1997)123:7(660)

Lourenço, P. B., Rots, J. G., & Blaauwendraad, J. (1995). Two approaches for the analysis of masonry structures - micro and macro-modeling. In *Heron* (Vol. 40, Number 4).

Lourenço, P. B., & Silva, L. C. (2020). Computational applications in masonry structures: From the meso-scale to the super-large/super-complex. *International Journal for Multiscale Computational Engineering*, *18*(1). https://doi.org/10.1615/IntJMultCompEng.2020030889

Luciano, R., & Sacco, E. (1997). Homogenization technique and damage model for old masonry material. *International Journal of Solids and Structures*, *34*(24). https://doi.org/10.1016/S0020-7683(96)00167-9

M

Magenes, G. (2006). Masonry Building Design in Seismic Areas: recent experiences and prospects from a European standpoint. *1st European Conference on Earthquake Engineering and Seismology*.

Mahdi, T. (2017). Seismic vulnerability of traditional masonry arches, vaults and domes. *Asian Journal of Civil Engineering*, *18*(3).

Malomo, D., Pinho, R., & Penna, A. (2020a). Applied Element Modelling of the Dynamic Response of a Full-Scale Clay Brick Masonry Building Specimen with Flexible Diaphragms. *International Journal of Architectural Heritage*, *14*(10). https://doi.org/10.1080/15583058.2019.1616004

Malomo, D., Pinho, R., & Penna, A. (2020b). Numerical modelling of the out-of-plane response of full-scale brick masonry prototypes subjected to incremental dynamic shake-table tests. *Engineering Structures*, *209*. https://doi.org/10.1016/j.engstruct.2020.110298

Malomo, D., Pinho, R., & Penna, A. (2020c). Simulating the shake table response of unreinforced masonry cavity wall structures tested to collapse or near-collapse conditions. *Earthquake Spectra*, *36*(2). https://doi.org/10.1177/8755293019891715

Malomo, D., & Pulatsu, B. (2024). Discontinuum models for the structural and seismic assessment of unreinforced masonry structures: a critical appraisal. In *Structures* (Vol. 62). https://doi.org/10.1016/j.istruc.2024.106108

Martelli, A. (2011). *La protezione degli edifici dal terremoto mediante moderne tecnologie*. ADEPRON. https://www.ingegneriastrutturale.net/documenti/articoli/adepron04_0021.pdf

Matuttis, H. G., & Chen, J. (2014). Understanding the Discrete Element Method: Simulation of Non-Spherical Particles for Granular and Multi-body Systems. In *Understanding the Discrete Element Method: Simulation of Non-Spherical Particles for Granular and Multi-body Systems* (Vol. 9781118567203). https://doi.org/10.1002/9781118567210

Meguro, K., & Hakuno, M. (1989). Fracture analyses of concrete structures by the modified distinct element method. *Doboku Gakkai Rombun-Hokokushu/Proceedings of the Japan Society of Civil Engineers*, (410 pt 1–12). https://doi.org/10.2208/jscej.1989.410_113

Meguro, K., & Hakuno, M. (1994). Application of the extended distinct element method for collapse simulation of a double-deck bridge. *Structural Engineering/Earthquake Engineering*, *10*(4).

MEGURO, K., IWASHITA, K., & HAKUNO, M. (1991). FRACTURE ANALYSES OF MEDIA COMPOSED OF IRREGULARLY SHAPED REGIONS BY THE EXTENDED DISTINCT ELEMENT METHOD. *Doboku Gakkai Ronbunshu*, *1991*(437). https://doi.org/10.2208/jscej.1991.437_37

Meguro, Kimiro, & Tagel-Din, H. (1997). A new efficient technique for fracture analysis of structures. *Bulletin of Earthquake Resistant Structure Research Center, Institute of Industrial Science, University of Tokyo*, *30*, 103–116.

Meguro, K, & Tagel-Din, H. (1997). A new simplified and efficient technique for fracture behavior analysis of concrete structures. *Fracture Mechanics of Concrete Structures Proceedings FRAMCOS-3*.

Meguro, K., & Tagel-Din, H. (1999). Simulation of buckling and post-buckling behavior of structures using applied element method. In *Bulletin of Earthquake Resistant Structure, IIS, University of Tokyo 32*.

Meguro, K., & Tagel-Din, H. (2000). Applied element method for structural analysis: Theory and application for linear materials. *Structural Engineering/Earthquake Engineering*, *17*(1).

Menegotto, M., & Pinto, P. E. (1973). Method of Analysis for Cyclically Loaded R.C. Plane Frames Including Changes in Geometry and Non-Elastic Behavior of Elements under Combined Normal Force and Bending. *IABSE Symposium on Resistance and Ultimate Deform Ability of Structures Acted On by Well Defined Repeated Loads*.

Milani, G., & Lourenço, P. B. (2009). A discontinuous quasi-upper bound limit analysis approach with sequential linear programming mesh adaptation. *International Journal of Mechanical Sciences*, *51*(1). https://doi.org/10.1016/j.ijmecsci.2008.10.010

Milani, G., Lourenço, P. B., & Tralli, A. (2006a). Homogenised limit analysis of masonry walls, Part I: Failure surfaces. *Computers and Structures*, *84*(3–4). https://doi.org/10.1016/j.compstruc.2005.09.005

Milani, G., Lourenço, P. B., & Tralli, A. (2006b). Homogenised limit analysis of masonry walls, Part II: Structural examples. *Computers and Structures*, *84*(3–4). https://doi.org/10.1016/j.compstruc.2005.09.004

Milani, G., Milani, E., & Tralli, A. (2009). Upper bound limit analysis model for FRP-reinforced masonry curved structures. Part II: Structural analyses. *Computers and Structures*, *87*(23–24). https://doi.org/10.1016/j.compstruc.2009.07.010

Milani, G., Rossi, M., Calderini, C., & Lagomarsino, S. (2016). Tilting plane tests on a small-scale masonry cross vault: Experimental results and numerical

simulations through a heterogeneous approach. *Engineering Structures*, *123*. https://doi.org/10.1016/j.engstruct.2016.05.017

Milani, G., & Tralli, A. (2012). A simple meso-macro model based on SQP for the non-linear analysis of masonry double curvature structures. *International Journal of Solids and Structures*, *49*(5). https://doi.org/10.1016/j.ijsolstr.2011.12.001

Miller, S. A., Collettini, C., Chiaraluce, L., Cocco, M., Barchi, M., & Kaus, B. J. P. (2004). Aftershocks driven by a high-pressure CO2source at depth. *Nature*, *427*(6976). https://doi.org/10.1038/nature02251

Modena, C., Valluzzi, M. R., Da Porto, F., & Casarin, F. (2011). Structural aspects of the conservation of historic masonry constructions in seismic areas: Remedial measures and emergency actions. *International Journal of Architectural Heritage*, *5*(4–5). https://doi.org/10.1080/15583058.2011.569632

Moratti, M., Gaia, F., Martini, S., Tsioli, C., Grecchi, G., Casotto, C., Calvi, G. M., Hertog, D. Den, Calvi, P. M., & Proestos, G. T. (2019). A methodology for the seismic multilevel assessment of unreinforced masonry church inventories in the Groningen area. *Bulletin of Earthquake Engineering*, *17*(8). https://doi.org/10.1007/s10518-019-00575-7

Muntendam-Bos, A. G., Hoedeman, G., Polychronopoulou, K., Draganov, D., Weemstra, C., van der Zee, W., Bakker, R. R., & Roest, H. (2022). An overview of induced seismicity in the Netherlands. *Geologie En Mijnbouw/Netherlands Journal of Geosciences*, *101*(2). https://doi.org/10.1017/njg.2021.14

N

National Civil Protection Service. (2013). *Manuale per La Compilazione Della Scheda per Il Rilievo Del Danno Ai Beni Culturali, Chiese - Modello A-DC* (Simona Papa & Giacomo Di Pasquale, Eds.).

Nelms, H. (1981). The structure of Newgrange. In *Antiquity* (Vol. 55, Number 213). https://doi.org/10.1017/S0003598X00116175

NEN. (2020). *NPR 9998:2020 – Assessment of buildings in case of erection, reconstruction and disapproval – Basic rules for seismic actions: Induced earthquakes*. Nederlands Normalisatie-instituut (NEN).

O

O'Dwyer, D. (1999). Funicular analysis of masonry vaults. *Computers and Structures*, *73*(1–5). https://doi.org/10.1016/S0045-7949(98)00279-X

OFMConv – Order of Friars Minor Conventual. (2022). 25 anni fa la Basilica di San Francesco veniva riaperta al pubblico. In *https://www.ofmconv.net/en/25-anni-fa-la-basilica-di-san-francesco-veniva-riaperta-al-pubblico/*. OFMConv.net.

Okamura, H., & Maekawa, K. (1983). *Non-Linear Analysis and Constitutive Models of Renforced Concrete*.

Oktiovan, Y. P., Davis, L., Wilson, R., Dell'Endice, A., Mehrotra, A., Pulatsu, B., & Malomo, D. (2023). Simplified Micro-Modeling of a Masonry Cross-Vault for Seismic Assessment Using the Distinct Element Method. *International Journal of Architectural Heritage*. https://doi.org/10.1080/15583058.2023.2277328

Oppenheim, I. J., Gunaratnam, D. J., & Allen, R. H. (1989). Limit State Analysis of Masonry Domes. *Journal of Structural Engineering*, *115*(4). https://doi.org/10.1061/(asce)0733-9445(1989)115:4(868)

P

Pandey, B. H., & Meguro, K. (2004). Simulation of brick masonry wall behavior under in-plane lateral loading using applied element method. *13th World Conference on Earthquake Engineering, Vancouver, BC, Canada, August*, (1664).

Pegon, P., & Anthoine, A. (1997). Numerical strategies for solving continuum damage problems with softening: Application to the homogenization of masonry. *Computers and Structures*, *64*(1–4). https://doi.org/10.1016/S0045-7949(96)00153-8

Pelà, L., Bourgeois, J., Roca, P., Cervera, M., & Chiumenti, M. (2016). Analysis of the effect of provisional ties on the construction and current deformation of mallorca cathedral. *International Journal of Architectural Heritage*, *10*(4). https://doi.org/10.1080/15583058.2014.996920

Pellegrini, D. (2023). Pre- and Post-Diction Simulation of the Seismic Response of a Masonry Cross Vault Tested on a Shaking Table. *International Journal of Architectural Heritage*, *18*(12). https://doi.org/10.1080/15583058.2023.2242812

Penna, A., Calderini, C., Sorrentino, L., Carocci, C. F., Cescatti, E., Sisti, R., Borri, A., Modena, C., & Prota, A. (2019). Damage to churches in the 2016 central Italy earthquakes. *Bulletin of Earthquake Engineering*, *17*(10). https://doi.org/10.1007/s10518-019-00594-4

Pulatsu, B., Erdogmus, E., & Lourenço, P. B. (2019). Simulation of Masonry Arch Bridges Using 3D Discrete Element Modeling. In *RILEM Bookseries* (Vol. 18). https://doi.org/10.1007/978-3-319-99441-3_94

R

Rossi, M., Calderini, C., Roselli, I., Mongelli, M., Canio, G. De, & Lagomarsino, S. (2020). Seismic analysis of a masonry cross vault through shaking table tests: The case study of the Dey Mosque in Algiers. *Earthquake and Structures*, *18*(1). https://doi.org/10.12989/eas.2020.18.1.057

S

Saltelli, A., Tarantola, S., Campolongo, F., & Ratto, M. (2004). Sensitivity Analysis in Practice. A Guide to Assessing Scientific Models. In: Probability and Statistics Series. In *Analyzing Uncertainty in Civil Engineering*.

Sathiparan, N., Mayorca, P., Kourosh Nasrollahzadeh, N., Guragain, R., & Meguro, K. (2005). Experimental Study on In-plane and Out-of-plane Behavior of Masonry Wallettes Retrofitted by PP-Band Meshes. *SEISAN KENKYU*, *57*(6). https://doi.org/10.11188/seisankenkyu.57.530

Sathiparan, N., Mayorca, P., & Meguro, K. (2012). Shake table tests on one-quarter scale models of masonry houses retrofitted with PP-band mesh. *Earthquake Spectra*, *28*(1). https://doi.org/10.1193/1.3675357

Scacco, J., Ghiassi, B., Milani, G., & Lourenço, P. B. (2020). A fast modeling approach for numerical analysis of unreinforced and FRCM reinforced masonry walls

under out-of-plane loading. *Composites Part B: Engineering*, *180*. https://doi.org/10.1016/j.compositesb.2019.107553

Szołomicki, J., Berkowski, P., & Barański, J. (2015). Computer modelling of masonry cross vaults strengthened with fiber reinforced polymer strips. *Archives of Civil and Mechanical Engineering*, *15*(3). https://doi.org/10.1016/j.acme.2014.05.006

T

Tagel-Din, H., & Meguro, K. (1999). Applied element simulationfor collapse analysis of structures. *Bulletin of Earthquake Resistant Structure Research Center, Institute of Industrial Science, University of Tokyo*, *32*, 113–123.

Tagel-Din, H., & Meguro, K. (2000a). Applied element method for dynamic large deformation analysis of structures. *Structural Engineering/Earthquake Engineering*, *17*(2). https://doi.org/10.2208/jscej.2000.661_1

Tagel-Din, H., & Meguro, K. (2000b). APPLIED ELEMENT METHOD FOR SIMULATION OF NONLINEAR MATERIALS: THEORY AND APPLICATION FOR RC STRUCTURES. In *JSCE* (Vol. 17, Number 2).

Theodossopoulos, D., & Sinha, B. (2008). Structural safety and failure modes in Gothic vaulting systems. ... *Int. Seminar on Structural* ....

Theodossopoulos, D., Sinha, B. P., & Usmani, A. S. (2003). Case Study of the Failure of a Cross Vault: Church of Holyrood Abbey. *Journal of Architectural Engineering*, *9*(3). https://doi.org/10.1061/(asce)1076-0431(2003)9:3(109)

V

Valluzzi, M. R., Da Porto, F., Garbin, E., & Panizza, M. (2013). *Experimental characterization of out-of-plane behaviour of infill masonry walls strengthened with composite materials*.

Van Der Pluijm, R. (1997). Non-linear behaviour of masonry under tension. *Heron*, *42*(1).

Van Elk, J., Doornhof, Di., Bommer, J. J., Bourne, S. J., Oates, S. J., Pinho, R., & Crowley, H. (2017). Hazard and risk assessments for induced seismicity in Groningen.

Geologie En Mijnbouw/Netherlands Journal of Geosciences, *96*(5). https://doi.org/10.1017/njg.2017.37

Van Mele, T., McInerney, J., DeJong, M. J., & Block, P. (2012). Physical and Computational Discrete Modelling of Masonry Vault Collapse. *Structural Analysis of Historical Constructions, Vols 1-3*.

van Zijl, G. P. A. G. (2004). Modeling Masonry Shear-Compression: Role of Dilatancy Highlighted. *Journal of Engineering Mechanics*, *130*(11). https://doi.org/10.1061/(asce)0733-9399(2004)130:11(1289)

Vicente, R., Parodi, S., Lagomarsino, S., Varum, H., & Silva, J. A. R. M. (2011). Seismic vulnerability and risk assessment: Case study of the historic city centre of Coimbra, Portugal. *Bulletin of Earthquake Engineering*, *9*(4). https://doi.org/10.1007/s10518-010-9233-3

W

Wendland, D. (2005). Some considerations on the shape of the caps of vaults. *Structural Analysis of Historical Constructions*.

Williams, M. S., Albuerne, A., Lawson, V., & Yip. F. (2012). Model Scale Shaking Table Tests on Masonry Barrel and Cross Vaults. *15 WCEE*.

Z

Zampieri, P., Simoncelo, N., Tetougueni, C. D., & Pellegrino, C. (2018). A review of methods for strengthening of masonry arches with composite materials. In *Engineering Structures* (Vol. 171). https://doi.org/10.1016/j.engstruct.2018.05.070